

**ESTIMATION OF PEELING AND FOLDING MECHANISM
OF WHITE-COATED PAPERBOARD USING NON-LINEAR
SPRING MODEL OF FLUFFING BASED DELAMINATION**

毛羽立ち剥離非線形ばねモデルによる白板紙の引き剥が
しと折り曲げ機構の評価

JINA WEERAYUT

ジナ ウェラユット

**A Thesis Submitted in Partial Fulfillment of the Requirements for the
Degree of Doctor of Engineering in Information Science and
Control Engineering**

Nagaoka University of Technology

August 2018

I would like to dedicate this thesis to my loving parents, คุณพ่อศไกร คุณแม่กัลยา

**TITLE: ESTIMATION OF PEELING AND FOLDING
MECHANISM OF WHITE-COATED PAPERBOARD
USING NON-LINEAR SPRING MODEL OF FLUFFING**

AUTHOR: JINA WEERAYUT

DATE OF ISSUE: AUGUST 2018

Acknowledgment

Firstly, I would like to express my sincere gratitude to my academic advisor Prof. Dr. Nagasawa Shigeru, a professor of Department of Mechanical Engineering, Nagaoka University of Technology, for his invaluable guidance, support and consistent encouragement I received throughout my doctoral student life. Even though he was very busy with his works, he had never left me alone to face difficulties arisen during the research work. Furthermore, the achievement of my study in a Doctoral course could not be possible without his valuable comments. It was a great experience has been working with him.

Besides my advisor, I would like to thank the rest of my thesis committee: Prof. Dr. Koguchi Hideo, Assoc. Prof. Dr. Kurahashi Takahiko, Assoc. Prof. Dr. Isobe Hiromi, Assoc. Prof. Dr. Miyashita Yukio, for their insightful comments and encouragement. Their expert guidance and valuable comments have improved the thesis content and the presentation.

My sincere thanks also goes to Asst. Prof. Dr. Seksan Chaijit, who partly motivated me to continue my study in the doctoral course at Nagaoka University of Technology and gave me a lot of useful information during the application to the course. Special thanks to Dr. Pusit Mitsomwang for his kindness instruction and great suggestions about my research work and Mr. Yuichi Igarashi for his kindness teaching and great suggestions about my experiment. I would also like to thank all laboratory members for their continuous support and contribution during my study period.

I am deeply indebted to the funding support (Monbukagakusho scholarship) from the Japanese government, providing financial support during studying at the Nagaoka University of Technology.

Finally, I would like to express my deep sense of gratitude to my parents and brother, Mr. Yotkrai Jina, Mrs. Kanlaya Jina and Mr. Panuwit Jina, for their support and encouragement throughout the course during my study.

WEERAYUT JINA

Nagaoka University of Technology

August 2018

Abstract

Delamination of white-coated paperboard is one of the most important roles for making a crease line of paper box and tray in the package converting industry, because the folding of crease is well used for making shapes of boxes and trays. The delamination of interlayers occurs during a folding process of creased paperboard. In order to inspect the strength or resistance of delamination, some measuring methods, such as the Z-directional tensile test (ZDTT), the peeling cohesion test (PCT) were examined in the first stage. The delamination and folding mechanism are important for making a high precious size of box, smart folding shapes and a certain strength of folded lines. To measure the resistance of forming and the stiffness of delaminated paperboard are necessary for estimating the folding performance of locally delaminated zone.

First, concerning an in-plane detaching resistance of a white-coated paperboard subjected to a peeling deformation, the z-directional (out-of-plane) tensile test (ZDTT) and the peel cohesion test (PCT) were investigated experimentally and numerically. Since the paperboard is composed of fibrous plies, its detaching mechanism seems to be different from a crack propagation of a fragile material. In this work, an internal breaking criteria and transient de-lamination phenomena of a weak-bonded layer of a white-coated paperboard were experimentally investigated through the ZDTT and the PCT. The detaching resistance in the normal direction was estimated with the proposed non-linear fluffing model using a finite element method (FEM) code to characterize the peeling deformation of the weak-bonded layer. A white-coated paperboard of 0.45 mm thickness (basis weight of 350 g m⁻²) was chosen for conducting the PCT and the ZDTT. An anaphase yielding resistance of detaching was revealed through the ZDTT of the paperboard. The relationship between the pulling force and the curvature radius of delaminated upper layer of the paperboard were discussed in the PCT. The FEM simulation of the PCT of the paperboard was analyzed using an isotropic-elastic model, which was developed through the ring crush test, and compared with the 3 point bending test. The results were as follows: (1) The out-of-plane detaching resistance of in-plane layer of a white-coated paperboard was experimentally characterized through the PCT by the

maximum peak line force at the early stage and the stationary line force. These line forces were almost independent to the paper-making direction. (2) A fluffing profile of the de-laminated layer and the thickness of the peeled upper layer experimentally depended on the pulling velocity. (3) Regarding the detaching resistance of peeled layer, a fluffing model was proposed in the developed simulation model. Equivalent fibers based fluffing model that were derived from the ZDTT experiment (approximated as discretely distributed nonlinear springs) well explained the existence of the maximum peak point of peeling force and saturated peel resistance.

Second, to develop a numerical simulation model of the folding process of a creased paperboard and to reveal the deformation characteristics of the creased paperboard, a cantilever type bending moment measurement was experimentally examined with a 0.43 mm thickness white-coated paperboard. To verify the folding response of the creased part, the initial crease (the scored depth) was varied within a certain range, and the lamination numbers were discussed with 2-8 layers. A fluffing resistance model based on the z-directional (out-of-plane) tensile test was initially developed and simulated using isotropic elasto-plastic solid properties. However, since the fluffing resistance was restricted in the normal direction of the detached interface, the in-plane shear resistance was not considered in the early stage. When investigating the folding process of a creased part, it was found that the in-plane shear resistance and its breaking limit was the primary characteristics. Therefore, in this work, in order to characterize the delamination and bulging deformation, the internal breaking criteria was numerically analyzed using a new combination model. A general purpose finite element method (FEM) code MARC was applied to develop a combination model comprising the out-of-plane fluffing subroutine and the in-plane shear glue strength. Through the FEM simulation of the folding process of creased paperboard, the following results were revealed: (1) The simulated bulging profile of the creased part and its bending moment resistance well matched with the corresponding experimental result at the stationary folding state for the folding angle $>20^\circ$, when using the combination model. The saturated bending moment resistance was characterized by the yielding stress and the folded geometrical mode. (2) The in-plane shear glue strength characterized the bulging patterns of the interlayer delamination in the folding process of the scored zone. (3) The initial delaminated

span of the scored zone was estimated as >150% of the creasing width. (4) The initial gradient of the bending moment resistance was characterized by the scored depth and the elastic modulus. (5) The transient response of bending moment at the early stage was characterized by the softening effect model (as partially deleted).

Third, to reveal deformation behavior under a compressive loading using V-Block fixtures, the developed combination model of shear glue strength and fluffing normal strength was conducted for analyzing the bending behavior of creased paperboard, using the in-plane MD tensile properties. An FEM analysis was simulated the compressive load using V-Block fixtures. The simulated folding deformation of the creased part of paperboard was compared with the experiment. The results of this study were as follows: (1) The compressive load tended to decrease with the scored depth and the folded angle. This tendency was well simulated and explained using the combination model. (2) The value of the yield strength characterized the bending moment for a certain large folding angle $> 60^\circ$. (3) The combination of the fluffing normal and the shear glue strength under the in-plane compressive state was well described the bulging mode of folded portion, when comparing the experimental result for the scored depth of $d_{as} = 0.2$ mm.

List of contents

	Page
Acknowledgement	i
Abstract	ii
List of contents	v
Nomenclature	ix
Chapter	
1 Introduction	1
1.1 Introduction to creasing process	1
1.1.1 History of creasing process and its principle	1
1.2 Motivation and problem statement	4
1.3 Objectives of research work	6
1.4 Scope of research work	6
1.5 Organization of treatise	7
2 Estimation of detaching resistance of a peeled in-plane layer of a white-coated paperboard using fluffing resistance model	13
2.1 Introduction	13
2.2 Analysis condition and preliminary investigation	15
2.2.1 Specimens	15
2.2.2 Estimation of elastic properties for compressive strength by ring crush test	16
2.2.3 Anaphase yield resistance model based on ZDTT	18
2.2.4 Method of Peel Cohesion Test (T-peel test)	21
2.2.5 FEM model for PCT	23
2.3 Results and discussions	27
2.3.1 Experimental peeling load response and deformation of peeled layer	27

List of contents (Continued)

	Page
2.3.2 Peeling load response and deformation of the worksheet on simulation	30
2.4 Conclusions	34
3 Analysis of the folding process of creased paperboard using a combined fluffing resistance and shear yield glue model	39
3.1 Introduction	39
3.2 Analysis conditions, estimated methods and the mechanical model of worksheet	42
3.2.1 Specimens	42
3.2.2 Out-of-plane detaching resistance model of specimens based on ZDTT	43
3.2.3 Experimental initial creasing of specimens	45
3.2.4 Experimental bending moment	46
3.3 Estimation of in-plane shear strength properties	47
3.4 FEM simulation model	49
3.4.1 FEM simulation model for non-scoring	49
3.4.2 FEM simulation model for scoring	51
3.4.3 FEM simulation model for folding	54
3.5 Results and discussion	55
3.5.1 Experimental bending moment resistance with the scoring depth	55
3.5.2 Bending moment resistance for non-creasing state	56
3.5.3 Combination effect of shear glue strength and fluffing normal strength	59
3.5.4 Effects of lamination numbers	63
3.5.5 Bulged profile of the creased part	64

List of contents (Continued)

	Page
3.5.6 Effects of length of delaminated zone.....	66
3.5.7 Effects of fluffing model on the creasing and folding process.....	68
3.5.8 Softening effect model on the creasing and folding process under the shallow indentation and the indentation depth.....	69
3.6 Conclusions.....	76
4 Analysis of folding process of creased paperboard subjected to in-plane compressive load using the combination model.....	81
4.1 Introduction.....	81
4.2 Preliminary investigation and experimental methods.....	82
4.2.1 Specimens.....	82
4.2.2 Out-of-plane detaching resistance model of specimens based on ZDTT.....	83
4.2.3 Estimation of the in-plane shear strength properties.....	86
4.2.4 Experimental initial creasing and working conditions.....	88
4.2.5 Experimental compressive load using V-Block fixtures.....	89
4.3 FEM simulation model.....	91
4.3.1 FEM simulation model for non-scoring.....	91
4.3.2 FEM simulation model for scoring.....	92
4.3.3 FEM simulation model for compressive load using V-Block fixtures.....	95
4.4 Estimation method of bending moment response under compressive load using V-Block fixtures.....	96
4.5 Results and discussion.....	97
4.5.1 Experimental compressive load using V-Block fixtures.....	97
4.5.2 Compressive load response of the worksheet on the simulation model using V-Block fixtures.....	98
4.5.3 Equivalent bending moment response under compressive load using V-Block fixtures for non-scoring.....	101

List of contents (Continued)

	Page
4.5.4 Equivalent bending moment response under compressive load using V-Block fixtures for scoring.....	104
4.6 Conclusions.....	107
5 Conclusions and prospects.....	111
5.1 Conclusions.....	111
5.2 Prospects.....	112
Appendixes.....	113
Appendix A User-defined subroutine of USPRNG.....	113
How to write the User Subroutine code.....	114
How to call the User Subroutine file on MARC Mentat 2015.....	114
How to check the output file of the User Subroutine on MARC Mentat 2015.....	117
Appendix B Apparatuses and tools.....	118
Appendix C List of publications.....	122
Biography.....	126

Nomenclature

Symbol	Definition
ZDTT	Z-directional (out-of-plane) tensile test
PCT	Peel cohesion test
MD	Machine direction for paper making
t	Thickness of work sheet /mm
t_p	Thickness of weak-bonded peeled layer in PCT /mm
t_b	Thickness of base paperboard /mm
L_{ZDTT}	Length of the specimen for ZDTT test /mm
B_{ZDTT}	Width of the specimen for ZDTT test /mm
$t_{p\ ZDTT}$	Thickness of weak-bonded peeled layer in ZDTT /mm
$e_z = x$	Elongation in ZDTT /mm
σ	Tensile stress in ZDTT /MPa
a_1-a_4, b_1-b_4, c_1	Coefficients of Eq.(1), (2), and (3)
$f_{ZDTT} = \sigma \cdot L_{ZDTT}$	Tensile line force in ZDTT
U	Distance between the 1st end and 2nd end of nonlinear spring which is joined to nodes on the peeled layer /mm
K	Stiffness of nonlinear spring in USPRNG subroutine
L_{PCT}	Length of the specimen for peeling test /mm
B_{PCT}	Width of the specimen for peeling test /mm
V	Experimental feed velocity of vertical motion of gripper point of peeled layer /mm·s ⁻¹
u_x	Horizontal displacement of base paper by table motion /mm
u_y	Vertical displacement of gripper point of peeled layer /mm
t_{ep}	Virtual elapsed time /s
v_y	Virtual feed velocity of the vertical motion of gripper point of peeled layer /mm·s ⁻¹
v_x	Virtual feed velocity of the horizontal motion of base paper /mm·s ⁻¹
L_{ip}	Length of initial peak that was equivalent to be 2.67 mm in this work, was equivalent to be the length of initial peak of the experimental result
$h = h_1-h_0$	Vertical displacement of edge of the peeled layer from the edge of base paperboard
h/t_p	Normalized peeling displacement per the thickness of peeled layer
$f_p (=F_p/b)$	Tensile line force of paperboard in PCT /kN·m ⁻¹
E_{RC}	Equivalent elasticity modulus derived from a ring crush test /MPa

Nomenclature (Continued)

Symbol	Definition
ν	Poisson's ratio
f_{pmax}	Maximum peak tensile line force in PCT / $\text{kN}\cdot\text{m}^{-1}$
f_{pc}	Average of saturated (stationary) resistance in PCT / $\text{kN}\cdot\text{m}^{-1}$
r_p	Curvature radius of peeled layer sheet /mm
σ_Y	The yield stress of specimen in the in-plane MD /MPa
V	Experimental indentation velocity of creasing rule / $\text{mm}\cdot\text{s}^{-1}$.
l_{dn}	Distance or length between the end of both notches in the in-plane shearing test /mm
w_s	The width of the specimen in an in-plane shearing test /mm
t_s	Thickness of paperboard of in-plane shearing test /mm
d_n	Depth of notches / mm
t_{ds}	Thickness of double-sided tape of in-plane shearing test /mm
t_m	Thickness of metal plate of in-plane shearing test /mm
$\tau_{B(inMD)}$	Breaking shear strength in the in-plane MD shearing test /MPa
s_t	Shear strength parameter in the glue contact function /MPa
L_{CST}	Length of the specimen for CST test /mm
W_{CST}	Width of the specimen for CST test /mm
B	Width of channel die /mm
d	Indentation depth of creasing rule /mm
d_{as}	Permanent depth after scoring by creasing rule /mm
h	Height difference (step) of rubber from the creasing rule /mm
r	Radius of a creasing rule /mm
b	Thickness of a creasing rule /mm
$\gamma = 2dB^{-1}$	Normalized indentation depth (nominal shear strain)
θ	folding angle (°)
M	Bending line moment resistance = bending moment resistance per unit width against folding / $\text{Nm}\cdot\text{m}^{-1}$
M_{90}	Bending line moment resistance at the folding angle of $\theta = 90^\circ$ / $\text{Nm}\cdot\text{m}^{-1}$
ω	Rotation velocity of fixture for folding (rps) ($= 2\pi\omega \text{ rad}\cdot\text{s}^{-1}$)
c_b	Thickness of 1st layer of paperboard /mm
μ_b	Friction coefficient between creasing rule and paperboard
μ_d	Friction coefficient between grooved plate (die) and paperboard
μ_t	Friction coefficient between paperboard and rubber fixtures
μ_{el}	Friction coefficient between each layer (interface layer) of scoring area
μ_c	Friction coefficient between paperboard and pin of load cell
L_{vb}	Length of the specimen for V-Block test /mm
W_{vb}	Width of the specimen for V-Block test /mm
L	Arm length of worksheet /mm

Nomenclature (Continued)

μ_{rd}	Friction coefficient between the deformable body and the upper-lower rigid body
μ_{ad}	Friction coefficient between the deformable body and the protector
μ_{vb}	Friction coefficient between the deformable body and V-Block fixtures

CHAPTER 1

INTRODUCTION

1.1 Introduction to creasing process

1.1.1 History of creasing process and its principle

Paper and paperboard are two common material used in almost all industries. They are highly recyclable and environment friendly materials, which results in a rapid utilization growth of these materials. However, the research works and relative fields of the mechanical properties of this popular and essential material are quite limited, especially the mechanism of paperboard converting. Paperboard die cutting, includes creasing, is wide spread in many fields such as foods, stationery packaging. Iggesund paperboard. (2014) proposed the conceptions for analysis of a paperboard have been published. In this article, the die-cutting and creasing operations were discussed. Gąsiorek. (2013) applied the Smoothed Particle Hydrodynamics (SPH) for the modeling of cutting composite bundles applying a guillotine. For the improvement of productivity or the development of quality on die cutting (Grebe, 1973; Hofer, 1994; Fellers et al., 1992) reported the evaluation of durability on die tools and the estimation of material properties on paperboard were clarified. Creasing is one of most essential mechanical behavior or processing technique for paperboard die cutting (Carey, 1992), due to the affected of the failure state in the folding process was based on the creasing stage. The die cutting and creasing process are widely applied for converting sheet materials in various industries, i.e. automobiles, electronic circuits, insulation and protective films, packaging, etc.

Moreover, the requirement of dimensional precision for cut products and creasing products and various shapes of cut parts and creasing parts, various types of the die cutting are developed and used such as folding, bending, printing, etc. **Fig. 1-1** shows some sheet material forming processes based on the principle of the creasing process.



Fig. 1-1 Examples of forming processes based on creasing principle.

The quality of the creasing product is affected not only by the material mechanical properties and creasing condition but also by other problems, caused by crushing or abrasion, folding failure in paperboard, delamination of paperboard. Therefore, the mechanical response of crease lines is introduced and verified on the basis of experimental tests (Giampieri et al., 2011). Creasing process is the process of using the creasing rule that is indented onto the paperboard. Creasing process can be done on either Flatbed or Rotary presses. One of the significant advantages of flatbed die creasing is tooling costs are kept to a minimum and its suitable for the complicated creasing pattern. The different combinations of materials are extremely suited to the process of flatbed die creasing. The flatbed dies creasing process, which is also referred to as shearing, indentation, creasing or pushing process, is illustrated in **Figure.1-2**.

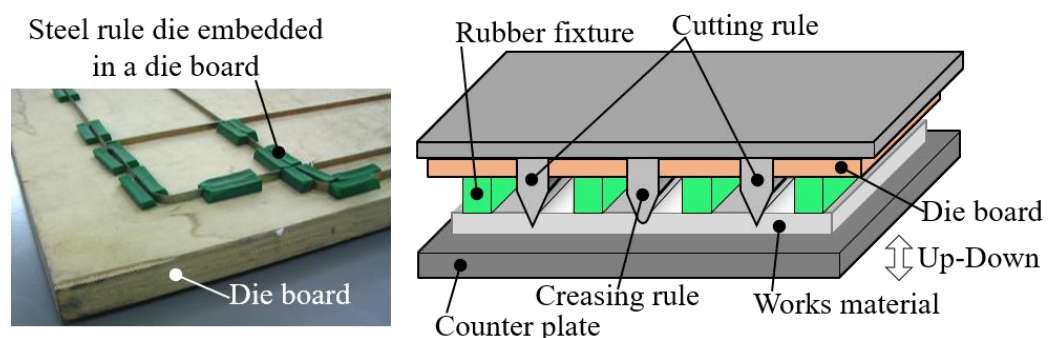


Fig.1-2 Flatbed die-cutting and creasing

A worksheet is pressed on a cutting plate by a rubber fixture and performed by a die designed patterns embedded in a die board. Die pattern will cut the work material sheet in a reciprocal up-down motion without any stopper. The final step in the creating

die involves the addition of ejection rubber. The rubber pads are adhered to the substrate to support eject the material after cutting. Die-cutting and creasing are faster and more stable than other methods. However, the tooling costs are cheap and the precision method for creasing the complicated pattern.

Sudo had studied the effect of detachment behavior on creasing deformation of the paperboard (Sudo et al., 2005). However, the detachment behavior on the creased paperboard are not sufficiently discussed from the aspect of the internal bonding strength model with the lamination structure. Thus, this thesis work intends to contribute to the effort of perception of the paperboard peeling mechanism. The experimental and finite element methods will be conducted. Li et al. (2018) reported the fracture behavior inclusive the fiber bridging offering by applying a potential based cohesive law. Gong et al. (2017) proposed the resistance (R)-curve and assumed fiber bridging tractions decreasing non-linearly concerning the crack opening displacement. Höwer et al. (2018) offered traction-separation law comprised a standard initial cohesive component, which estimated for the initial interfacial stiffness and energy release rate, along with a new constitutive to consider for the fiber bridging and contribution to the delamination process. For the explanation of large-scale failure process zones, Sørensen et al. (2003) applied the cohesive laws by the determination of the J integral and end-opening of the cohesive zone of double cantilever beam specimens loaded with pure bending moments. Borgqvist et al. (2016) showed the appearance of the limited bands for the in-plane strength in compression of paperboard in folding. By modification, the in-plane yield parameters to the short-span compression test (SCT).

Paperboard is a thick, single or multiple paper-based materials composed of fluffing structure. Wathén (2006) reported the Z-directional fiber strength is less sensitive to fiber degradation than axial fiber strength. The fiber properties have an essential influence on the fracture properties of paper.

Besides, the fluffing structure can apply to deep drawing process. Awais et al. (2017) reported on the effect of creases on the formability. Linvill et al. (2017) showed the hinge model had included wrinkle initiation. To observe the forming ability, the digital image correlation (DIC) can provide a vivid account of the buckling of box panels (Viguié et al., 2013).

In this research work, the paperboard comprises a pulp fiber structure matrix and a clay coated layer. The fiber layer consists of multiple plies (Reinhard et al., 2013). There are several problems in the forming process such as folding failure and delamination line in the converting processes. An example of a picture illustrating the paperboard structure for the delaminated line is shown in **Fig. 1-3** (it was copied from the original resource: Bhattacharya et al. (2016)).

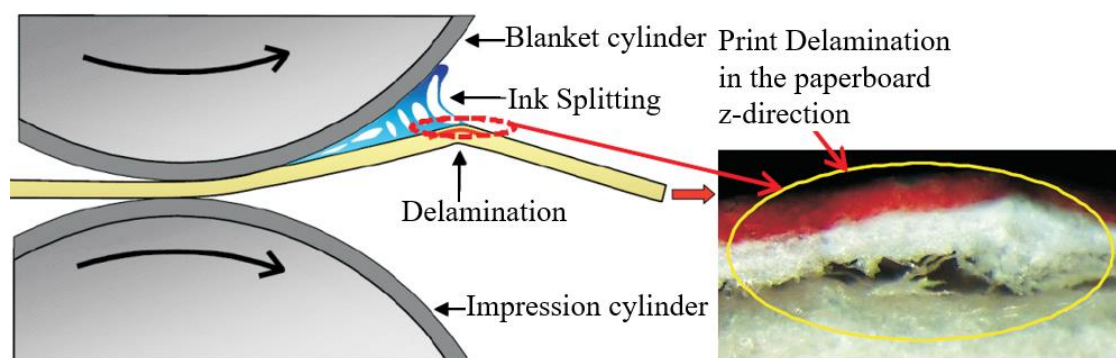


Fig. 1-3 Delamination of paperboard in offset printing process, (Bhattacharya et al. 2016).

1.2 Motivation and problem statement

Nowadays, the paperboard converting product become quite attractive materials for various applications, especially packaging product and printing industry. Laminated paperboard is a popularly used packaging material. Its use is expanding every year, mostly because it is almost 100% recyclable and inexpensive. Paperboard can be converted into packages by relatively forthright processes such as cutting, creasing, folding and glueing (Beex et al., 2009). However, a problem in paperboard converting is the folding failure during the forming process. Cracked folds provide product less appealing to consumers and also compromise their durability. The quality of folds and the possibility of cracking depend on the creasing stage. Namely, the creasing stage is essential for preventing the folding failure of paperboard, and the creased lines must be stably folded without any surface failures. In practice, both processes are improved

using experimental knowledge, but systematic studies of the mechanics supporting both processes especially cracking are rare. Beex et al. (2009) reported the upper plies under a high pressured state, are loaded in in-plane tension which may cause the top layer to break. The delamination mechanism is quite important to estimate the creasing deformation of white-coated paperboard or corrugated paperboard. Some researchers reported the importance of anisotropic elasticity of raw paper sheet and delamination behaviors were explained through FEM simulation models and experiments (Nagasawa et al., 2006, 2013). Sudo et al. (2005) described a feasibility study about the effect of inner detachment behavior on creasing deformation of a paperboard applying a distributed resistance model of nonlinear springs, which was explained in the MARC subroutine: USPRNG (MSC software, 2003, 2010a, 2010b); however, Sudo's model did not consider the shear resistance. In this work, therefore, a 0.45mm thickness white-coated paperboard was examined by varying the feed velocity. The in-plane tensile line force f_p was observed during the peeling process with respect to the peeling elongation h/t_p of the coated paperboard in order to investigate the feed velocity effect on the peeling load response. Numerical simulation and experimentation researches the deformation and cracking characteristics of a white-coated paperboard during the creasing process of a white-coated paperboard have been reported in recent years (Sudo et al., 2005). It was found that the breaking of the top layer is a frequent problem, especially for high grammage layers. Hence, the purpose of this study is to introduce the material models for layers and an internal bonding strength of paperboard, respectively. Additionally, the delamination and damage in the creasing and folding processes are also considered. In point of view, the investigations were carried out from both experimentation and numerical simulation. However, another research work did not discuss the effect of the peeling load resistance of a white-coated paperboard. Therefore, the detaching criteria of the in-plane layer are not yet revealed in general. In this study, an internal breaking criteria and transient de-lamination were discussed with a combination model comprising the fluffing normal resistance (derived from ZDTT) and the glue breaking resistance as the shear yielding stress (based on the in-plane shear test and the frictional shear sliding) for considering a couple of creasing and folding conditions. The FEM model was simulated base on the experimental observation that

was obtained using a load cell and a CCD camera tool. It was included the continuum model that was described as the physical behavior of white-coated paper. On the other hand, the delamination model was described the fluffing normal resistance (derived from ZDTT) and the breaking shear yielding stress (based on the in-plane shear test) between the interlayers of the paperboard.

Moreover, to get smart/preferable crease profiles of paperboard sheets is very difficult. Anyway, in order to promote the die cutting technology for the converting industry of paperboard sheet materials, the understanding of their cutting and creasing characteristics is crucial.

1.3 Objectives of research work

In this thesis work, the author aims to investigate the material properties and the forming properties of paperboard. There are several research works have been studied (Li et al., 2016; Östlund, 2017; McDonald et al., 2017). In this study, the detaching resistance of a white-coated paperboard was studied and investigated. The main objectives of the research works are followings.

- (i) To describe an in-plane detaching resistance of a white-coated paperboard subjected to a peeling deformation.
- (ii) To develop a numerical simulation model of the folding process of a creased paperboard and to reveal the deformation characteristics of the creased paperboard.
- (iii) To reveal the deformation behavior under the compressive load using V-Block fixtures.

1.4 Scope of research work

In this research work, the material objects were considered: a 0.45 mm thickness, basis weight 350 g·m⁻² of a white-coated paperboard. The white-coated paperboard was investigated based on the uni-axial tensile test of specimens. The peeling test was investigated in the machine direction (MD). The *T*-peel test was applied for mechanical investigation of the peel behavior according to ASTM-D1876-01 (2001), (Pugno and Abdalrahman, 2012). The word “*T*-peel” in this research, it means that indicates the

existence of one peel arm, which is bent by 90°. Deformation behaviors of the worksheets and their peeling load resistance which were recorded by a CCD camera and a load cell were main peeling results used for discussing about effects of peeling conditions of the worksheet's peeling characteristics.

In addition, the peeling problems of a white-coated paperboard were numerically studied by finite element method (FEM) analysis. All simulations were carried out under the assumptions of two-dimensional (plane-strain) condition. The worksheets were assumed to be the isotropic elasticity properties. The large-strain analysis method was considered with the updated Lagrange procedure for all of the simulations. Both processes in FEM simulation and experiment have been taken in to account in studying with the folding mechanics of paperboard. In order to characterize the delamination and bulging deformation, an internal breaking criteria was numerically analyzed using a new combination model. A general purpose finite element code was applied to develop a combination model, which comprises the out-of-plane fluffing subroutine and the in-plane shear glue strength.

1.5 Organization of treatise

This treatise consists of five chapters. In each chapter, main contents are constructed as follows:

Chapter 1, *General introduction*, this chapter describes general of die cutting such as its history, principle and advantages. The author also explains the motivation and problem statement for this research work. The objectives and scope of the research are clarified.

Chapter 2, *Estimation of detaching resistance of a peeled in-plane layer of a white-coated paperboard using fluffing resistance model*. The author describes the necessity of the detaching resistance of a white-coated paperboard that is subjected to a peeling deformation. Experimental backgrounds of forming processes of packaging containers subjected to the peeling strength of paperboard. The simulated peeling load response and deformation of the worksheet when applying a fluffing model are presented and discussed.

Chapter 3, *Analysis of the folding process of creased paperboard using a combined fluffing resistance and shear yield glue model*. In this chapter, the experimental results of bending moment resistance concerning the scoring depth are clarified. The development and verification of a combined fluffing resistance and shear yield glue model for the folding simulation are illustrated. By using the proposed method, shear glue strength and fluffing normal strength with respect to the folding deformation of the creased paperboard are discussed.

Chapter 4, *Analysis of folding process of creased paperboard subjected to in-plane compressive load using the combination model*. In this chapter, the author aims to reveal deformation behavior under the compressive load using V-Block fixtures. In this investigation, the applicability of the in-plane tensile properties was applied to an in-plane compressive load test of a creased white-coated paperboard through the FEM simulation. The applicability of the shear glue strength and fluffing normal strength were conducted. For these studies, an FEM analysis was performed to simulate the compressive load using V-Block fixtures. For the comparison, the simulated and experimented folding deformation of the creased part of paperboard was discussed and their relationships were explained.

Chapter 5, *Conclusions*, the author wrote this chapter to summarize essential supplements disclosed in this thesis work. Recommendations for future works were also explained.

References

- American Society for Testing and Materials (ASTM), Standard Test Method for Peel Resistance of Adhesives (*T*-peel test), D1876-01, (2001), pp.1–3
- Awais, M., Sorvari, J., Tanninen, P. and Leppänen, T., Finite element analysis of the press forming process, *International Journal of Mechanical Sciences*, Vol.131–132, (2017), pp.767–775.
- Beex, L. A. A. and Peerlings, R. H. J., An experimental and computational study of laminated paperboard creasing and folding, *International Journal of Solids and Structures*, Vol.46, (2009), pp.4192–4207.
- Bhattacharya, A., Kumar, P., Debarde, S. and Chandrasekhar, Y., Engineered Paperboards for Boosting Packaging Performance, *Quarterly Journal of Indian Pulp and Paper Technical Association*, Vol.28(4), (2016), pp.2.
- Borgqvist, E., Wallin, M., Tryding, J., Ristinmaa, M. and Tudisco, E., Localized Deformation in Compression and Folding of Paperboard, *Packaging Technology and Science*, Vol.29(7), (2016), pp.397–414.
- Carey B.K., *Packaging Productivity*, Vol.1-1, (1992), pp.16–21.
- Christer Fellers., Sören Östlund. and Petri Mäkelä., Evaluation of the Scott bond test method, *Nordic Pulp and Paper Research Journal, Paper Physics*, Vol. 27, No.2, (2012), pp.231–236.
- Fellers, C., Fredlund M. and Wagberg, P., *Tappi Journal*, Vol.4, (1992), pp.103-109.
- Gašiorek, D., The application of the smoothed particle hydrodynamics (SPH) method and the experimental verification of cutting of sheet metal bundles using a guillotine, *Journal of Theoretical and Applied Mechanics*, Vol.51(4), (2013), pp.1053–1065.
- Giampieri, A., Perego, U. and Borsari, R., A constitutive model for the mechanical response of the folding of creased paperboard, *International Journal of Solids and Structures*, Vol.48, (2011), pp.2275–2287.
- Gong, Y., Zhao, L., Zhang, J., Wang, Y. and Hu, N., Delamination propagation criterion including the effect of fiber bridging for mixed-mode I/II delamination in CFRP multidirectional laminates, *Composites Science and Technology*, Vol.151, pp.302–309.

- Grebe, W., Hofer, H., *Allgemeine Papier-Rundschau*, Vol.9, (1973), pp.292–300.
- Hofer, H., Wurth, V., *Papier+Kunststoff Verarbeiter*, Vol.10, (1994), pp.33–38.
- Höwer, D., Lerch, B., Bednarczyk, B., Pineda, E., Reese, S. and Simon, J., Cohesive zone modeling for mode I facesheet to core delamination of sandwich panels accounting for fiber bridging, *Composite Structures*, Vol.183(1), (2018), pp.568–581.
- Iggesund paperboard., *Die-cutting and creasing, Reference Manual*, (2014), pp.174–185
- Koubaa, A. and Koran, Z., Measure of the internal bond strength of paper/board, *Tappi Journal*, Vol.78, No.3 (1995), pp.103–111.
- Linville, E., Wallmeier, M. and Östlund, S., A constitutive model for paperboard including wrinkle prediction and post-wrinkle behavior applied to deep drawing. *International Journal of Solids and Structures*, Vol. 117, (2017), pp.143–158.
- Li, Y., Edward, S., Reese, S. and Simon, J., Anisotropic elastic-plastic deformation of paper : In-plane model, *International Journal of Solids and Structures*, Vol.100-101, (2016), pp.286–296.
- Li, Y., Reese, S. and Simon, J.W., Modeling the fiber bridging effect in cracked wood and paperboard using a cohesive zone model, *Engineering Fracture Mechanics*, Vol.196, (2018), pp.83–97.
- McDonald, J.D. and Kerekes, R.J., Pragmatic mathematical models of wet pressing in papermaking, *BioResources*, Vol.12(4), (2017), pp.9520–9537.
- MSC Software, *Marc document: Theory and User Information*, Vol. A, (2010a), pp.567–568, 655.
- MSC Software, *Marc document: User Subroutines and Special Routines*, Vol.D, (2010b), pp.265–267.
- Nicola M, Pugno. And Tamer Abdalrahman., *Peeling Experiments of Double Side Adhesive Tapes Suggests the Feasibility of Graphene Nanocomposites with Gigantic Toughness*, *Nanoscience and Nanotechnology Letters*, Copyright © 2012 American Scientific Publishers, Vol. 4, (2012), pp.1–4

- Östlund, S., Three-Dimensional Deformation and Damage Mechanisms in Forming of Advanced Structures in Paper, The 16th Pulp and Paper Fundamental Research Symposium, (2017), pp.1–86.
- Pugno, N. and Abdalrahman, T., Peeling Experiments of Double Side Adhesive Tapes Suggests the Feasibility of Graphene Nanocomposites with Gigantic Toughness, Nanoscience and Nanotechnology Letters, Vol.4, (2012), pp.1–4, American Scientific Publishers.
- Scandinavian Pulp, Paper and Board Testing Committee., Z-directional tensile strength, SCAN-P 80:98, (1998) pp.1–3.
- Nagasawa, S., Yamagata, D., Fukuzawa, Y. and Murayama, M., Stress analysis of wedged rupture in surface layer of coated paperboard, Journal of Materials Processing Technology, Elsevier Science, Vol. 178, (2006), pp.358–363.
- Nagasawa, S., KOMIYAMA, Y., MITSOMWANG, P., Finite Element Analysis of Corrugated Board on Rotary Creasing Process, Journal of Advanced Mechanical Design, Systems and Manufacturing, Vol. 7, No.2, (2013), pp.103–114.
- Reinhard, S., Werner, A., Werner, K. and Martin, T., Chapter 17 Surface Sizing and Coating, Handbook of paper and board (ed., Holik, H.), Vol.2, (2013), pp.747–772, WILEY-VCH Verlag and KGaA, Weinheim.
- Sørensen, B.F. and Jacobsen, T.K., Determination of cohesive laws by the J integral approach, Engineering Fracture Mechanics, Vol.70(14), (2003), pp.1841–1858.
- Stenberg, N., Fellers, C. and Östlund, S., Measuring the stress-strain of paperboard in the thickness direction, Journal of Pulp and paper science, Vol.27, (2001), pp.213–221.
- Sudo, A., Nagasawa, S., Fukuzawa, Y. and Katayama, I., Analysis of exfoliation of laminated layers and creasing deformation of paperboard, Proceedings of The Hokuriku-Shinetsu District Annual Conference of Japan Society of Mechanical Engineers, No.047-1, (2005), pp.35–36 (in Japanese), DOI: 10.1299/jsmehs.2005.42.35.
- Viguié, J. and Dumont, P.J.J., Analytical post-buckling model of corrugated board panels using digital image correlation measurements, Composite Structures, Vol. 101, (2013), pp.243–254.

Wathén, R., Studies on fiber strength and its effect on paper properties. KCL re-inventing paper, (2006), pp.1–98.

CHAPTER 2

ESTIMATION OF DETACHING RESISTANCE OF A PEELED IN-PLANE LAYER OF A WHITE-COATED PAPERBOARD USING FLUFFING RESISTANCE MODEL

2.1 Introduction

As mentioned in chapter 1, When making a packaging box of a paperboard, a creasing process, which is composed of the first stage: scoring by a creasing knife and the second stage: folding, is widely used (Kirwan, 2013). Since the delamination occurs during the folding process of scored paperboard, a reasonable estimation of bending mechanism of a folded part under delaminating is necessary for performing a stable and smart folding and designing a suitable strength of inner delamination of paperboard. The delamination behavior is not only an essential feature of crease folding but also a primary factor of failure modes when tearing or shearing a laminated material. Regarding the estimation of detaching resistance, the peel cohesion test (PCT) or T-peel test (Koubaa, 1995; ASTM-D1876-01, 2001; Fellers et al., 2012; Pungo et al., 2012) and the z-directional (out-of-plane) tensile test (ZDTT) (Scandinavian Pulp, Paper and Board Testing Committee-SCAN-P 1998) are well used for measuring the bonding strength of the delamination layer of paperboard and the bonding strength of peeled metallic foil stacked on adhesive mat.

There are several reports for estimating the anisotropic properties of paperboard and the delamination-based folding resistance in a crease making process. Material properties of a thickness direction was analyzed by several researchers (e.g., Stenberg, et al., 2001). Thakker et al. (2008) reported the nonlinear local buckling of folded raw sheet of corrugated fiberboard, using the orthotropic elasto-plasticity. Nagasawa et al. (2006) reported about the orthotropic elasticity of paperboard during a wedge cutting process, and the surface breaking behaviors was explained through FEM simulation and experiments. Sudo et al. (2005) showed a feasibility study about the effect of inner detachment behavior on creasing deformation of the paperboard using a distributed

resistance model of nonlinear springs, which was described in the MARC subroutine: USPRNG (MSC software, 2003, 2010), although Sudo's model was not considered with the shear resistance. The ink-tack delamination of a paperboard that comprised softly connected plies was investigated (Hallbäck et al., 2006) for assessing the effect of elastic moduli of each layer on the ink-tack delamination event. In order to simulate the delamination and folding resistance of creased paperboard, a cohesive damage model was considered for explaining the bulging of a creased part (Beex and Peerlings, 2009). Gong et al. (2017) proposed the resistance (R)-curve and assumes fiber bridging tractions decreasing non-linearly concerning the crack opening displacement. Höwer et al. (2018) offered traction-separation law comprises a standard initial cohesive component, which estimates for the initial interfacial stiffness and energy release rate, along with a new constitutive to consider for the fiber bridging contribution to the delamination process. Li et al. (2018) described the fracture behavior inclusive the fiber bridging offering by applying a potential based cohesive law. Sørensen et al. (2003) used the cohesive laws for explaining large-scale failure process zones, by the determination of the J integral and end-opening of the cohesive zone of double cantilever beam specimens loaded with pure bending moments. The cohesive damage model seems to be convenient for adjusting the shear slide and normal detaching in a delaminated layer, but it is not based on the real fluffing behavior. Wathén (2006) explained the Z-directional fiber strength is less sensitive to fiber degradation than axial fiber strength. The fiber properties have an essential influence on the fracture properties of paper. In this work, a white-coated paperboard was chosen for examining the PCT and ZDTT. In the PCT, the in-plane pulling (tensile) line force and the corresponding z-directional elongation of the upper layer peeled from the paperboard was observed during the peeling process to investigate the fluffing detachment of the weak-bonded layer as shown in **Fig. 2-1**. To develop a simplified mechanical model of detaching resistance of weak-bonded in-plane layer of a paperboard, an FEM model has been utilized with the MARC user's subroutine USPRNG, which comprises anaphase yielding resistance derived from the z-direction tensile test in the FEM simulation. In this study, this model was known as the fluffing model, which was composed of distributed nonlinear spring joints. The fluffing model based on experimental data of ZDTT is our original method for solving an in-plane detaching behavior of multiple

plies. The fluffing-based peeling model has been discussed for characterizing the experimental features.

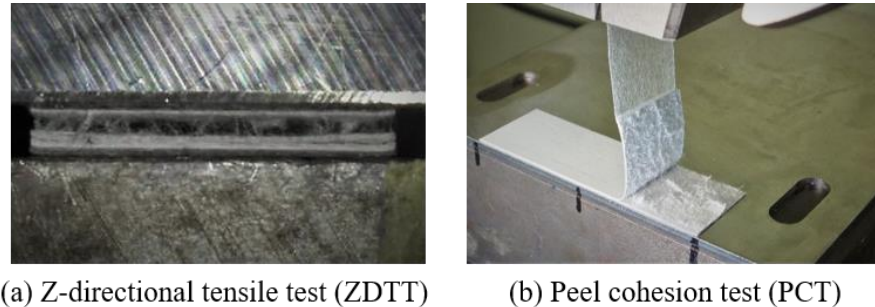


Fig. 2-1 Example of z-directional (out-of-plane) tensile test and peel cohesion test of paperboard.

2.2 Analysis condition and preliminary investigation

2.2.1 Specimens

For a peeling experiment, a commercially recycled white-coated paperboard that had a thickness $t = 0.45$ mm and nominal basis weight of $350 \text{ g}\cdot\text{m}^{-2}$ was chosen. Its fiber and pulp analysis was summarized in **Table 2-1**, while the in-plane tensile properties of the paperboard in the making machine direction (MD) were shown in **Table 2-2**. **Figure 2-2** shows an example of in-plane tensile stress–strain diagram of the paperboard.

Table 2-1 Size of fiber and pulp combination ratio of white-coated paperboard 350 (measured by Kajaani-FS300) L-BKP. Broad-leaved lumber (hard wood), bleaching kraft pulp; N-BKP: Needle-leaved lumber (soft wood), bleaching kraft pulp; NTMP: Needle-leaved, thermal mechanical pulp; L(n): based on number of fibers in each fibrillation index class; L(l): based on length weighted number of fibers in each fibrillation index class; L(w): based on weight-weighted number of fibers in each fibrillation index class; CWT: Wall thickness of cell; Width: average width of fiber.

Unit	Pulp combination ratio/%			Projected length of fiber/mm			Size/ μm		Section area/ μm^2
	L-BKP	N-BKP	N-TMP	L(n)	L(l)	L(w)	Width	CWT	CSA
Value	64.7	16.0	19.3	0.56	0.99	1.52	18.2	4.8	256.6

Table 2-2 In-plane tensile properties of a white-coated paperboard in MD. The tensile feed velocity was $0.33 \text{ mm}\cdot\text{s}^{-1}$ (strain rate: 0.00183 s^{-1}). The tensile procedure was based on JIS-P8113. The average (maximum–minimum) of ten samples was shown.

	Young's modulus E/MPa	Yield strength σ_Y/MPa	Tensile strength σ_B/MPa	Breaking strain ε_B
MD	5220 (4900–5490)	28.5 (27.7–29.2)	42.5 (40–43.73)	0.021 (0.018–0.023)

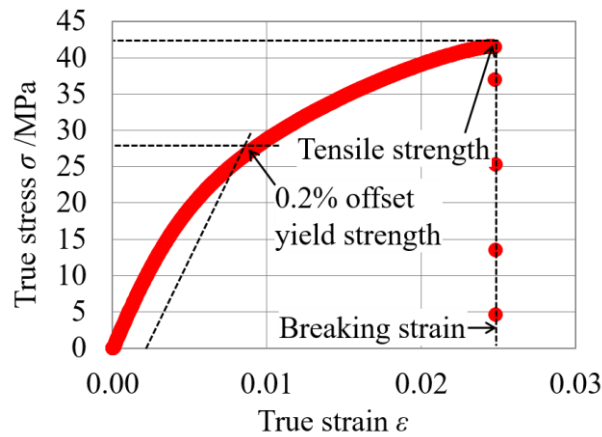


Fig. 2-2 In-plane tensile stress–strain diagram (feed velocity $V = 0.33 \text{ mm}\cdot\text{s}^{-1}$).

2.2.2 Estimation of elastic properties for compressive strength by ring crush test

Although some articles for deformation analysis of a paperboard or corrugated board using the orthotropic elastic model have been published (Nagasawa et al., 2006, 2013a, 2013b; Komiyama et al., 2013), a large deformation of orthotropic elastic model is generally unstable for numerical simulation. In this work, since the peeling resistance in the weak-bonded layer was macroscopically discussed with the pull-up force and the curvature of peeled layer, the peeled-off layer was assumed to be equivalently isotropic elastic, and the corresponded Young's modulus was investigated for developing an FEM model. This equivalent Young's modulus was examined using several evaluation tests: the in-plane tensile test (as shown in **Table 2-2**), an in-plane ring crush test (JIS-P8126, 2005), and an out-of-plane three points bending test (ASTM-D790-2, 2002).

According to our preliminary investigation, the Young's modulus value of 5220 MPa (MD) was fairly large (high stiffness) to estimate the bending deflection behavior of a peeled thin layer. It was obvious because the real behavior was based on a sort of

orthotropic elasticity, and the thickness direction must have a small value of that. The authors examined a few cases of the out-of-plane three points bending test (based on ASTM-D790-2, 2002), and they observed that the equivalent Young's modulus of the out-of-plane three points bending test was smaller than that of the in-plane tensile test. However, the result of the three points bending method seems to be difficult to detect a value of equivalent Young's modulus without discussing the mechanical condition of bending tool. Among those two evaluation methods (in-plane tensile and out-of-plane three points bending), the in-plane ring crush test seems to be stable and well-known in the packaging industry for detecting the value of the equivalent Young's modulus. Therefore, the ring crush test (JIS-P8126, 2005) was conducted for detecting the equivalent MD elastic modulus E_{RC} .

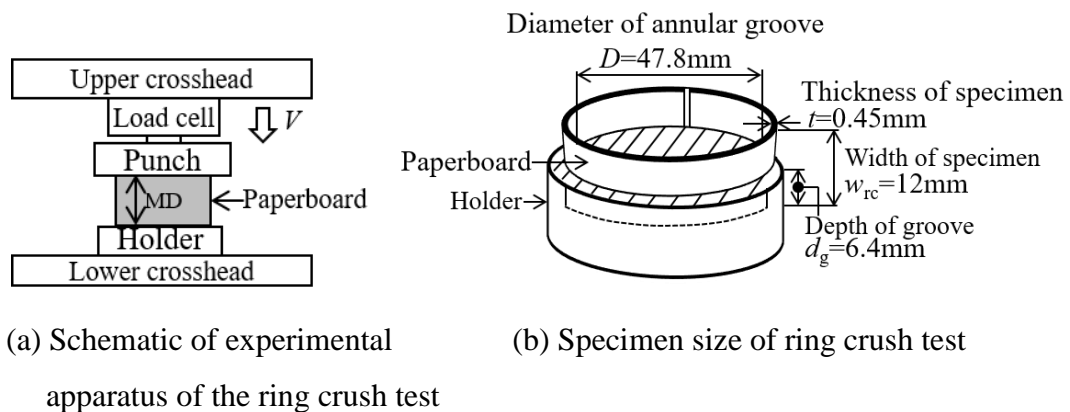


Fig. 2-3 Schematic diagram and specimen size of the ring crush test.

Figure 2-3 (a) and **(b)** shows the schematic diagram and specimen size of the ring crush test. The specimen holder was a circular annular groove with a fixed outside diameter of 47.8 mm. The depth of this groove was 6.4 mm. The bottom of the groove was flat, and its walls were perpendicular to the bottom. The width and length of the specimen were 12 mm and 150 mm, respectively. The velocity of the ring crush test was chosen as $0.1 \text{ mm}\cdot\text{s}^{-1}$. The specimens were prepared 10 pieces. **Figure 2-4** shows the experimental result of the ring crush test. The equivalent Young's modulus was estimated as $E_{RC} = 533 \text{ MPa}$ from the in-plane MD ring crush test.

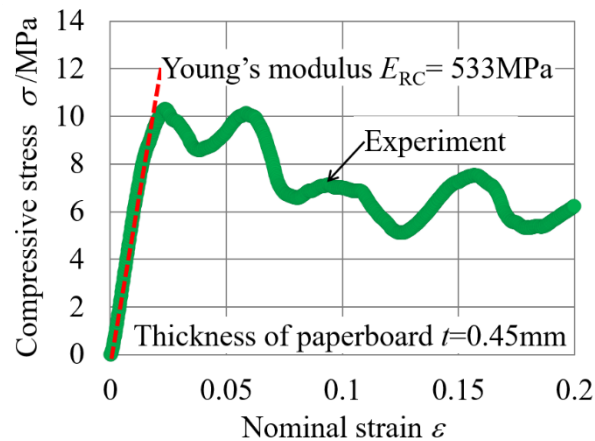
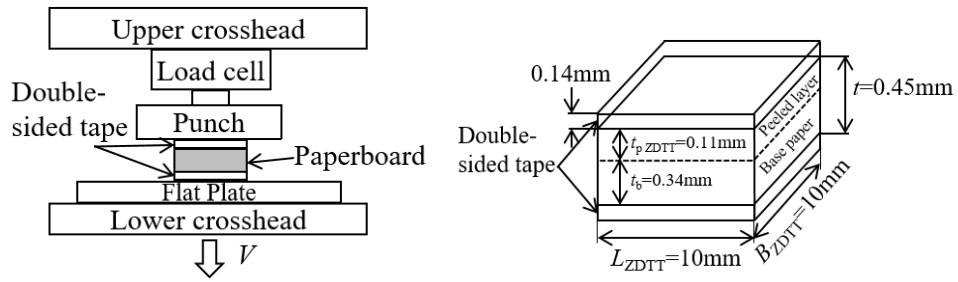


Fig. 2-4 Relationship between compressive stress and nominal strain of the ring crush test.

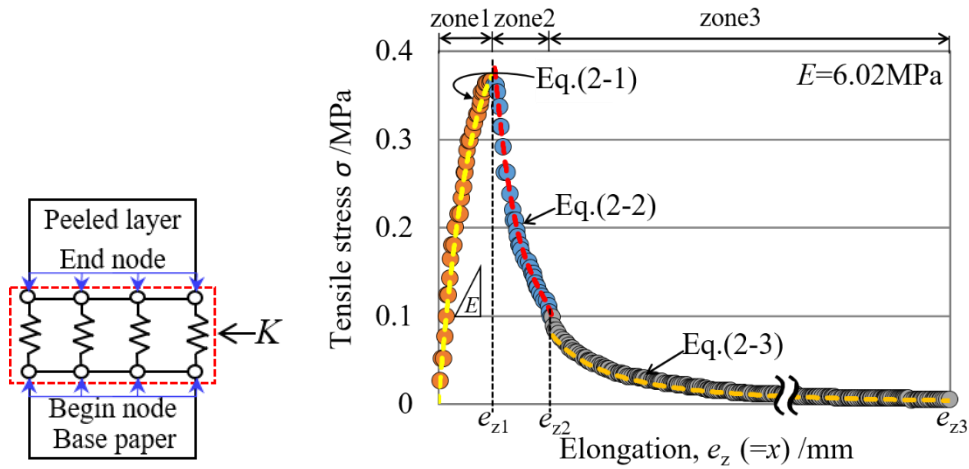
2.2.3 Anaphase yield resistance model based on ZDTT

The ZDTT model is used for explaining the detaching behavior of a fibrous-wire-(fluffing)-based resistance of a white-coated paperboard to determine the z-direction (thickness direction) tensile strength of a paperboard (Koubaa, Scandinavian Pulp, Paper and Board Testing Committee-SCAN-P, Stenberg, Fellers, et al., 1995, 1998, 2001, 2012). **Figure 2-5** shows the relationship between tensile stress and elongation in the thickness direction. **Figure 2-5 (a)** shows the schematic of the experimental apparatus of ZDTT. An acrylic-based double-sided adhesive tape NWK-15S was inserted beneath the lower worksheet and upper the worksheet for stacking on the lower crosshead. The velocity in the experiment of ZDTT was chosen as $0.1 \text{ mm}\cdot\text{s}^{-1}$. **Figure 2-5 (b)** shows the specimen size of the ZDTT test. The specimens were prepared 10 pieces as a square sheet with a length of $L_{\text{ZDTT}} = 10 \text{ mm}$, a width of $B_{\text{ZDTT}} = 10 \text{ mm}$, and the thickness of 0.45 mm . **Figure 2-5 (c)** show the lower surface of peeled layer and the upper surface of base paper. Here, the interface was joined by the proposed fluffing non-linear springs.



(a) Schematic of experimental apparatus of ZDTT

(b) Specimen size



(c) Fiber bridging between the lower surface of the peeled layer and the upper surface of base paper

(d) Tensile stress response diagram of ZDTT ($t = 0.45$)

Fig. 2-5 Relationship between tensile stress and elongation in the thickness direction.

Figure 2-5 (d) shows the tensile stress response diagram of the ZDTT and shows the fitting state between the experimental data and approximation curves. Here the elongation e_z was subdivided into three zones: zone1, zone2 and zone3 as shown in **Fig. 2-5 (d)**. The tensile stress σ was approximated with e_z by using Eq. (2-1), (2-2), and (2-3), respectively. Equation (2-1) and (2-2) were approximated by the third order polynomial expressions, and Eq. (2-3) was approximated by the power law. Comparing the Young's modulus based on the in-plane tensile test properties $E_{(\text{in-plane})}$ and the Young's modulus that was derived by **Fig. 2-5 (d)** in the thickness direction $E_{(\text{ZDTT})}$, they were fairly different with each other. $E_{(\text{in-plane})}$ was about 100% larger than that of $E_{(\text{ZDTT})}$. However, in the ZDTT mode, since the detached layer was kept in a plane (flat), the isotropic material model is assumed in the ZDTT model.

$$\sigma = a_1 e_z^3 + a_2 e_z^2 + a_3 e_z + a_4 \quad (0 < e_z < e_{z1}) \quad (2-1)$$

$$\sigma = b_1 e_z^3 + b_2 e_z^2 + b_3 e_z + b_4 \quad (e_{z1} < e_z < e_{z2}) \quad (2-2)$$

$$\sigma = c_1 e_z^2 \quad (e_{z2} < e_z < e_{z3}) \quad (2-3)$$

Table 2-3 shows the coefficient values of Eq. (2-1), (2-2), and (2-3). The generated thickness of a weak-bonded layer was estimated as t_p ZDTT = 0.11 (0.10–0.11) mm.

Table 2-3 Stiffness coefficient values of Eq. (2-1), (2-2), and (2-3).

e_{z1}	0.0835	e_{z2}	0.178	e_{z3}	2.192		
a_1	14.1	a_2	-5.35	a_3	0.71	a_4	0.0006
b_1	-0.56	b_2	0.27	b_3	-0.04	b_4	0.003
c_1	0.0015	c_2	-1.04				

The first zone of $0 < e_z < e_{z1}$ shows the elastic or elasto-plastic behavior before breaking at the weak-bonded layer. The zone of the second and third periods of $e_{z1} < e_z < e_{z3}$ is a sort of anaphase yielding behavior that is caused by the fluffing resistance of delamination.

The tensile stress σ is described with the detaching distance of e_z as in Eq.(2-1)–(2-3), and this seems to be caused by fluffing or drawing phenomena of fibers. Therefore, the anaphase yielding resistance of ZDTT is applied to the resistance of the detaching layer during PCT, when the detached distance of corresponded two nodes is considered in two-dimensional freedom. This fluffing model can be described using a user defined subroutine of USPRNG (MSC software, 2010). In this user defined subroutine, the bonding line force $f = \sigma L_{ZDTT}$ is defined by the stiffness K and the distance U between the first end and second end of the nonlinear spring, as shown in Eq.(2-4).

$$\sigma = (K \cdot L_{ZDTT}^{-1}) \cdot U \quad (2-4)$$

In the implementation of user defined subroutine, Eq. (2-4) was replaced to Eq.(2-1)–(2-3) using $e_z = U$. When $U > e_{z3}$, the nonlinear spring force is defined as zero. Namely, this is the breaking criteria which is based on ZDTT model.

2.2.4 Method of Peel Cohesion Test (T-peel test)

T-peel test was applied for the mechanical investigation of the peel behavior according to ASTM-D1876-01 (2001), (Pugno and Abdalrahman, 2012). The word “T-peel” means that the one peel arm is bent by 90° . **Figure 2-6** shows a schematic of the experimental apparatus and specimen configuration. The coated layer of the worksheet was set as the upper side. The starting position of the peeling process was shown in **Fig 2-6**. To keep the attitude of the pull-up tape in the vertical, the linear positioning stage was moved in the horizontal with the same feed velocity as the vertical pull-up velocity. **Figure 2-7** shows the profile parameters of the peeling process. Specimens were prepared as a rectangle sheet with a length $L_{PCT} = 50$ mm and a width $B_{PCT} = 15$ mm in the MD.

An acrylic based double-sided adhesive tape NWK-15S with a length of 50 mm and a width of 15 mm were inserted beneath the worksheet for stacking on the lower crosshead, while another double-sided adhesive tape with a length of 45 mm and a width of 15 mm was set up as shown in **Fig. 2-7**. Here the adhesive tape was bent by 90° with an attached length of 15 mm. The initial distance between the clamp and the specimen was 20 mm. The adhesive tape NWK-15S had a thickness of 0.14 mm. A load cell with the maximum load 10 kN was used in **Fig. 2-6**. Each specimen placed on the double-sided tape stacked on the counter plate which was fixed on the lower crosshead. The double-sided tape was fixed on the upper crosshead, which moved upward with a velocity of $V = 0.1, 0.25, 0.5,$ and $1.0 \text{ mm}\cdot\text{s}^{-1}$. The pull-up vertical displacement h was equal to the horizontal displacement of linear positioning stage.

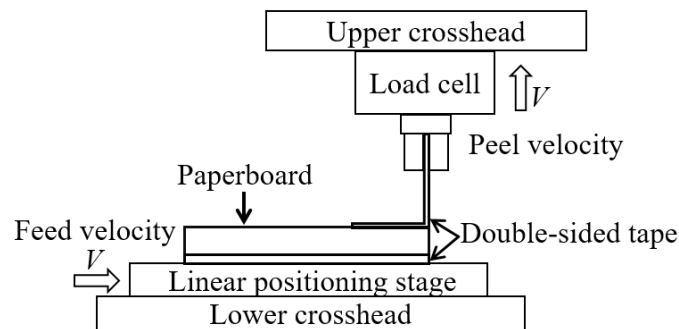


Fig. 2-6 Schematic of experimental apparatus.

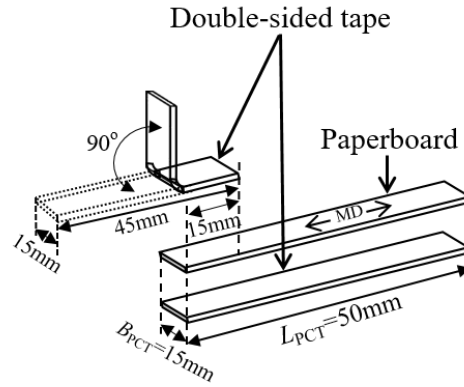


Fig. 2-7 Profile parameters on peeling process.

The line force $f (=F/b)$, the height of end part of peeled layer h , the inclined angle α_r , the cracked length L , and the coordinates of three points (a)(b)(c) were recorded with respect to the elapsed time for each feed velocity V , as shown in **Fig.2-8** and **Fig.2-9**.

Figure 2-8 shows an early stage when $\alpha_r \ll 90^\circ$ and $h/t_p < 10$, while **Fig. 2-9** shows a peeling deformation profile under the stationary stage when $\alpha_r \approx 90^\circ$. The curvature radius r_p were approximately calculated from the three points (a), (b), and (c), as defined in **Fig. 2-8** and **Fig. 2-9**. As mentioned below in the experimental result of PCT, the thickness of weak-bonded peeled layer t_p was about 0.11 mm when it was measured by a mechanical micrometer. This thickness was almost equal to that of ZDTT. Before the peeling test, the paperboard specimens were kept at a temperature of 296 ± 1 K and a relative humidity of $50 \pm 1\%$ in a controlled room for 24 h. The peeling test was conducted in the same room. Measurements were performed ten times for each case.

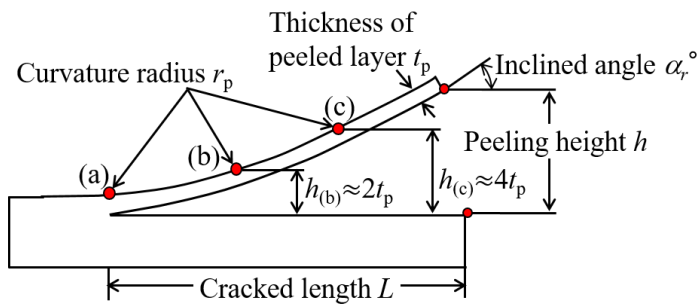


Fig. 2-8 Schematic diagram of early stage of peeling profile when $\alpha_r \ll 90^\circ$ and $h < 10t_p$.

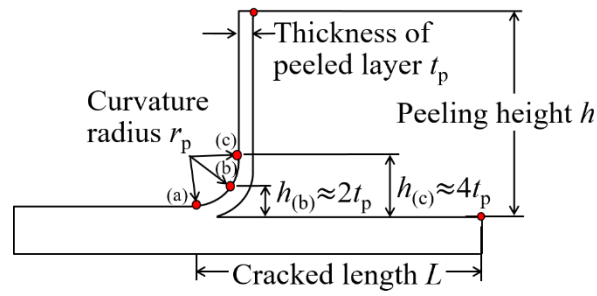


Fig. 2-9 Schematic diagram of peeling profile for stationary stage when $\alpha_f \approx 90^\circ$.

2.2.5 FEM model for PCT

The purpose of the numerical model is to explain the experimental observations described in the previous section and to predict the behavior of peeling mechanism at the early stage and/or stationary stage of a white-coated paperboard. An isotropic elastic behavior of deflection of a peeled layer and base paper were assumed. A general purpose finite element code, MSC.MARC 2012.1.0, was employed for simulating the peeling process. The updated Lagrange procedure and a large strain analysis were used. The thickness of the worksheet was $t = 0.45$ mm. Seeing the experiment of PCT, since the position (thickness) of weak-bonded layer was stably a certain constant, the peeled worksheet was modeled as a combination of a peeled layer with a thickness of $t_p = 0.11$ mm and a base paperboard with a thickness of $t_b = 0.34$ mm ($=t-t_p$).

The contact boundary of those two deformable objects (peeled layer and base paperboard) is assumed to be the same as the fluffing model, which was derived from ZDTT, for accounting the opening behavior of the peeled layer. Therefore, the user defined subroutine USPRNG that describes the detaching resistance of ZDTT with Eq.(2-1), (2-2), and (2-3) was adopted. A two-dimensional model was constructed in a full-length worksheet of $L_{PCT} = 50$ mm, as shown in **Fig. 2-10**. The number of divided elements of the worksheet was 8000, while that of total nodes was 10010. The four-node plane strain quadrilateral element type was adopted. The peeled layer and base paper were assumed to be elastically deformable, the lower side of base paperboard was fixed on a rigid counter plate, and the middle point of the right side of the peeled layer (a gripped node on the right side) was pulled up in the vertical direction.

As for the material properties of peeled surface layer, three kinds of testing data was measured and tried to apply to the peeling deformation of the thin surface layer as the isotropic elastic body. Here, the tree was 1) In-plane tensile test, 2) 3 point bending test, and 3) Ring crush test (in-plane compressive test) were compared. As the result, we concluded that the equivalent Young's modulus of 3 point test was naturally usable for simulating the bending and pulling in the peeling test. However, to measure the equivalent Young's modulus was unstable when changing the beam span and folded angle, whereas to measure the ring crush elastic modulus was stable and also its Young's modulus was fairly close to that of 3 point bending test. Therefore, as one of development technique, to use the ring crush test based Young's modulus for peeling test was proposed through the research. The in-plane tensile test based simulation of peeling was far different from other cases (3 point bending and ring crush test based simulation of peeling). The Young's modulus of the peeled layer and base paper were mainly assumed to be 533 MPa (derived from the ring crushed test) and the poisson's ratio was $\nu = 0.2$ (referred from Baum et al., 1981), except for the gripper jointed area which had the length $L_{ip} = 2.67$ mm (equal to the initial in-plane crack based on the experimental observation), as shown in **Fig. 2-10**.

According to a preliminary experiment of the adhesive tape NWK-15S, the in-plane tensile test (based on JIS-P8113) had the Young's modulus of $E = 350$ (337–362) MPa, while the out-of-plane tensile test (based on ZDTT) had the Young's modulus of $E = 1.13$ (0.93–1.31) MPa. Although the material property of adhesive tape is really anisotropic, an equivalent Young's modulus must be identified as an isotropic model. Thus, the behavior of the peeling mode was investigated by varying the value of the Young's modulus in the range of 1.13–350 MPa. In this work, a value of $E = 200$ MPa was assumed for matching to the experiment.

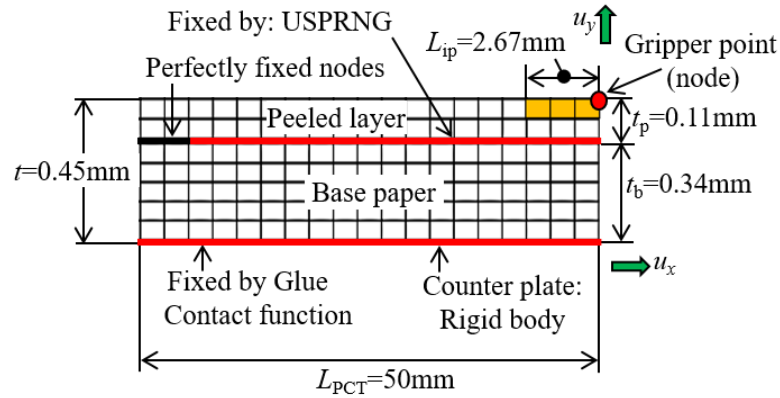


Fig. 2-10 Size definition and boundary condition of FEM model with the initial profile of worksheet for PCT. The bonding restriction on the specified peeled layer was modeled by the user defined subroutine USPRNG using the anaphase yielding criteria of Eq. (2-1), (2-2), and (2-3).

In the developed simulation model, the glue constraint was initially detached on the weak bonded layer, while the upper surface of base material and the lower surface of peeled layer (0.11 mm) was joined by the proposed fluffing non-linear springs. Here, the rest of non-peeled zone was defined as an uniform solid body without any cracking. Namely, as for the in-plane shearing, the shearing stability was considered by the uniform non-cracked body, and the cracking (peeling) resistance was completely determined by the normal resistance of fluffing non-linear springs. To protect any tangential slip between the peeled layer and base paperboard during a simulation process, the left side of the peeled layer was fixed for a certain range (10% of L_{PCT}) in both the horizontal and vertical directions. The peeling direction was chosen as parallel to the MD of worksheet. In addition, by seeing the fibrous-wire-based resistance, the nonlinear spring model was proposed by using the user defined subroutine USPRNG. The breaking criterion was considered with an anaphase yield resistance based on ZDTT. Here Eq. (2-1) was used in an elastic region, Eq. (2-2) was used for a detaching behavior between the peeled layer and base paper, and Eq. (2-3) was considered for a fibrous drawing (fluffing).

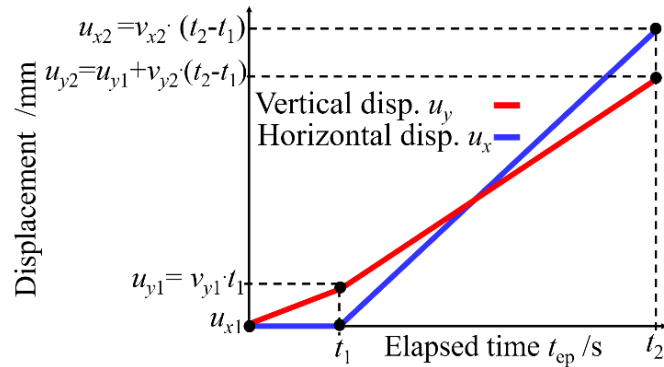


Fig. 2-11 Relationship between the vertical displacement of gripper point and the horizontal of base paper stacked on moving table.

Figure 2-11 shows the relationship between the vertical motion of the gripper point of the peeled layer (u_y) and the horizontal motion of the base paper stacked on moving table (u_x) in this FEM simulation. Here the moving velocity and time increment of gripper in simulation were virtually introduced for defining the incremental variation of forced displacement of the gripper in the MARC model. The virtual feed velocity of the gripper was empirically chosen as follows: the first stage vertical velocity of gripper v_{y1} was $4.62 \text{ mm}\cdot\text{s}^{-1}$ for $t_{ep} = 0 - t_1$ ($t = 0.05 \text{ ms}$), while the first stage horizontal velocity v_{x1} was $0 \text{ mm}\cdot\text{s}^{-1}$ for the same duration ($t_{ep} = 0 - t_1$). The corresponded vertical displacement of the gripper u_{y1} was $0.231 \text{ }\mu\text{m}$, and the horizontal displacement u_{x1} was 0 mm . The constant time step of increment was set as 0.05 ms in the first stage. In the second stage, the vertical velocity v_{y2} was set to $31 \text{ mm}\cdot\text{s}^{-1}$ for $t_{ep} = t_1 - t_2$ ($t_2 = 2.0 \text{ s}$), while the horizontal velocity of base paper v_{x2} was $39 \text{ mm}\cdot\text{s}^{-1}$ for the same duration ($t_{ep} = t_1 - t_2$). The constant time step of increment was set as 5 ms in the second stage. As the result, the vertical displacement of gripper u_{y2} was 62 mm , while the horizontal displacement of base paper u_{x2} was 78 mm at $t_{ep} = t_2 = 2 \text{ s}$. Moving of base paper was empirically delayed for a bit to avoid any unstable detaching on the peeled layer. Namely, after vertically elevating the gripper up to $0.23 \text{ }\mu\text{m}$ ($h/t_p = 0.002$, a quite small offset) without moving the table in the horizontal, the velocity ratio of vertical by horizontal was empirically fixed to $31/39 (=0.795)$ for the sake of keeping the attitude of upper layer sheet in 90° when $h/t_p \approx 50$. Since the experimental condition of feed velocity ratio was $v_y/v_x = 1.0$, that of simulation also seems to be 1.0 . However, when considering $v_{x2} = v_{y2} = 31 \text{ mm}\cdot\text{s}^{-1}$, the attitude angle of the gripper point was about 80° – 86° when $100 < h/t_p < 300$, although the peeling force was almost similar to that of the

case of $v_{y2}/v_{x2} = 31/59$. When considering $v_{x2} = 59 \text{ mm}\cdot\text{s}^{-1}$ and $v_{y2} = 31 \text{ mm}\cdot\text{s}^{-1}$ ($v_{y2}/v_{x2} \approx 0.53 < 1$), the upper layer is remarkably deflected in the out-of-plane. Moreover, the peeling force became negative in the early duration of $h/t_p < 70$, while the peeling force changed to the positive and became almost same as that of the experiment for $100 < h/t_p < 300$. To date, in this work, the virtual feed velocities $v_{x2} = 39 \text{ mm}\cdot\text{s}^{-1}$ and $v_{y2} = 31 \text{ mm}\cdot\text{s}^{-1}$ were used for discussing the simulation.

2.3 Results and discussions

2.3.1 Experimental peeling load response and deformation of peeled layer

Figure 2-12 shows the relationship between the normalized peeling displacement h/t_p and the tensile line force $f_p \text{ kN}\cdot\text{m}^{-1}$. Here the real feed velocity and pull-up (peel) velocity were equal with each other and chosen as 0.1, 0.25, 0.5, and 1.0 $\text{mm}\cdot\text{s}^{-1}$. The maximum peak tensile line force $f_{p\text{max}}$ was detected in the early stage of $h/t_p = 0\text{--}20$. Since the stationary state of f_p occurred for $h/t_p > 20$ but its response was varied randomly in a small extent, the average of f_p ($=f_{p\text{c}}$) was calculated for $20 < h/t_p < 100$ using the trapezoidal rule of numerical integration. The maximum peak $f_{p\text{max}}$ and the stationary average $f_{p\text{c}}$ were plotted in **Fig. 2-13**. It was found that $f_{p\text{max}}$ tended to decrease with the feed velocity, whereas $f_{p\text{c}}$ tended to increase with the feed velocity when $V < 0.3 \text{ mm}\cdot\text{s}^{-1}$. The ratio of $f_{p\text{max}}$ by $f_{p\text{c}}$ was about 3–4.

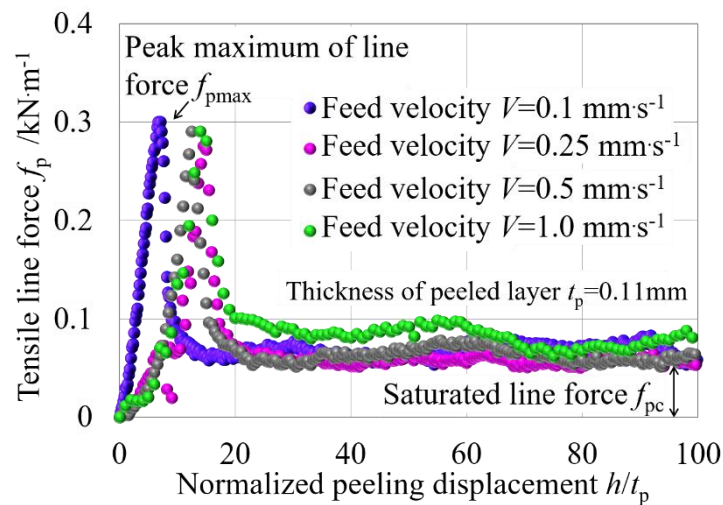


Fig. 2-12 Relationship between tensile line force and peeling displacement.

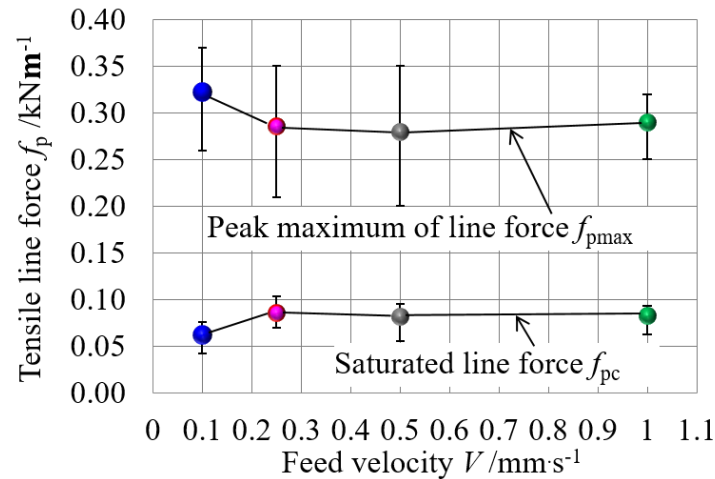


Fig. 2-13 Maximum peak and stationary average of tensile line force with respect to feed velocity.

Figure 2-14 and 2-15 show the representative side-view photographs of peeled specimens during PCT under the stationary state (for $20 < h/t_p < 400$). In those photographs, the curvature radius r_p of the peeled layer, the image scanning thickness, and the thickness by mechanical micrometer were also shown. The thickness profile was measured by the mechanical micrometer and image scanned average. The thickness of the image average tended to decrease with the feed velocity, whereas the thickness measured by the mechanical micrometer was almost invariant with the feed velocity. This difference seems to be caused by a variation in the scuffing height with the feed velocity. The curvature radius was estimated as shown in **Fig. 2-9**.

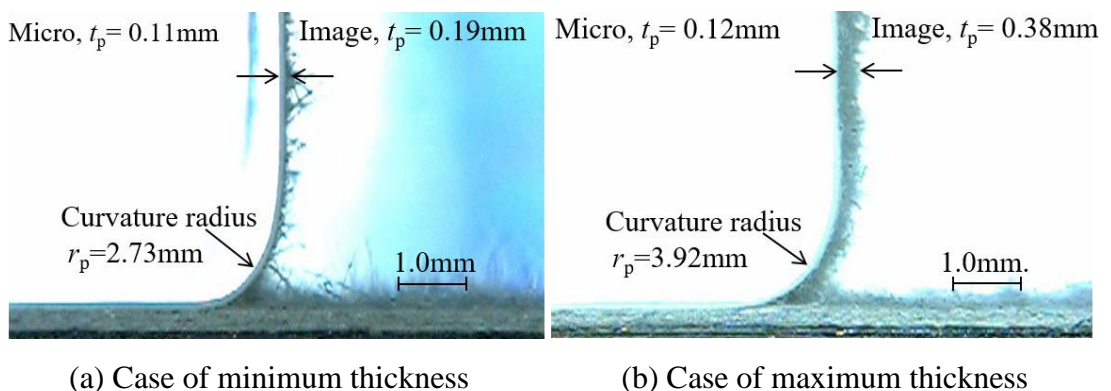


Fig. 2-14 Photographs of the side view of specimen during PCT at $V = 0.1 \text{ mm}\cdot\text{s}^{-1}$. Thickness of peeled layer: t_p , curvature radius: r_p .

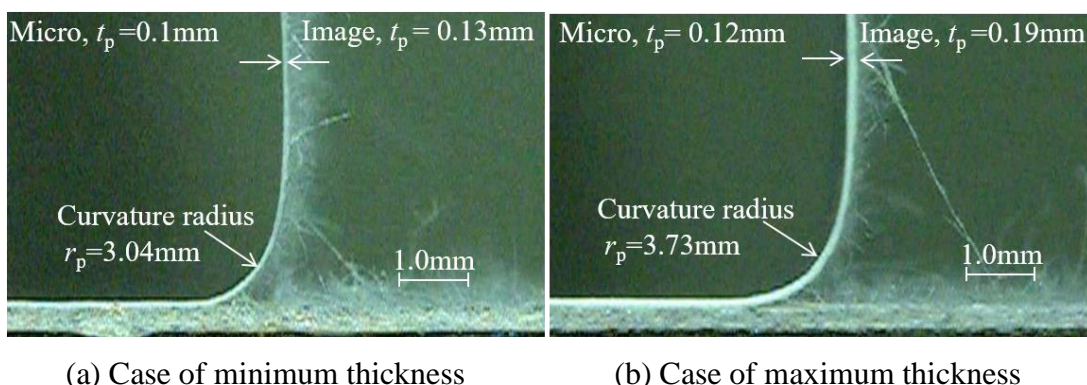


Fig. 2-15 Photographs of the side view of specimen during PCT at $V = 0.25 \text{ mm}\cdot\text{s}^{-1}$.
Thickness of peeled layer: t_p , curvature radius: r_p .

Figure 2-16 shows the normalized thickness of the peeled layer t_p with respect to the thickness of 0.45 mm of the worksheet. In this figure, the thickness measured by image processing tended to decrease with the feed velocity. This was caused by the variation of scuffing height, while the thickness measured by a mechanical micrometer was almost invariant with the velocity. **Figure 2-17** shows the relationship between the curvature radius r_p and the feed velocity. It was confirmed that the curvature radius tended to increase with the feed velocity.

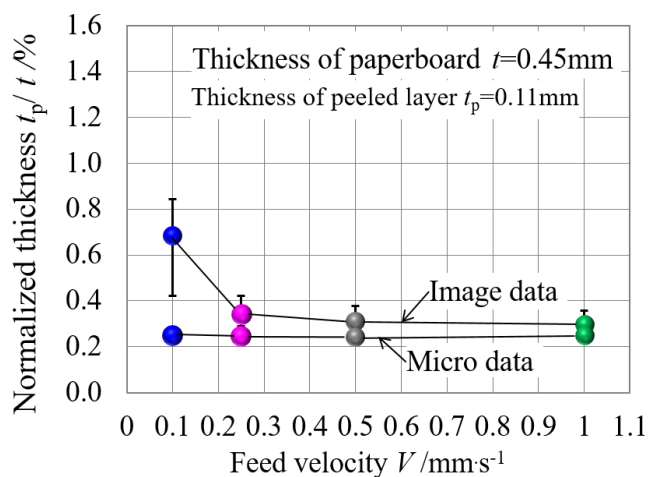


Fig.2-16 Thickness of peeled layer t_p .

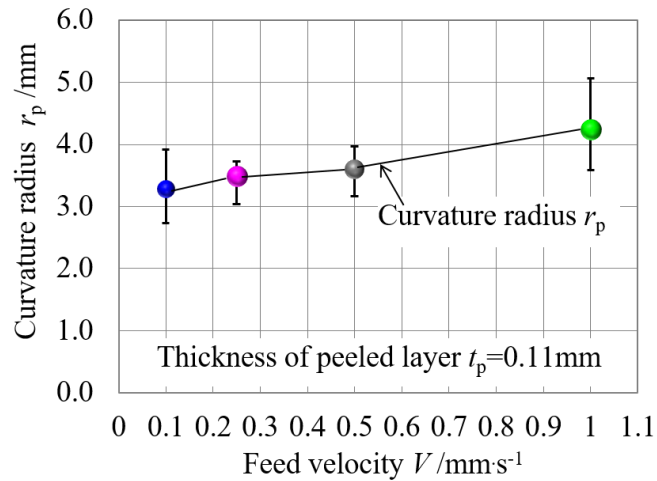


Fig. 2-17 Relationship between curvature radius r_p and the feed velocity.

2.3.2 Peeling load response and deformation of the worksheet on simulation

The proposed fluffing based FEM model was employed to simulate the peeling deformation of a white-coated paperboard. The maximum peak tensile line force $f_{p\max}$ was detected by the early stage of $h/t_p \approx 0-50$, while the stationary stage of f_{pc} occurred for $50 < h/t_p < 300$. In **Fig. 2-18**, “Exp.” shows the experimental relationship between the tensile line force and normalized peeling height for $h/t_p \leq 300$, while “FEM” shows the simulation result. In the experimental case, the feed velocity was $0.1 \text{ mm}\cdot\text{s}^{-1}$. The pull-up vertical displacement h was experimentally equal to the horizontal displacement L of linear positioning stage, while the ratio of h by L was empirically set to 0.795 for $0.04 < h/t_p < 300$. Seeing the simulation of **Fig. 2-18**, the peak maximum line force $f_{p\max}$ was 0.30 MPa, while the saturated line force f_{pc} was 0.05–0.08 MPa. This result was similar to the experimental result.

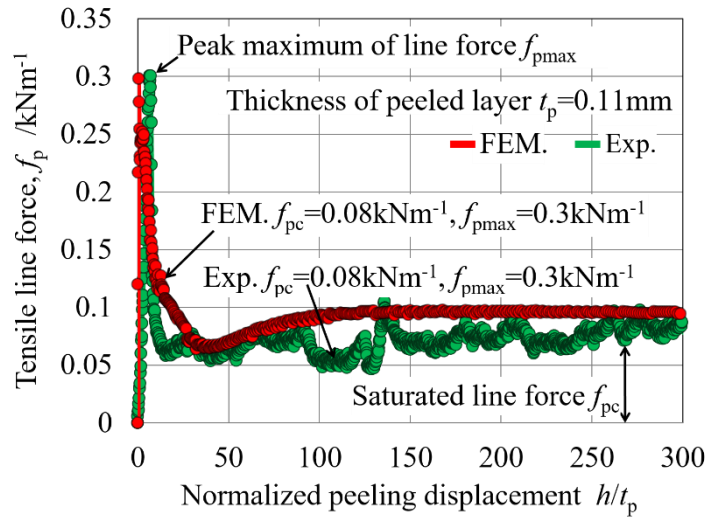


Fig. 2-18 Relationship between tensile line force and normalized peeling height (comparison of simulated with experimental result).

Figure 2-19 (a) shows a photograph of the experimental peeling deformation in the early stage of $h \approx 7.09t_p$, while **Fig. 2-19(b)** shows an FEM simulation at the peeling height of $h \approx 7.09t_p (=0.78 \text{ mm})$. The cracked length L and inclined angle of end point α_r were respectively $L \approx 24.3 t_p$ ($20t_p - 27.5t_p$) and $\alpha_r \approx 25^\circ$ ($23^\circ - 28^\circ$) in the experiment. However, the FEM simulation had $L \approx 24t_p$ and $\alpha_r \approx 29^\circ$ in the early stage. The curvature radius r_p was experimentally 2.7 (2.29–3.05) mm, and that of FEM simulation was approximately 2.6 mm. Hence, it was revealed that the proposed FEM simulation was fairly matched to the experimental response. Seeing **Fig. 2-19 (a)**, the detached profile of the double-sided adhesive tape was confirmed. Since the real details of detached profile were complicated deformation, the equivalent isotropic Young's modulus of $E = 200 \text{ MPa}$ was empirically introduced for the end zone of $L_{ip} = 2.67 \text{ mm}$ as mentioned in the **section 2.2.5**. When this end zone had the same Young's modulus as that of the upper layer $E = 533 \text{ MPa}$, the peak maximum of f_p was not so much changed but the reducing tendency was fairly different (small) in the range of $10 < h/t_p < 60$. This means that the early stage peeling is sensitively affected by the equivalent stiffness of the end zone of the peeled upper layer.

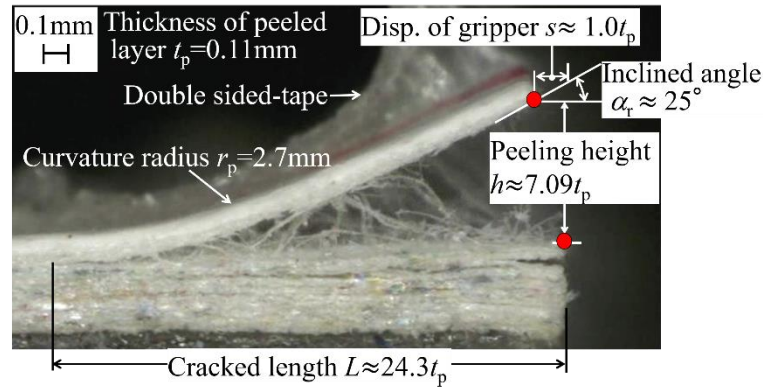
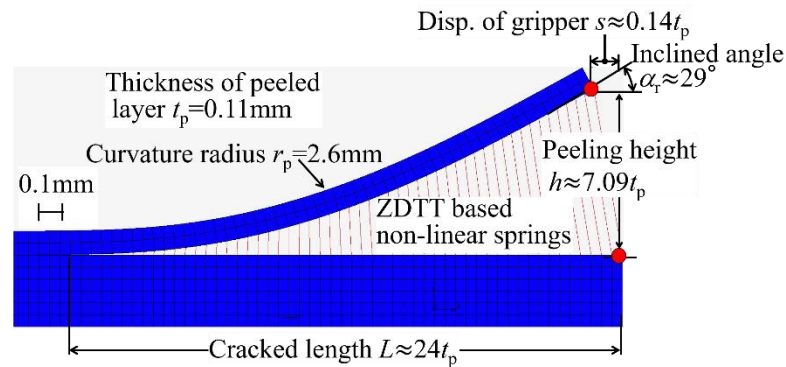
(a) Photograph of experiment at $h \approx 7.09t_p$.(b) FEM simulation at $h \approx 7.09t_p$.

Fig. 2-19 Representative side views of peeling deformation profile in the early stage $h < 20t_p$.

Figure 2-20 showed the peeling deformation profile in the stationary stage ($\alpha_t = 90^\circ$). Here, **Fig. 2-20 (a)** shows the experimental result, and **Fig. 2-20 (b)** shows the FEM simulation result. The curvature radius of the experiment was approximately 3.26 (2.73–3.92) mm, while that of the FEM simulation was about 2.63 mm. The ratio of the experimental average by FEM simulation was about 1.2. The ratios are fairly similar with each other. So far, the fluffing-based FEM model well explains the peak occurrence of the line force at the early stage and the saturated line force as compared to the experimental result.

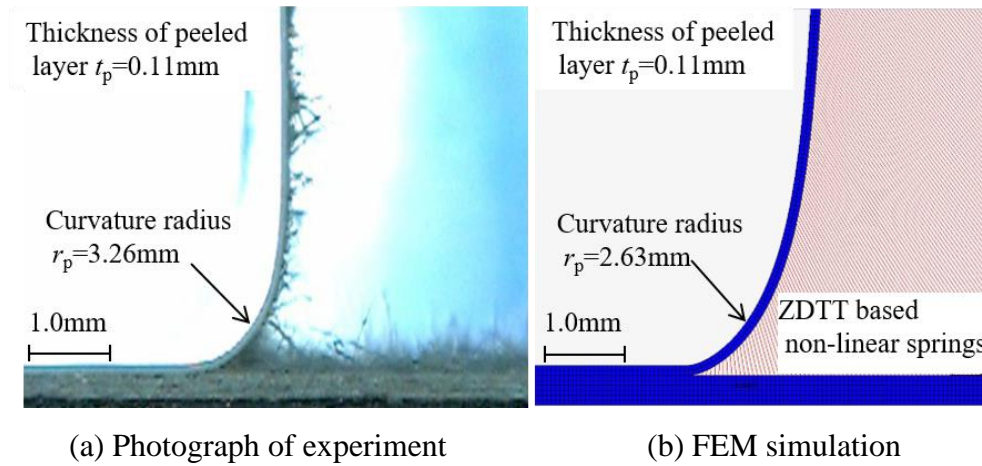


Fig. 2-20 Representative side views of peeling deformation profile in the stationary stage at $\alpha_r = 90^\circ$.

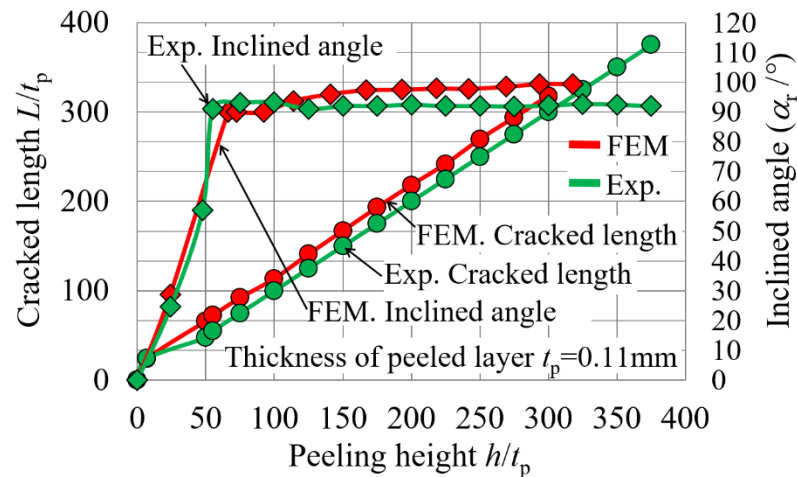


Fig. 2-21 Cracked length and inclined angle of peeling deformation profile

Figure 2-21 shows the FEM inclined angle α_r , the FEM cracked length L/t_p and the experimental cracked length L/t_p with respect to the peeling height h/t_p . Seeing the relationship between L/t_p and h/t_p , the experimental gradient of dL/dh was 0.989, while the FEM-simulation-based gradient of that was 0.998. Namely, since the derivative dL/dh is approximately 1, the increment of peeling height dh is balanced to the variation of cracked length dL . In this case, the fracture release rate of mode 1 is equal to the peeling line force itself. The experimental inclined angle α_r stably reached 90° for $h/t_p \approx 55-375$, while the FEM based inclined angle α_r was 90° when $h/t_p \approx 50-300$ ($L/t_p \approx 66-318$).

2.4 Conclusions

The peeling test of a 0.45-mm-thick coated paperboard was performed experimentally by varying the feed velocity $V = 0.1\text{--}1.0 \text{ mm}\cdot\text{s}^{-1}$. The detaching behavior of the weak-bonded layer was discussed with respect to the early stage and stationary stage by using the proposed fluffing model, which was based on the experimental result of ZDTT. The experimental features are as follows:

- (a) The weak-bonded layer thickness (peeled layer thickness) t_p was about 0.11 mm (24.4% of the thickness of 0.45 mm) in the examined paperboard. The peak maximum of line force $f_{p\max}$ occurred at the early stage (the ratio of peeling pull-up height by the peeled layer thickness h/t_p was less than 20), while the saturated line force f_{pc} was observed for $h/t_p > 20$.
- (b) The value of $f_{p\max}$ slightly decreased with the feed velocity V when $V < 0.25 \text{ mm}\cdot\text{s}^{-1}$ and it remained almost unchanged for $V > 0.25 \text{ mm}\cdot\text{s}^{-1}$. Conversely, the value of f_{pc} slightly increased when $V < 0.25 \text{ mm}\cdot\text{s}^{-1}$, while it remained almost unchanged for $V > 0.25 \text{ mm}\cdot\text{s}^{-1}$. The ratio of $f_{p\max}$ by f_{pc} was about 3–4.
- (c) The thickness of the image average t_p tended to decrease for $V < 0.25 \text{ mm}\cdot\text{s}^{-1}$, while the thickness measured by the mechanical micrometer t_p was almost invariant for all the measured V . This difference was explained by the variation of the scuffing height with V . Measured thickness of micrometer was different from that of image profile by the digital microscope when varying the feed velocity. This means that the fluffing height is varied with the peeling velocity. Average thickness is stably determined by the weak bonded layer position, but the fluffing height is varied with the peeling velocity.
- (d) The curvature radius r_p tended to increase with the feed velocity. Regarding the numerical simulation, the following was revealed.
- (e) The USPRNG user subroutine, fluffing model based on ZDTT response, can appropriately estimate the peeling deformation of the coated paperboard from the early stage up to the stationary stage. The existence of the early stage peak maximum of line force was characterized by the fluffing model.
- (f) The crack length and inclined angle of the peeled layer also matched well to the experimental results.

- (g) Even if the value of shearing glue parameter s_t was set up, the peeling response was not affected by the value of s_t . So far, it was revealed that the normal fluffing resistance was the main factor to determine the peeling resistance, but the shearing resistance was not any primary factor.
- (h) There are two features in the peeling response. One is the overshoot of load response as the crack initiation. Another is the stationary peeling resistance as the crack propagation. These two features were described by using the distributed fluffing non-linear springs. Namely, the fiber bridge mechanism is fundamentally described by the virtual fluffing non-linear springs. Here, the distributed pitch of virtual fluffing springs was designed as the order of the used minimum side length of the FE mesh size of the peeled layer. This is also one of the mechanism of peeling. The fiber bridge mechanism can be described by the virtual fluffing non-linear springs, by using appropriate pitch of distributed springs.

References

- American Society for Testing and Materials (ASTM), Standard Test Methods for Flexural Properties of Unreinforced and Reinforced Plastics and Electrical Insulating Materials, D 790-02, (2002), pp.146–154.
- American Society for Testing and Materials (ASTM), Standard Test Method for Peel Resistance of Adhesives (T -peel test), D1876-01, (2001), pp.1–3.
- Baum, G. A., Brennan, D. C. and Habeger, C. C., Orthotropic elastic constants of paper, *Tappi Journal*, Vol.64 No.8 (1981), pp.97–101.
- Beex, L. A. A. and Peerlings, R. H. J., An experimental and computational study of laminated paperboard creasing and folding, *International Journal of Solids and Structures*, Vol.46, (2009), pp.4192–4207.
- Fellers, C., Östlund, S. and Mäkelä P., Evaluation of the Scott bond test method, *Nordic Pulp and Paper Research Journal, Paper Physics*, Vol.27, No.2 (2012), pp.231–236.
- Gong, Y., Zhao, L., Zhang, J., Wang, Y. and Hu, N., Delamination propagation criterion including the effect of fiber bridging for mixed-mode I/II delamination in CFRP multidirectional laminates, *Composites Science and Technology*, Vol.151, pp.302–309.
- Hallbäck, N., Girlanda, O. and Tryding, J., Finite element analysis of ink-tack delamination of paperboard, *International Journal of Solids and Structures*, Vol.43, (2006), pp.899–912.
- Höwer, D., Lerch, B., Bednarczyk, B., Pineda, E., Reese, S. and Simon, J., Cohesive zone modeling for mode I facesheet to core delamination of sandwich panels accounting for fiber bridging, *Composite Structures*, Vol.183(1), (2018), pp.568–581.
- Japanese Industrial Standards (JIS), Standard Test Methods for Paper and board—Compressive strength—Ring crush method, P 8126, (2005), pp.1–10.
- Kirwan, J. M., *Handbook of Paper and Paperboard Packaging Technology* 2nd ed., (2013), pp. 268–287, Wiley- Blackwell.
- Komiyama, Y., Kon, W., Nagasawa, S. and Fukuzawa, Y., Effect of Structural Shape of Corrugated Medium on Flat Crush Characteristics of Corrugated Fiberboard,

- Journal of the Chinese Society of Mechanical Engineers, Transactions of the Chinese Institute of Engineers, Series C Vol.34 No.4, (2013), pp.361–369.
- Koubaa, A. and Koran, Z., Measure of the internal bond strength of paper/board, Tappi Journal, Vol.78, No.3 (1995), pp.103–111.
- Li, Y., Reese, S., and Simon, J.W., Modeling the fiber bridging effect in cracked wood and paperboard using a cohesive zone model, Engineering Fracture Mechanics, Vol.196, (2018), pp.83–97.
- MSC Software, Marc document: Theory and User Information), Vol.A, (2010a), pp.655. MSC Software, Marc document: User Subroutines and Special Routines), Vol.D, (2010b), pp.265–267.
- Nagasawa, S., Komiyama, Y. and Mitsomwang, P., Finite Element Analysis of Corrugated Board on Rotary Creasing Process, Journal of Advanced Mechanical Design, Systems, and Manufacturing, Vol.7, (2013a), pp. 103–114.
- Nagasawa, S., Mitsomwang, P., Chaijit, S. and Wongpatsa, W., Finite Element Analysis of Two Dimensional Deformation of Double-wall Corrugated Board on Creasing Process, Proceedings of the 3rd International Symposium on Engineering, Energy and Environments, Bangkok, (2013b), pp.338–343.
- Nagasawa, S., Yamagata, D., Fukuzawa, Y. and Murayama, M., Stress analysis of wedged rupture in surface layer of coated paperboard, Journal of Materials Processing Technology, Elsevier Science, Vol.178, (2006), pp.358–363.
- Pugno, N. and Abdalrahman, T., Peeling Experiments of Double Side Adhesive Tapes Suggests the Feasibility of Graphene Nanocomposites with Gigantic Toughness, Nanoscience and Nanotechnology Letters, Vol.4, (2012), pp.1–4, American Scientific Publishers.
- Scandinavian Pulp, Paper and Board Testing Committee., Z-directional tensile strength, SCAN-P 80:98, (1998) pp.1–3.
- Sørensen, B.F., and Jacobsen, T.K., Determination of cohesive laws by the J integral approach, Engineering Fracture Mechanics, Vol.70(14), (2003), pp.1841–1858.
- Stenberg, N., Fellers, C. and Östlund, S., Measuring the stress-strain of paperboard in the thickness direction, Journal of Pulp and paper science, Vol.27, (2001), pp.213–221.
- Sudo A., Nagasawa, S., Fukuzawa, Y. and Katayama, I., Analysis of exfoliation of laminated layers and creasing deformation of paperboard, Proceedings of The

Hokuriku-Shinetsu District Annual Conference of Japan Society of Mechanical Engineers, 047-1, (2005), pp.37–38 (in Japanese).

Thakkar, B. K., Gooren, L. G. J., Peerlings, R. H. J. and Geers, M.G.D., Experimental and numerical investigation of creasing in corrugated paperboard. *Philosophical Magazine*, Vol.88, (2008), pp.3299–3310.

Wathén, R., Studies on fiber strength and its effect on paper properties. KCL re-inventing paper, (2006), pp.1–98.

CHAPTER 3

ANALYSIS OF THE FOLDING PROCESS OF CREASED PAPERBOARD USING A COMBINED FLUFFING RESISTANCE AND SHEAR YIELD GLUE MODEL

3.1 Introduction

In the production of packaging containers, wedge-pushed cutting, creasing by the flatbed die cutter and the folding of creased lines are inevitable and determine the quality of containers (Kirwan, 2013). In the formation of blank patterns made of paperboard, a suitable residual stiffness of the creased parts is necessary for processing the fold of the paperboard in an automatic folder–gluer machine, and the creased lines must be stably folded without any surface failures as shown in **Fig. 3-1**. Namely, the creaser indentation depth against the paperboard must be controlled to retain the folding strength of the creased lines and the appropriate bulge that forms in the fold's interior. These procedures were empirically managed by experts in the past. However, to process this formation automatically in the folder–gluer machine, an appropriate prediction of the folding stiffness and the bulge profile with the specified creaser indentation depth is required.

Regarding the estimation of the crease deviation in the folds of eccentrically creased paperboards and the quasistatic folding stiffness concerning the creaser indentation depth were reported by (Nagasawa et al., 2001, 2008). Some bending strength testers were developed to investigate the bending moment and to record the deformation profile of the creased part during a folding process (Nagasawa et al., 2001, 2003, 2011, 2016). One of the bending moment measurement apparatuses (CST-J-1, Katayama Steel Rule Die Inc., Tokyo, Japan) is effective for controlling the bending rotation velocity and its sleeping time at a specified angle position of the creased part of a worksheet (CST-J-1, 2013; Nagasawa et al., 2015). Beex et al. (2009) proposed an FEM cohesive damage model for describing the bulging of the creased part to explain the delamination and folding resistance of a creased paperboard. Sudo et al. (2005) reported a feasibility study about the effect of inner detachment behavior on creasing

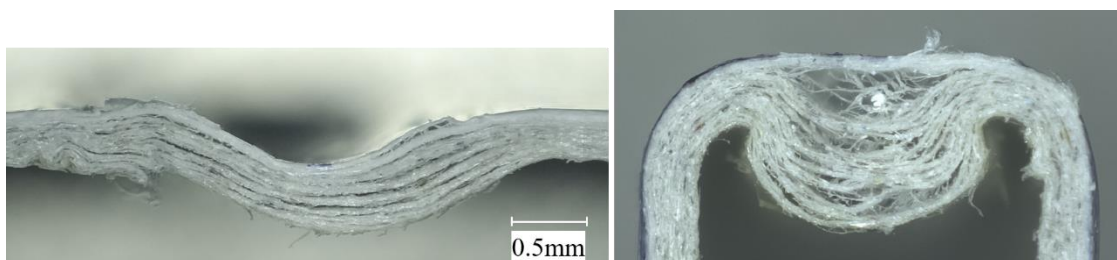
deformation of a paperboard using a distributed resistance model of nonlinear springs, which was described in the MARC subroutine: USPRNG (MSC software, 2003, 2010a, 2010b); however, Sudo's model did not discuss the shear resistance. Giampieri et al. (2011) reported an FEM model of a delaminated interface for simulating the folding behavior of a creased paperboard, which was considered the evolution of the damage variable with the imposed rotation angle. Hicks et al. (2003) proposed an FEM model to measure the internal energy during the delamination and buckling of laminated materials.

Regarding the delamination behavior of weak-bonded layers of white-coated paperboard, Jina et al. (2017) reported the fluffing model comprising anaphase yielding resistance derived from the z-directional tensile test (ZDTT) (Scandinavian Pulp, Paper and Board Testing Committee-SCAN-P, 1998), and the applicability of fluffing resistance to describe the peeling behavior of the weak-bonded layer was discussed using the FEM simulation. Here, although several reports used the orthotropic elastic or the orthotropic elastic-plastic model for simulating the limited cases (Murayama et al., 2005, Nagasawa et al., 2006, 2013a, 2013b; Komiyama et al., 2013), they were sometimes unstable for converging the numerical calculation, especially for a large deformation such as a folding. Therefore, in the previous work (Jina et al., 2017), the material properties of a paperboard were based on the isotropic elastic model with the in-plane compressive properties (the ring crush test), but the delamination of interlayers was considered by using the fluffing resistance of ZDTT. Because the fluffing model was relatively stable for peeling interlayers, it seems to be applicable to other deformations such as a large folding of paperboard after scoring by the creasing rule.

According to the development of the peeling model (Jina et al., 2017), because the glue model comprised a normal yield and the shear yield stress was unstable and far different from the real resistance, glue based detaching was not suitable for simulating the peeling process of a paperboard. However, a certain shear resistance near the peeled edge was necessary for successfully executing the fluffing-model-based simulation, although the peeling force was almost unaffected by the in-plane shear resistance. So far, to apply the fluffing model to the folding deformation of the creased part, a new consideration of the shear resistance in the delaminated layers must be investigated.

In this work, the bending characteristics of a white-coated paperboard, which was previously subjected to the creasing rule indentation, was numerically investigated

under the cantilever type folding, to develop a deformation model of the creased part of the paperboard. An FEM model was developed to simulate the bulging deformation and bending moment response of CST-J-1. To develop a mechanical model of detaching resistance of the delaminated layers of paperboard, a combination of the normal-directional fluffing resistance, which was implemented by the use of a MARC user's subroutine USPRNG based on ZDTT, and the in-plane shear yielding stress was introduced. The peeling model (Jina et al., 2017) was not affected by the in-plane shearing resistance, because the peeling force was mainly determined by the out-of-plane (normal directional) detaching stress and the bending stiffness of the peeled thin layer. However, in the case of the folding of a creased part, the bulged crease zone tends to be detached (same as the peeled state), whereas the folded inside left-right zones are a little out of the creased position. They are compressed in the thickness direction and are sheared/slide in the in-plane direction for each laminated layer. Hence, the authors investigated a combination model comprising the fluffing normal resistance (derived from ZDTT) and the glue breaking resistance as the shear yielding stress (based on the in-plane shear test and the frictional shear sliding) for discussing a couple of creasing conditions. Here, to verify the bending behavior of multiple plies, the effects of layer numbers were discussed. The initial creasing process with the creasing rule indentation depth and the folding process as a cantilever type (CST-J-1 model) were also investigated in the FEM simulation and were compared with the experimental results.



(a) Creasing failure state

(b) Folding failure state

Fig. 3-1 Example of creasing and folding failures state of paperboard.

3.2 Analysis conditions, estimated methods and the mechanical model of worksheet

3.2.1 Specimens

A white-coated paperboard comprises a pulp fiber structure matrix and a clay coated layer. The fiber layer comprises multiple plies and the coated layer is a mixture of ground calcium carbonate, kaolin and a binder (Reinhard et al., 2013). In this work, a commercially recycled white-coated paperboard with a thickness $t = 0.43$ (0.42–0.44) mm and a nominal basis weight of $350 \text{ g}\cdot\text{m}^{-2}$ was chosen. Its fiber and pulp analyses were summarized in **Table 3-1**, whereas the in-plane tensile properties of the paperboard in the machine direction of paper making (MD) were shown in **Table 3-2**. The specimens were prepared as a rectangle sheet, the width of which was 15mm, the length was 220mm, and the gauge length (distance of fixtures) was 180mm. These mechanical properties were almost the same as that reported in the previous work (Jina et al., 2017).

Table 3-1 Size of fiber and the pulp combination ratio of white-coated paperboard 350 (measured by Kajaani-FS300) L-BKP: Broad-leaved lumber (hard wood), bleaching kraft pulp; N-BKP: Needle-leaved lumber (soft wood), bleaching kraft pulp; NTMP: Needle-leaved, thermal mechanical pulp; L(n): based on number of fibers in each fibrillation index class; L(l): based on length weighted number of fibers in each fibrillation index class; L(w): based on weight-weighted number of fibers in each fibrillation index class; CWT: Wall thickness of cell; Width: average width of fiber (Jina et al., 2017).

Unit	Pulp combination ratio/%			Projected length of fiber/mm			Size/ μm		Section area/ μm^2
	L-BKP	N-BKP	N-TMP	L(n)	L(l)	L(w)	Width	CWT	CSA
Value	64.7	16.0	19.3	0.56	0.99	1.52	18.2	4.8	256.6

Table 3-2 In-plane tensile properties of a white-coated paperboard in machine direction (MD). Tensile feed velocity was $0.33 \text{ mm}\cdot\text{s}^{-1}$ (strain rate: 0.00183 s^{-1}). The tensile procedure was based on JIS-P8113. The average (minimum – maximum) of five samples was shown.

	Young's modulus E/MPa	Yield strength σ_Y/MPa	Tensile strength σ_B/MPa	Breaking strain ε_B
MD	5400 (5350–5460)	27.2 (26.6–27.6)	43.2 (42–43.86)	0.021 (0.02–0.022)

3.2.2 Out-of-plane detaching resistance model of specimens based on ZDTT

Regarding the out-of-plane (the thickness direction) detaching resistance, the ZDTT model was used for fixing the detaching layers (the interfaces of plies) of the paperboard. Jina et al. (2017) reported the ZDTT relation between the tensile stress and elongation in the thickness direction, as shown in **Fig. 3-2**. **Figure 3-2 (a)** indicates the schematic of the experimental apparatus of ZDTT. An acrylic-based double-sided adhesive tape NWK-15S was inserted beneath the lower and upper worksheet for stacking the lower crosshead. The feed velocity in the experiment of ZDTT was chosen as $0.1 \text{ mm}\cdot\text{s}^{-1}$. In this report, the specimens were prepared in 10 pieces as a square sheet with a length of $L_{\text{ZDTT}} = 10 \text{ mm}$, a width of $B_{\text{ZDTT}} = 10 \text{ mm}$ and a thickness of 0.45 mm . In this work, the average thickness of the paperboard was updated as 0.43 mm , due to a new population. **Figure 3-2 (b)** shows the tensile stress response diagram of the ZDTT and shows the fitting state between the experimental data and approximation curves. Here, the elongation e_z was subdivided into three zones: zone1, zone2 and zone3 as shown in **Fig. 3-2 (b)**. Here, $e_z (= x)$ is equal to a displacement of the lower crosshead. The tensile stress σ was approximated with e_z by using Eqs. (3-1)–(3-3) (Jina et al., 2017). **Table 3-3** shows the coefficient values of Eqs. (3-1)–(3-3). The generated thickness of weak-bonded layer was estimated as $t_{\text{p ZDTT}} = 0.11 (0.10\text{--}0.11) \text{ mm}$. The first zone of $0 < e_z < e_{z1}$ shows the elastic or elasto-plastic behavior before breaking at the weak-bonded layer. The zone of second and third periods of $e_{z1} < e_z < e_{z3}$ is a sort of an anaphase yielding behavior that is caused by the fluffing resistance of delamination.

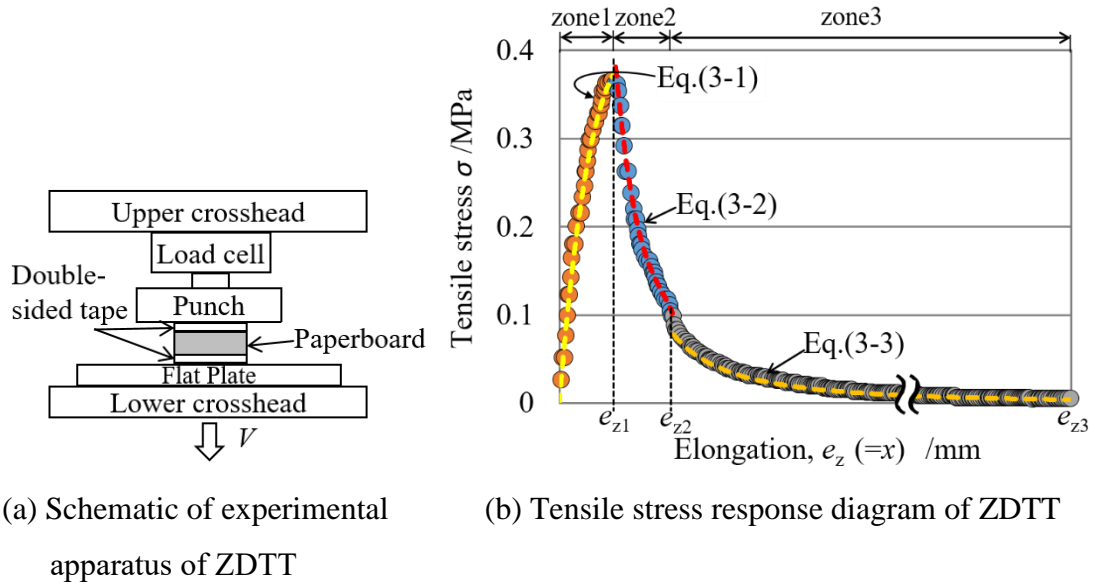


Fig. 3-2 Relations between the tensile stress and elongation in the thickness direction (Jina et al., 2017) ($t = 0.45$ mm).

The nominal tensile stress σ is described with the detaching distance of e_z as Eqs.(3-1)–(3-3), and this seems to be caused by fluffing or the drawing phenomena of fibers. Therefore, the anaphase yielding resistance of ZDTT is applied to the resistance of detaching layers during a folding process of the creased part. This fluffing model can be described using a user-defined subroutine of USPRNG (MSC software, 2010a, 2010b). Here, all the side edges of specimen were simply cut off by using a shaving knife, and any additional notches were not processed on the side edges.

$$\sigma = a_1 e_z^3 + a_2 e_z^2 + a_3 e_z + a_4 \quad (0 < e_z < e_{z1}) \quad (3-1)$$

$$\sigma = b_1 e_z^3 + b_2 e_z^2 + b_3 e_z + b_4 \quad (e_{z1} < e_z < e_{z2}) \quad (3-2)$$

$$\sigma = c_1 e_z^2 \quad (e_{z2} < e_z < e_{z3}) \quad (3-3)$$

Table 3-3 Stiffness coefficient values of Eq. (3-1), (3-2), and (3-3).

e_{z1}	0.0835	e_{z2}	0.178	e_{z3}	2.192		
a_1	14.1	a_2	-5.35	a_3	0.71	a_4	0.0006
b_1	-0.56	b_2	0.27	b_3	-0.04	b_4	0.003
c_1	0.0015	c_2	-1.04				

In this user-defined subroutine, the bonding line force $f = \sigma L_{ZDTT}$ is specified by the stiffness K and the distance U between the first and second ends of the nonlinear spring, as shown in Eq. (3-4).

$$\sigma = (K \cdot L_{ZDTT}^{-1}) \cdot U \quad (3-4)$$

In the implementation of a user-defined subroutine, Eq. (3-4) was replaced with Eqs. (3-1)–(3-3) using $e_z = U$. When $U > e_{z3}$, the nonlinear spring force is defined as zero. Namely, this is the breaking criteria based on the ZDTT model.

3.2.3 Experimental initial creasing of specimens

The specimens were prepared as 5 pieces of a rectangle formed white-coated paperboard, which had a width $W_{CST} = 20$ mm and length $L_{CST} = 40$ mm. All the paperboard specimens were kept in a temperature of 296 ± 1 K and a relative humidity of $50\% \pm 1\%$ in a controlled room for 24 h. The creasing stage was performed in the same room. Measurements were performed five times for each case. **Figure 3-3** shows the scoring state of a paperboard specimen using a round-edge knife (a creasing rule with a radius of $r = 0.355$ mm and thickness of $b = 0.71$ mm) with the rubber fixtures, of which the shore hardness was 40 A. The height difference (step) of rubber from the creasing rule was 1.4 mm, and the height of rubber was 7 mm. Using the paperboard thickness t and the thickness of the creasing rule b , the groove width B was empirically chosen as $2t + b = 1.6$ mm. The paperboard was scored by the creasing rule with a changing indentation depth d . The quantity $\gamma = 2d/B$ is defined here as the normalized indentation depth (Kirwan, 2013; Nagasawa et al., 2015). The creaser direction angle ϕ was chosen as 90° with respect to the MD, as shown in **Fig. 3-4**. The values of γ were chosen as 0.4, 0.7 and 1.0. The feed velocity was chosen as $V = 0.0167$ mm·s⁻¹. **Figure 3-5** shows the depth and width profile of scoring process. **Figure 3-5 (a)** shows the indentation depth of creasing rule d , whereas **Figure 3-5 (b)** shows the profile after scoring, namely, the depth after scoring d_{as} and the width after scoring w_p . **Table 3-4** shows the indentation depth of creasing rule d and the profile parameters d_{as} and w_p after scoring.

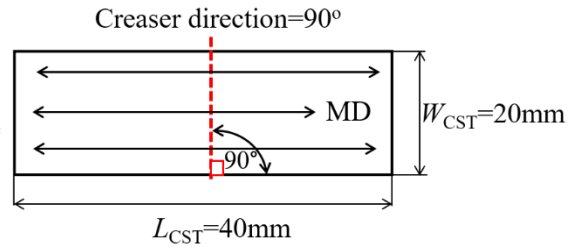
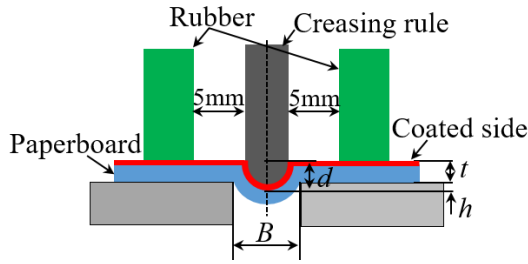


Fig. 3-3 Schematic of the scoring apparatus **Fig. 3-4** Creaser direction of paperboard

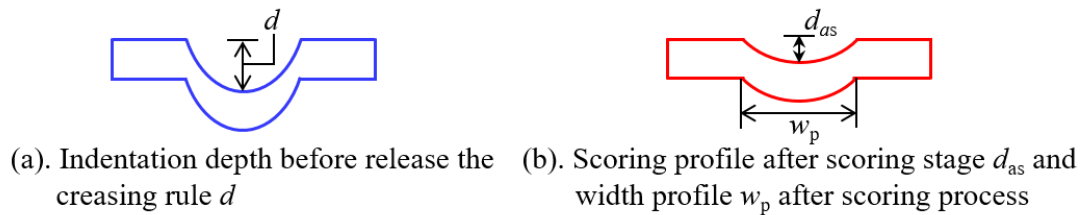


Fig. 3-5 Depth and width profile of the scoring stage.

Table 3-4 Scoring profile of experiment.

Normalized indentation depth γ	Indentation depth before release d /mm	Profile after scoring	
		Depth d_{as} /mm	Width w_p /mm
0.4	0.32	0.1 (0.09–0.11)	1.88 (1.79–1.94)
0.7	0.56	0.2 (0.18–0.2)	1.97 (1.79–2.08)
1.0	0.8	0.32 (0.3–0.34)	2.13 (2.02–2.19)

3.2.4 Experimental bending moment

To estimate the bending resistance of a white-coated paperboard, the folding experiment of the cantilever type (CST-J-1) was carried out. The specimen was taken over from the scoring stage described in section 3.2.3. The experiment was performed five times for each case. **Figure 3-6** shows a schematic of the CST-J-1 apparatus (Nagasawa et al., 2011, 2015; Katayama Steel Rule Die., 2013), and the loading process and deformed state of the specimen are shown. **Figure 3-7** is an example of the relation between the folding angle θ and the bending line moment (resistance for the unit width) M . Here, the rotation velocity ω of the fixture was set to 0.05 rps and the folding angle was increased up to 90° . In order to compare later the simulation with the experiment, the moment M_{90} (at $\theta = 90^\circ$) was recorded.

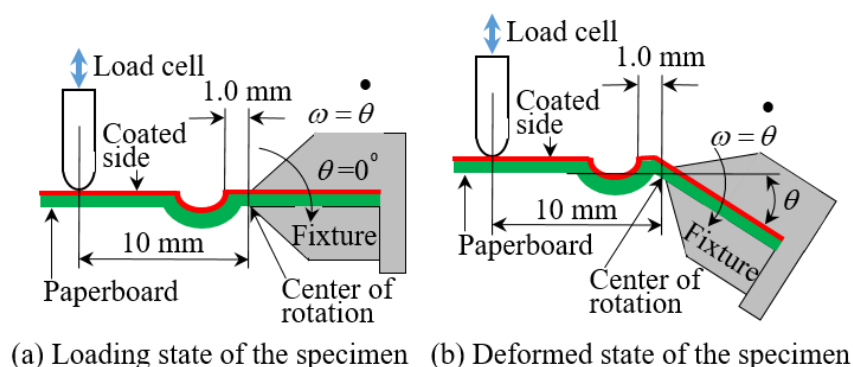


Fig. 3-6 Bending test apparatus using CST-J-1 (loading process).

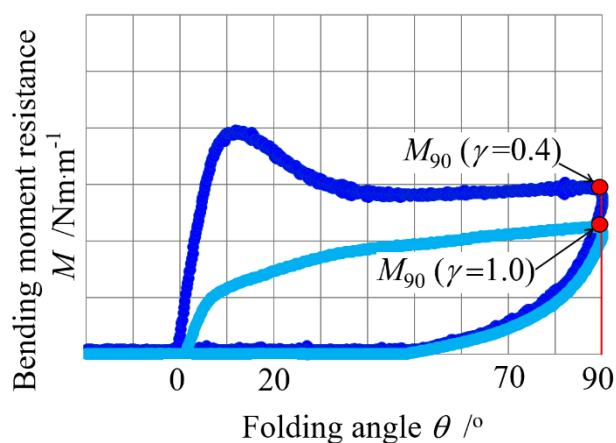


Fig. 3-7 Analysis parameters at tracking point of 90° in the bending moment response.

3.3 Estimation of in-plane shear strength properties

The in-plane shear yielding stress test seems to be related to the creasing deformation. Therefore, the in-plane shear yielding test (based on ASTM-D3846-79, 1990) was conducted for estimating the breaking shear yielding stress under a free compressive state in the thickness direction. It seems to be a sort of a lower bound shear strength. On the other hand, the upper bound of shear strength is expected as the in-plane yielding shear stress of the worksheet. To investigate the lower bound shear strength, the MD direction was considered. **Figure 3-8** shows the schematic of the shearing test apparatus and the specimen size. The specimen was fixed by an acrylic-based double-sided adhesive tape NWK-15S that was inserted between the metal plate and the worksheet. The velocity in the experiment of the shearing test was chosen as $0.1 \text{ mm}\cdot\text{s}^{-1}$. The specimens were prepared as 10 pieces of a rectangle sheet, the notches of which was made by a hand knife. The specimen had an effective length of $l_{\text{dn}} = 3 \text{ mm}$

and a width of $w_s = 10$ mm. Namely, the nominal area of in-plane sheared zone was 30 mm^2 . The thickness of double-sided tape $t_{ds} = 0.14$ mm and the thickness of metal plate $t_m = 0.22$ mm were used. The lower side of the metal plate was fixed, whereas the upper side of metal plate was pull up. **Figure 3-9** shows the relation between the nominal shear stress $\tau = P/(w_s \cdot l_{dn})$ and the displacement of the metal plate. In the figure, the shear strength $\tau_{B(\text{inMD})}$ (lower bound) was a breaking value recorded as the maximum $\tau_{B(\text{inMD})} = 1.63(1.23\text{--}2.03)$ MPa, whereas the in-plane MD shearing yield strength (upper bound) was estimated as $\sigma_Y/1.732 = 15.7$ MPa from **Table 3-2**. The strain energy with areal density until the breakage was roughly estimated as 2.2 $\text{J}\cdot\text{mm}^2$ from **Fig. 3-9**.

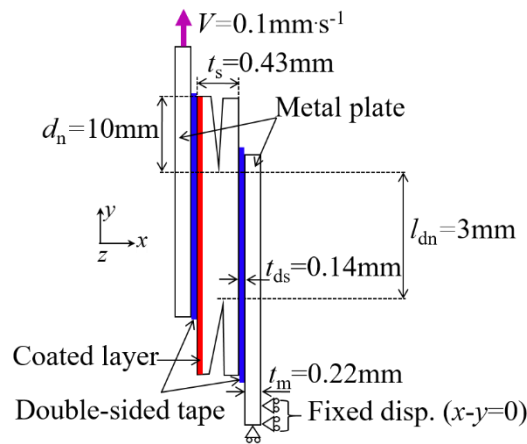


Fig. 3-8 Schematic of the shearing test apparatus

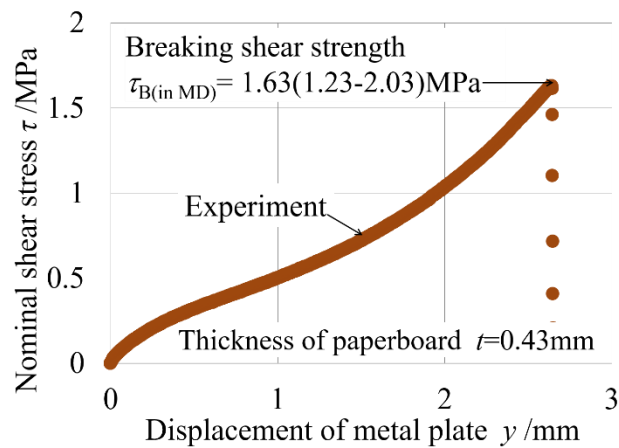


Fig. 3-9 Relation between the nominal shear stress and displacement of the metal plate in the in-plane shearing test.

In this work, due to the use of a general purpose FEM code (MSC.MARC 2015), the shear-stress-yield-based glue model was employed. Since the normal breaking

resistance of delaminated layers is considered as the fluffing resistance (ZDTT based nonlinear spring model), only the shear resistance of delaminated layers is considered as the glue breaking model, which is controlled by the GLUED CONTACT option (MSC software, 2010a). The glued contact is generally released when Eq. (3-5) is satisfied. Here, τ_{if} and σ_{if} are the contact shear and normal stress, respectively. s_t , s_n , and m are the user-defined parameters of breakage. In this model, the normal resistance s_n was not considered due to the use of fluffing model, and then the index of m becomes arbitrarily determined.

When any node is released on the delaminated layer due to the breaking criteria of Eq. (3-6), the node on the delaminated layer obeys the rule of frictional CONTACT (MSC software, 2010a) between the two bodies (upper/lower layers). The contact stress is calculated using the contact force divided by equivalent areas for shell elements. The glue breaking criteria was fundamentally defined by the in-plane shear stress of the shearing test. Therefore, $s_t=1.63$ MPa was assumed to be the first trial value. However, due to the stress concentration at the cracked edge and the frictional restriction under a compressive-strained state, the macroscopic deformation of the creased zone must be verified using an appropriate amplified factor of the shear strength parameter s_t . In the following simulation, the early stage slipping pattern of the delamination of interlayers and the saturated bending moment resistance at a large folded state (e.g., at $\theta = 90^\circ$) are verified by varying the shear strength parameter $s_t = 1.63\text{--}16$ MPa.

$$(\sigma_{if}/s_n)^m + (\tau_{if}/s_t)^m = 1 \quad (3-5)$$

$$(\tau_{if}/s_t) = 1 \quad (3-6)$$

3.4 FEM simulation model

3.4.1 FEM simulation model for non-scoring

A general purpose finite element code, MSC.MARC 2015, was used to simulate the non-scoring process. The updated Lagrange procedure and a large strain analysis used for a two-dimensional model (plane strain). The thickness of the worksheet was $t = 0.43$ mm. **Figure 3-10** shows the FEM non-scoring model based on the bending stage. The bending model was two dimensional (plane strain), an isotropic

elasto-plastic model was assumed by using the in-plane tensile testing properties in the MD. The mesh model was made of a full model, because the folding deformation was not symmetric with the center position. Here, the deformable body assumed to be the thick layer which was the thickness that of $t=0.43\text{mm}$, and the folding resistance of worksheet is characterized by the in-plane yielding stress.

The size of the specimen and boundary condition were shown in **Fig. 3-10**. The longitudinal length was assumed to be $L_{CST} = 25\text{ mm}$. The number of divided elements of the worksheet was 16949, whereas that of the total nodes was 66843. The eight-node plane strain quadrilateral element type 27 was adopted. The Young's modulus of the deformable body was assumed to be 5400 MPa from **Table 3-2**, and the Poisson's ratio was $\nu = 0.2$ (Baum et al., 1981). The yield stress was assumed to be 27.2 MPa (**Table 3-2**) and perfect-plastic. According to the friction coefficient of the load cell end of bending tester CST-J-1 against the paperboard μ_{lc} was 0 (no friction), the arm length between the center of a rotator and the load cell end was 10 mm, the rotator fastened the deformable body and they were fixed by using the GLUE CONTACT function. Here, the load cell and rotator were assumed to be rigid bodies. The angular displacement of the rotator was up to 90° on the clockwise (-1.57 radians), the incremental angle was chosen as 0.0157 radians for each step in the simulation. The total increment was 100 steps for simulating the folding stage.

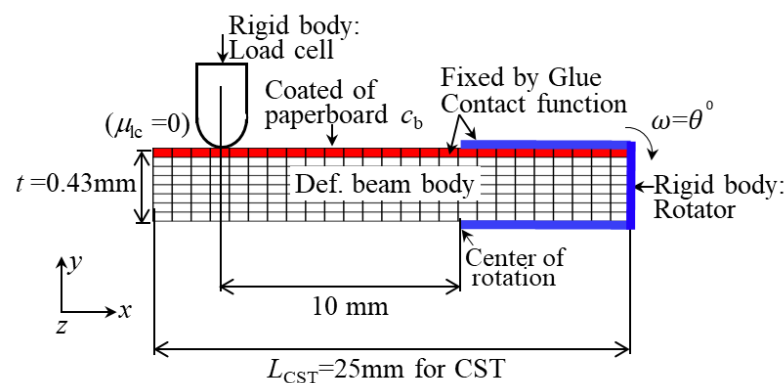


Fig. 3-10 Schematic of the non-scoring apparatus for FEM model. The interlayers were not delaminated.

3.4.2 FEM simulation model for scoring

A general purpose finite element code, MSC.MARC 2015, was employed for simulating the scoring process. The updated Lagrange procedure and a large strain analysis were used for a two dimensional model (plane strain). The thickness of the worksheet was $t = 0.43$ mm. **Figure 3-11** shows the FEM scoring model based on the experimental scoring process. Since the bending was two dimensional (plane strain), an isotropic elasto-plastic model was assumed by using the in-plane tensile testing properties in the MD. The mesh model was made of a full model, because the folding deformation was not symmetric with the scored-center position. Although the mechanical properties of thickness direction are different from this isotropic model, since the scored zone is initially de-laminated and the geometrical profile is fitted to the real experimental scored depth, the bending resistance seem to be characterized by the in-plane stiffness and resistance. Here, the layer detaching resistance is considered as the bonding resistance, and the bending resistance of each layer is characterized by the in-plane yielding stress. Although the number of plies were 8 for the considered specimens, the model of delamination layers assumed 3, 5, 7 and 8 layers for verifying the effects of layer numbers as shown in **Table 3-5**. The upper layer defined as the 1st layer had the thickness of $c_b = 0.11$ mm (Jina et al., 2017), whereas the other layers were defined as the following four cases: (1) Interlayers comprised 2nd and 3rd layers of 0.16 mm. (2) Interlayers comprised 2nd–5th layers of 0.08 mm. (3) Interlayers comprised 2nd–7th layers of 0.053 mm. (4) Interlayers comprised 2nd–8th layers of 0.046 mm. Here, since the representative coated paperboard of $360 \text{ g}\cdot\text{m}^{-2}$ empirically has 8 layers in the paper making process, the fourth case was mainly used in the following simulation.

The breaking criteria of the bonded interfaces in the creasing zone were based on the fluffing model and the shear breaking glue model. Namely, a new combination model was introduced. The subroutine USPRNG that described the detaching resistance of ZDTT with Eqs. (3-1)–(3-3) was adopted. The shear breaking glue model was assumed to have the glue tangential strength parameter s_t chosen as five cases: 1.63 MPa (as the lower bound strength based on the in-plane shearing test); 6 MPa (3.7 times of 1.63 MPa); 11 MPa (6.8 times of 1.63 MPa); 14 MPa (8.6 times of 1.63 MPa); and 16 MPa (10 times of 1.63 MPa, also estimated as the Mises shear yield of $\sigma_Y/1.732 = 15.7$ MPa).

The size of the specimen and boundary condition were shown in **Fig. 3-11**. The longitudinal length was assumed to be $L_{CST} = 25$ mm. The number of divided elements of the worksheet was 16949, whereas that of the total nodes was 66843. The eight-node plane strain quadrilateral element type 27 was adopted. The Young's modulus of the deformable body was assumed to be 5400 MPa from **Table 3-2**, and the Poisson's ratio was $\nu = 0.2$ (Baum et al., 1981). The yield stress was assumed to be 27.2 MPa (**Table 3-2**) and perfect-plastic. The deformable body comprised two parts: (1) Each layer was permanently fixed at the left and right outside and (2) Each layer was bonded by the USPRING joints of Eq. (3-4) and the shear glue of Eq. (3-6) at the central creased zone. The tools were assumed to be rigid bodies as following: creasing rule (round-edge knife), die (grooved counter plate) and rubber fixtures.

Regarding the friction coefficient of tools and worksheet, the kinetic friction coefficient between the noncoated paperboard and the counter plate was 0.4 (Murayama et al., 2005). The friction coefficient of the postal cardboard against the postal cardboard was also measured as 0.5–0.7 (Nagasawa et al., 2009). In this simulation work, to avoid any unstable state of FEM execution, all the friction coefficients were assumed to be appropriate values for each area as shown in **Table 3-5**. The friction coefficient μ_{el} with the interlayers of the paperboard was 0.7. The sliding condition of contact area against the tools was assumed to be slippery. Namely, the friction coefficients μ_b , μ_d of the creasing rule and the grooved plate (channel die) against the paperboard were 0.1. The friction coefficient μ_r of the rubber fixture against the paperboard was assumed to be zero (no friction). The edge radius of groove was 0.1 mm, whereas the width of groove (channel die) was 1.6 mm. The lower grooved counter plate (die) was fixed, as shown in the vertical and horizontal axes (x, y-axis) in **Fig. 3-11**.

The indentation depth of the creasing rule was chosen as shown in **Table 3-6**. Seeing **Table 3-4**, the indentation depth of creasing rule d , and the permanent depth after scoring d_{as} were fairly different with each other due to the spring back effect. It seems to be caused by the in-plane isotropic assumption of elasto-plastic behavior against the real orthotropic behavior. In order to compare the experimental result and the simulation, the permanent scoring depth based on the experimental result was approximately prepared in the simulation: $d_{as} = 0.1, 0.2$ and 0.32 mm. These parameters d_{as} were used in the simulation for discussing the cantilever type (CST-J-1) folding as shown in **Table 3-6**. Since the length of the detached zone was not known previously,

it was chosen as $L = 1.6$ (based on the width of channel die), 2.4 and 6.2 mm for investigating the effects of detached zone on the creasing deformation. Here, the $d_{as} = 0.2$ mm was chosen as the representative case for the simulation of folding process.

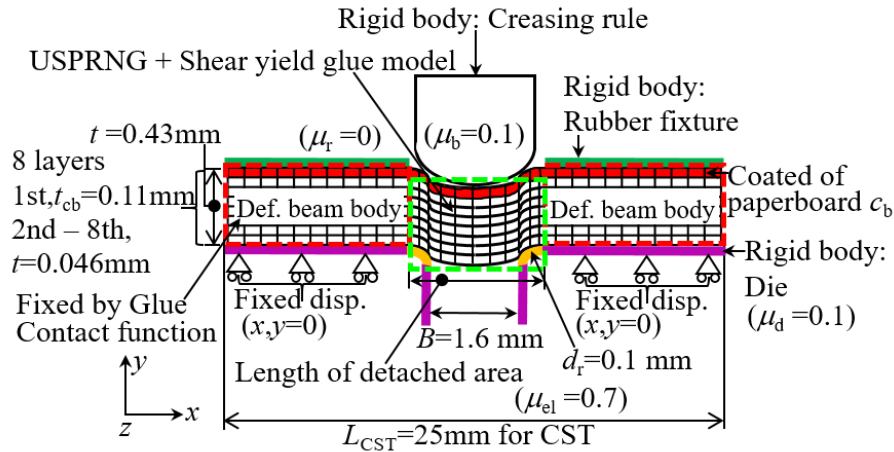
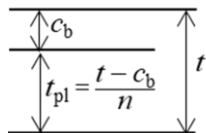


Fig. 3-11 Schematic of the scoring apparatus for FEM model. The bonding restriction on the specified of the detaching layer (creasing area) was modeled by the user's subroutine USPRNG using the criteria of Eqs. (3-1)–(3-3) and the shear yield glue model.

Table 3-5 Model conditions for FEM simulation.

Object type	Worksheet	Friction coefficients:
Young's modulus E /MPa	5400	$\mu_{el} = 0.7,$
Poisson's ratio	0.2	$\mu_b, \mu_d = 0.1,$
Yield strength σ_Y /MPa	27.2	$\mu_r, \mu_c = 0$ (no friction)
Thickness of worksheet t /mm	0.43	Shear strength parameter of glue joint: $s_t = 1.63, 6.0, 11.0, 14.0$ and 16.0 /MPa
Thickness of 1st layer c_b /mm	0.11	
t_{pl} /mm for 2nd–3rd layers, in case of $n = 2$	0.16	Length of the detached zone: $L = 1.6, 2.4, 6.2$ /mm
t_{pl} /mm for 2nd–5th layers, in case of $n = 4$	0.08	
t_{pl} /mm for 2nd–7th layers, in case of $n = 6$	0.053	
t_{pl} /mm for 2nd–8th layers, in case of $n = 7$	0.046	



Definition of the thickness of interlayers when assuming $(n+1)$ plies

t_{pl} : the thickness of each interlayer, n : the number of interlayers

Table 3-6 Scoring profile of FEM.

Indentation depth before release d /mm	Profile after scoring	
	Depth d_{as} /mm	Width w_p /mm
0.13	0.1	1.64
0.23	0.2	1.65
0.35	0.32	1.61

3.4.3 FEM simulation model for folding

In order to compare with the experimental observations described in section 3.2.4 and to predict the behavior of bending and bulging of creased part, a cantilever type (CST-J-1) folding was carried out as shown in **Fig. 3-12**. This simulation was taken over from the scoring stage described in section 3.4.2. Additional conditions were as follows: the friction coefficient of the load cell end of bending tester CST-J-1 against the paperboard μ_{lc} was 0 (no friction), the arm length between the center of rotator and the load cell end was 10 mm, the rotator fastened the deformable body and they were fixed by using the GLUE CONTACT function. Here, the load cell and rotator were assumed to be rigid bodies. The angular displacement of the rotator was up to 90° on the clockwise (-1.57 radians), the incremental angle was chosen as 0.0157 radians for each step in the simulation. The total increment was 100 steps for simulating the folding stage.

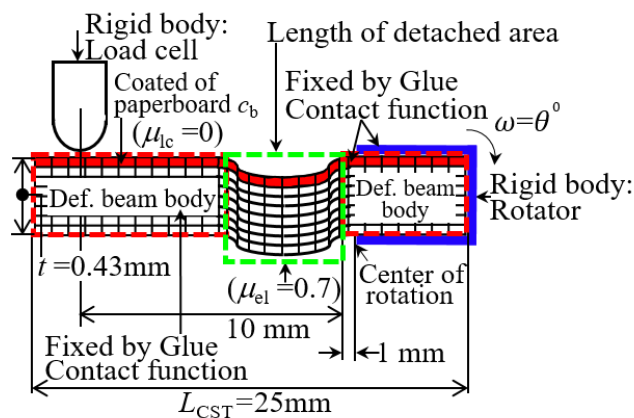


Fig. 3-12 Size definition and boundary condition of FEM CST model. The detaching layer (creasing-area) based on the user's subroutine USPRNG using the criteria of Eqs. (3-1)–(3-3) and the shear yield glue model.

The simulation was discussed with respect to the next two categories: (C1) First, in order to verify the necessity of combination of the fluffing normal and the shear glue strength with the detaching resistance in the interlayers, the scored depth d_{as} was chosen as 0.1, 0.2 and 0.32 mm, and the length of the delaminated zone was chosen as $L = 2.4$ mm (1.5 times of channel die width). Comparison of d_{as} was done for verifying the applicability of this combination model. The number of delamination layers was chosen as 3, 5, 7 and 8 layers, and the effect of layer numbers was discussed. Here, the 8 layers model was mainly used as the representative case. Regarding the magnitude of in-plane shear glue strength, the shear strength parameter s_t was chosen as 1.63, 6.0, 11.0, 14.0 and 16.0 MPa, respectively. (C2) In the second, to customize the size of delaminated zone, the length of the delaminated zone was chosen as $L = 1.6$ (based on the width of channel die), 2.4 and 6.2 mm. Here, the scored depth d_{as} was chosen as 0.2 mm, while the number of delamination layers was chosen as 8.

3.5 Results and discussion

3.5.1 Experimental bending moment resistance with the scoring depth

Figure 3-13 shows the experimental relationship between the bending moment resistance M and folding angle θ when choosing the scored depth $d_{as} = 0.1, 0.2$ and 0.32 mm. The bending moment resistance tended to decrease with the scored depth d_{as} . **Figure 3-14** shows the sectional views of creased part of experimental specimens folded at $\theta = 20^\circ$ and 90° . Here, the case of $d_{as} = 0.1$ mm was shown in the subfigures (a) and (b), the case of $d_{as} = 0.2$ mm was shown in the subfigures (c) and (d), the case of $d_{as} = 0.32$ mm was shown in the subfigures (e) and (f), respectively.

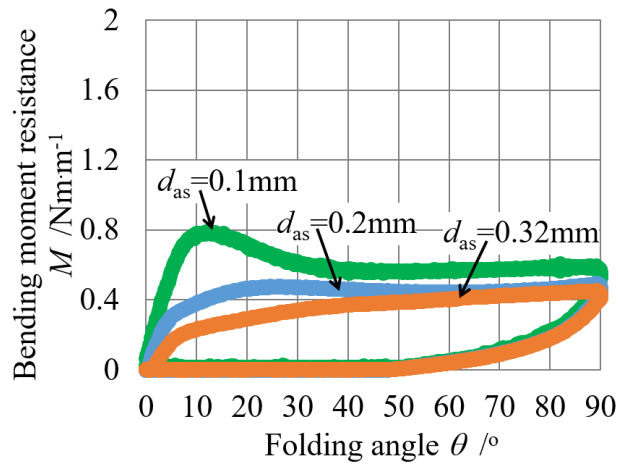


Fig. 3-13 Relationship between bending moment resistance and folding angle in the experiment when choosing $d_{as} = 0.1, 0.2,$ and 0.32mm .

Scored depth d_{as}	$\theta=20^\circ$	$\theta=90^\circ$
$d_{as}=0.1\text{ mm}$	(a).	(b).
$d_{as}=0.2\text{ mm}$	(c).	(d).
$d_{as}=0.32\text{ mm}$	(e).	(f). 1mm.

Fig. 3-14 Sectional views of creased part of paperboard in the experiment when folding at $\theta = 20^\circ$ and 90° . Photographs were arranged in: (a) and (b) as $d_{as} = 0.1\text{ mm}$, (c) and (d) as $d_{as} = 0.2\text{ mm}$, and (e) and (f) as $d_{as} = 0.32\text{ mm}$.

3.5.2 Bending moment resistance for non-creasing state

Figure 3-15 shows the relationship between bending moment resistance M and folding angle θ of the paperboard. Here, the non-creasing state was representatively chosen as $d_{as} = 0\text{ mm}$ in the experiment and FEM simulation. The result was found that the FEM simulation based bending moment response almost matched that of the experimental result.

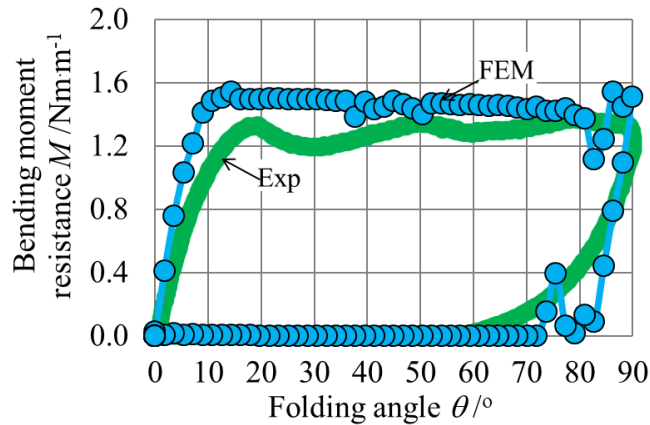


Fig. 3-15 Relationship between bending moment resistance and folding angle in the experiment and FEM simulation model when choosing $d_{as} = 0$ mm (non-creasing state). In the FEM simulation model, the interlayers were not delaminated.

Figure 3-16 shows the vector diagrams of maximum σ_{p1} (tensile state) and minimum σ_{p2} (compressive state) principal stresses at the folding angle 90° for $d_{as} = 0$ mm (non-scored). Seeing the **Fig. 3-16 (a)** the upper side was shown the tensile state σ_{p1} , whereas the **Fig. 3-16 (b)** the lower side was shown the compressive state σ_{p2} .

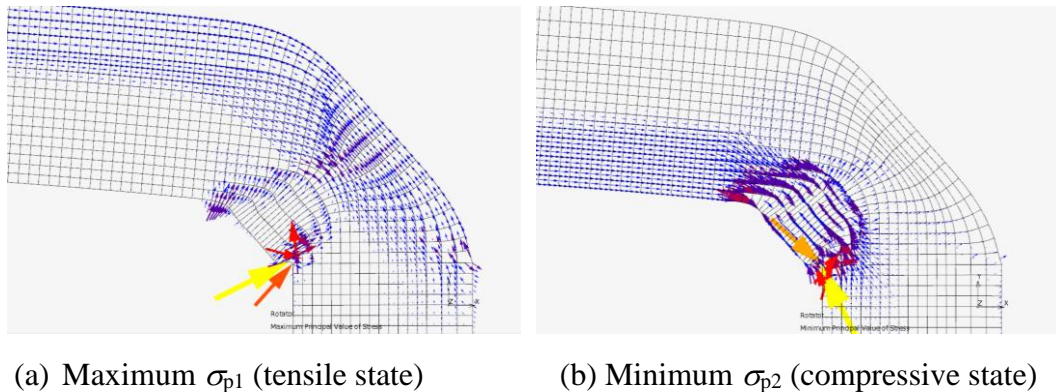


Fig. 3-16 Vector diagrams of σ_{p1} and σ_{p2} principal stresses at the folding angle 90° for $d_{as} = 0$ mm (non-scored).

Figure 3-17 shows contour band diagrams with the magnitude of the maximum σ_{p1} and minimum σ_{p2} principal stresses when choosing the folding angle 90° for $d_{as} = 0$ mm (non-scored). Here, the case of tensile state σ_{p1} was shown in the subfigure (a), the case of compressive state σ_{p2} was shown in the subfigure (b), respectively. From the figure mentioned below, the subsequent features were shown: (i) A high tensile state,

shown by the yellow band ($\sigma_{p1} > 53.06$ MPa), was detected in the upper zone. (ii) A high compressive stress was dominant in the center of the lower zone.

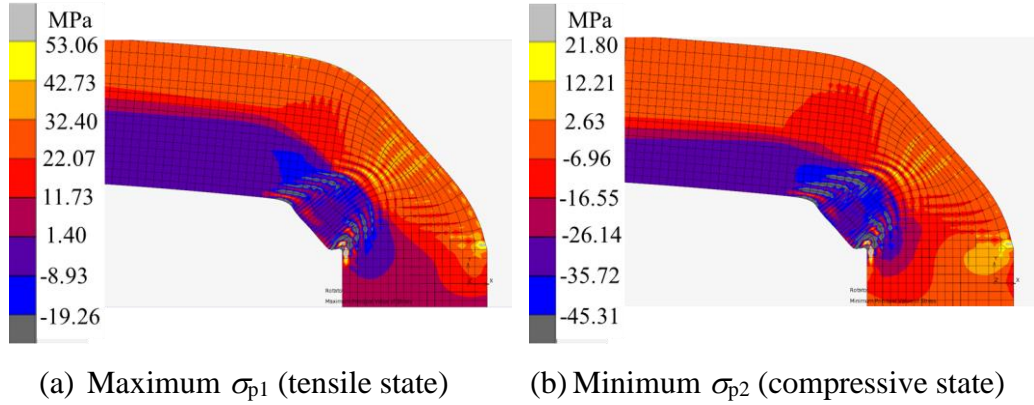


Fig. 3-17 Contour band diagrams of σ_{p1} and σ_{p2} principal stresses at the folding angle 90° for $d_{as} = 0$ mm (non-scored).

Figure 3-18 shows the norm of σ_{p1} and σ_{p2} were detected along the center of the thickness direction. The σ_{p1} was estimated in length between of 0–0.30mm, whereas the σ_{p2} was estimated in length between of 0.34–0.43mm. The average value of σ_{p1} was 36.57 MPa, whereas the σ_{p2} was -36.55 MPa

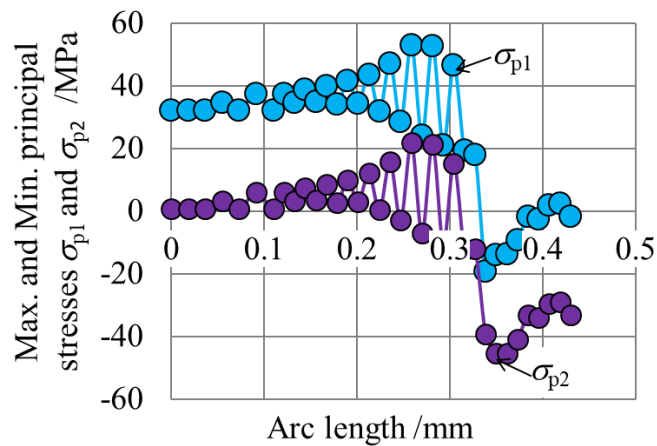


Fig. 3-18 Magnitude of σ_{p1} and σ_{p2} principal stress of worksheet at the folding angle 90° for $d_{as} = 0$ mm (non-scored).

3.5.3 Combination effect of shear glue strength and fluffing normal strength

The case C1 described in section 3.4.3 was investigated. **Figure 3-19** shows the relationship between bending moment resistance M and folding angle θ of the paperboard. Here, the permanent scored depth was representatively chosen as $d_{as}=0.1$ mm in the experiment and FEM simulation. Here, the experimental result was referred from **Fig. 3-13**. **Figure 3-20** shows the relationship between bending moment resistance M_{90} at $\theta = 90^\circ$ and shear strength parameter s_t . When choosing $s_t = 11$ MPa for $90^\circ > \theta > 20^\circ$, the FEM simulation based bending moment almost matched that of experimental result. However, when choosing $s_t > 14$ MPa, the FEM simulation based bending moment tended to be remarkably larger than that of experiment, owing that any detaching deformation disappeared at the scored zone and then there was not appropriate bulging.

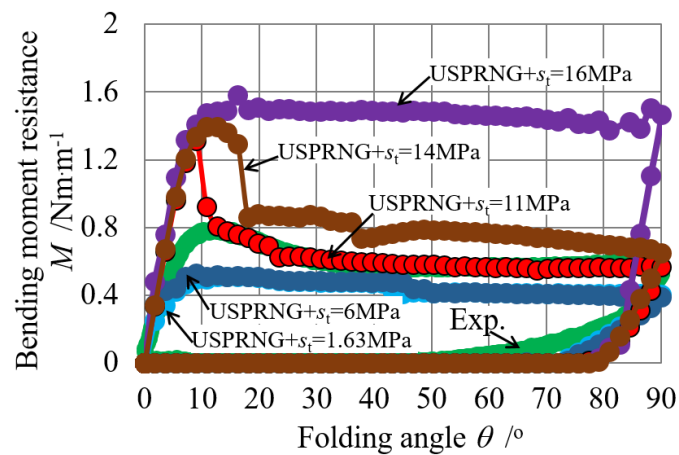


Fig. 3-19 Relationship between bending moment resistance and folding angle. Simulated conditions were as follow: the scored depth $d_{as} = 0.1$ mm, the number of layers 8, the length of delaminated zone $L = 2.4$ mm, and the detaching criteria was the fluffing plus the shear strength parameter $s_t = 1.63, 6.0, 11.0, 14.0$ and 16.0 MPa.

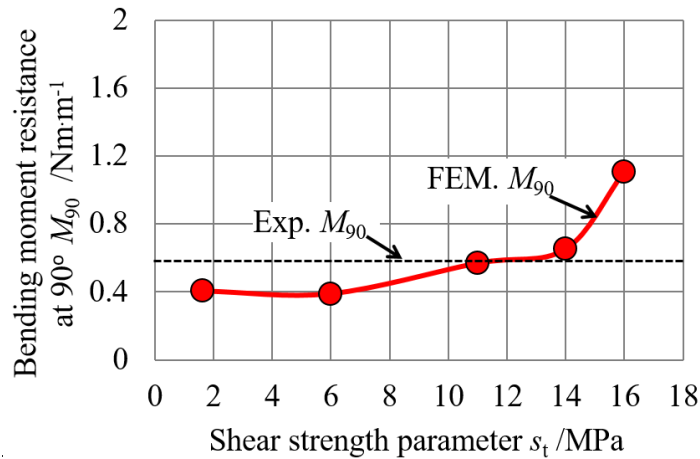


Fig. 3-20 Relationship between bending moment resistance and shear strength parameter s_t at the folding angle 90° . The simulated conditions were the same as that of **Fig.3-19**.

Figures 3-21 and **3-22** show contour band diagrams with the magnitude of the maximum (principal) shear stress τ_{\max} when choosing the shear strength parameter s_t as 1.63 and 11 MPa, respectively. In case of $s_t = 1.63$ MPa, as shown in **Fig. 3-21**, the bulge of scored part was obviously insufficient compared with that of the experimental result shown in **Fig. 3-14 (b)**. In case of $s_t=11$ MPa, as shown in **Fig. 3-22**, the bulge of scored part was relatively similar to that of experimental result. Seeing these contour band diagrams, the Mises shear stress (yielding level) of $15.7 \text{ MPa} = \sigma_y/\sqrt{3}$ occurred at the contact zone of interlayers in both cases. This seems to be caused by the frictional shear sliding under a high pressured contact with the interlayers. Namely, it is found that the shear strength parameter s_t does not determine the maximum shear stress, but affects the early stage slipped pattern of interlayers. In this work, $s_t/\tau_{B(\text{inMD})} = 6.7$ was relatively suitable for making the bulging profile and the saturated bending moment resistance M_{90} .

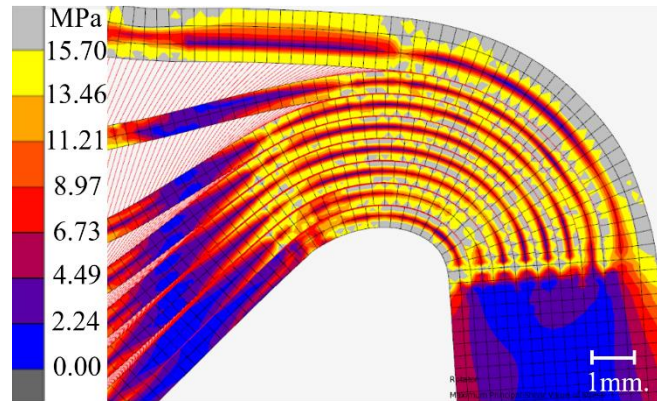


Fig. 3-21 Contour bands diagram of the maximum shear stress τ_{\max} when choosing $s_t = 1.63$ MPa for the folding angle of 90° . Other simulated conditions were as follows: the scored depth $d_{as} = 0.1$ mm, the length of delamination zone $L = 2.4$ mm, and the detaching criteria was the fluffing plus the shear strength.

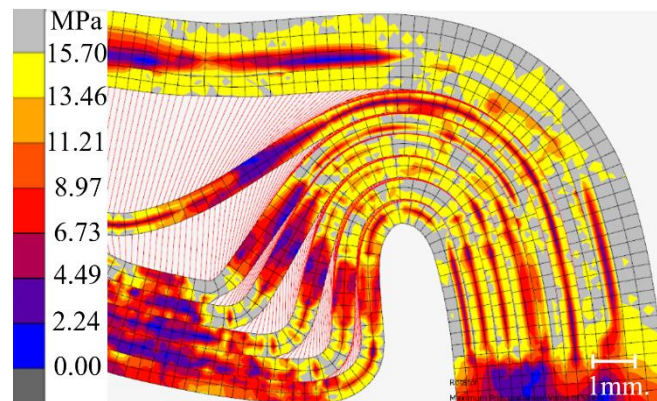


Fig. 3-22 Contour bands diagram of the maximum shear stress τ_{\max} when choosing $s_t = 11.0$ MPa for the folding angle of 90° . Other simulated conditions were as follows: the scored depth $d_{as} = 0.1$ mm, the length of delamination zone $L = 2.4$ mm, and detaching criteria was the fluffing plus the shear strength.

Seeing the cases of $s_t > 11$ MPa in **Fig. 3-19**, the simulated response had a large overshoot at the early stage ($\theta = 10 \sim 20^\circ$), whereas the experimental result had not such an overshoot response. This numerical overshoot appeared to be caused by bulging of scored zone due to the use of the isotropic elasto-plastic model based on the tensile test in the MD. Although the scored zone of specimen seemed to be softened by the indentation

of creasing rule, the FEM model used the in-plane tensile test properties for all the range of specimen.

Seeing the bending moment response at the early stage ($\theta < 10^\circ$) in **Fig. 3-19**, the initial gradient $G_i = \partial M / \partial \theta$ (for $0 < \theta < 2^\circ$) of simulation appeared to be a little larger than that of experiment, although G_i is almost independent to s_t . In order to reveal the effect of permanent scored depth d_{as} on the folding deformation of creased paperboard, the initial gradient G_i and the saturated bending moment M_{90} was investigated. According to the experimental reports, G_i and M_{90} tended to be decreased with $\gamma = 0.2-1.0$ (Nagasawa et al., 2001, 2003).

Figure 3-23 shows the normalized initial gradient G_i/G_{i0} for $d_{as} = 0.1, 0.2$ and 0.32 mm. Here, in the FEM simulation, the shear parameter was $s_t = 11$ MPa and the delaminated zone was $L = 2.4$ mm, and G_{i0} was the initial gradient when $d_{as} = 0$. The experimental G_{i0} was $0.14 \text{ Nm} \cdot \text{m}^{-1} \text{deg}^{-1}$ and that of simulation model was $0.23 \text{ Nm} \cdot \text{m}^{-1} \text{deg}^{-1}$, respectively. Therefore, the initial stiffness of FEM model was about 60% larger than that of experiment, owing that the isotropic elasto-plastic model in in-plane MD was considered in the FEM model. Nevertheless, the FEM simulation and the experimental results had a similar dependency on G_i with that of the scored depth. Namely, the geometrical feature of scored depth is the primary factor for determining the initial gradient G_i . Regarding the mismatching for $d_{as} > 0.2$ mm, the material properties (such as the Young's modulus and yielding stress) seem to be changed by deep indentation of creasing rule at the scored zone, and then a sort of the work softening seems to reduce the initial gradient actually.

Figure 3-24 shows the relationship between the bending moment resistance M_{90} at the folding angle 90° when choosing $d_{as} = 0.1, 0.2$ and 0.32 mm under $s_t = 11$ MPa. Comparing the FEM simulation with the experimental result for each scored depth, they were fairly matched with each other. So far, it is found that the determination procedure of the shear strength parameter s_t in the FEM simulation is applicable to the folding of creased paperboard when watching the saturated folding angle. In this work, the right angle folding was verified for $d_{as} = 0.1-0.32$ mm.

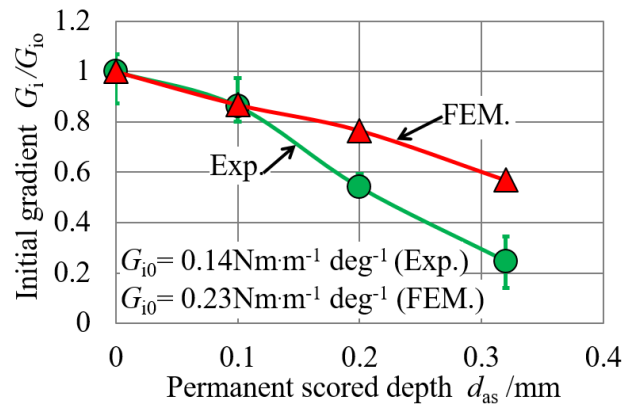


Fig. 3-23 Effect of permanent scored depth d_{as} on the initial gradient of bending moment. In the FEM simulation, the length of de-lamination area was $L = 2.4$ mm, and detaching criteria was based on the fluffing plus shear glue of $s_t = 11.0$ MPa.

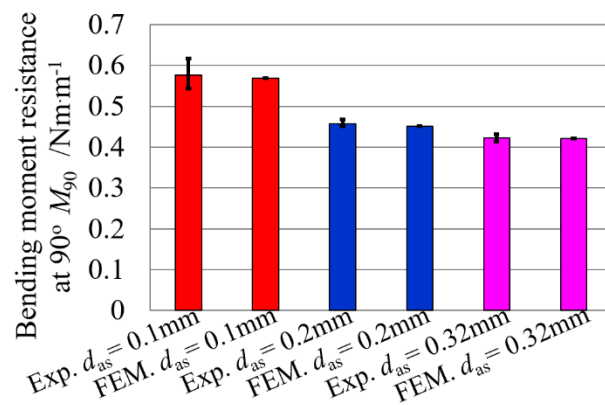


Fig. 3-24 Relationship between bending moment resistance at the folding angle of 90° for experiment and FEM simulation. The scored depth was $d_{as} = 0.1, 0.2$ and 0.32 mm. In the FEM simulation, the length of de-lamination area was $L = 2.4$ mm, and detaching criteria was based on the fluffing plus shear glue of $s_t = 11.0$ MPa.

3.5.4 Effects of lamination numbers

Because the prepared paperboard had the thickness of 0.43 mm and its lamination numbers were empirically estimated as 8 layers, the FEM simulation was mainly discussed by using the 8 layers model. As the sensitivity of layer numbers on the bending stiffness seems to be important for designing or estimating the folding stiffness, the effects of layer numbers on the bending moment at the saturated state of $\theta = 90^\circ$ were investigated here while virtually varying the layer numbers. **Table 3-7** shows the experimental and FEM-simulated bending moment M_{90} at $\theta = 90^\circ$ when

varying d_{as} under $s_t = 11$ MPa when concerning the lamination numbers of 3, 5, 7 and 8 layers. From this table, the following features were disclosed: (1) When the lamination layers were 8 layers, M_{90} of the FEM model almost agreed with that of experiment for $d_{as} = 0.1, 0.2$ and 0.32 mm. The 8 layer model seems to be suitable for the describing the bulging of paperboard. (2) When the lamination numbers was less than 8 layers, as the bending stiffness of each layer is remarkably increased (related to the cube of its thickness) and the freedoms of buckling of delaminated layer are changed, the saturated bending moment resistance M_{90} seems to increase with decreasing layer numbers.

As the result, using the proposed model (isotropic, in-plane tensile properties based material properties, 8 layers with the combination detaching criteria by the fluffing resistance of Eq. (3-4) and shear glue resistance of $s_t = 11$ MPa), the FEM simulation of bending moment response was similar to the experimental response for three kinds of scored depth: $d_{as} = 0.1, 0.2$ and 0.32 mm.

Table 3-7 Experimental and FEM based bending moment resistances M_{90} with respect to d_{as} .

Depth d_{as} /mm	Experimental results /Nm m ⁻¹	FEM results /Nm m ⁻¹			
		3 layers	5 layers	7 layers	8 layers
0.1	0.58 (0.54–0.62)	1.09	0.97	0.91	0.57
0.2	0.46 (0.45–0.47)	1.0	0.88	0.8	0.45
0.32	0.42 (0.41–0.43)	1.06	0.82	0.63	0.42

3.5.5 Bulged profile of the creased part

Figure 3-25 shows the sectional views of the FEM folded parts for the folding angle of $\theta = 20^\circ, 90^\circ$. **Fig. 3-25 (a)** defines the height h_b and the width w_b of bulged inside part. **Figure 3-25 (b)–(e)** illustrated the FEM simulation result at the folding angle of $\theta = 20, 90^\circ$ when choosing the scored depth of $d_{as} = 0.1, 0.2$ mm. Here, the FEM model conditions were as follow: the length of delaminated area was $L = 2.4$ mm, the de-lamination resistance was considered as the fluffing model of USPRNG plus the shear glue parameter of $s_t = 11$ MPa.

The FEM deformation profile well described the inside bulging and delamination state at the center zone for both the cases of $d_{as} = 0.1$ and 0.2 mm. **Figure 3-26** shows the height h_b and the width w_b of the bulged inside part of the experiment

and the FEM simulation for the folding angle $\theta = 20^\circ, 30^\circ, 50^\circ, 70^\circ$ and 90° , when choosing $d_{as} = 0.1$ and 0.2 mm. Seeing this figure, the width w_b of FEM simulation was similar but a little smaller (15%–24%) than that of the experiment for the folding angle of 20° – 90° , while the height h_b of FEM simulation was well matched to the experimental result for the folding angle. The case of $d_{as} = 0.32$ mm were similar to the case of $d_{as} = 0.2$ mm, except for the gap extent of the width between the FEM simulation and experiment. Namely, the width of FEM simulation was a little smaller (20%–26%) than that of the experiment.

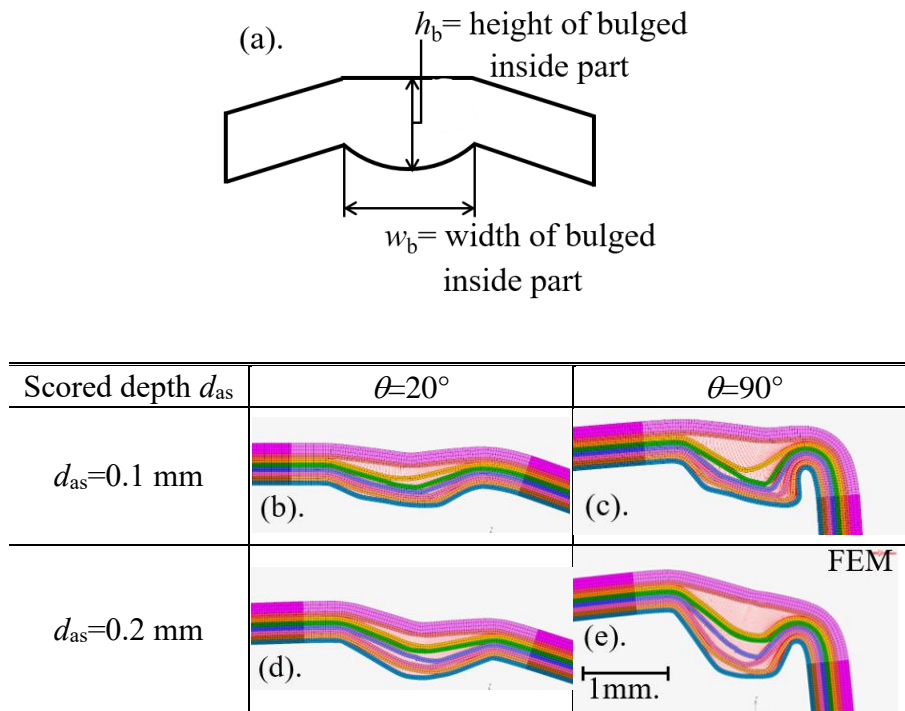


Fig. 3-25 Sectional views of folded part of paperboard in the FEM simulation with respect to 20° and 90° . (a) Definition of the height and the width for bulged profile. (b) and (c): at $d_{as} = 0.1$ mm. (c) and (d): at $d_{as} = 0.2$ mm. In the FEM simulation, $L = 2.4$ mm, the lamination was 8 layers, and the detaching criteria was based on the fluffing resistance plus shear glue of $s_t = 11$ MPa.

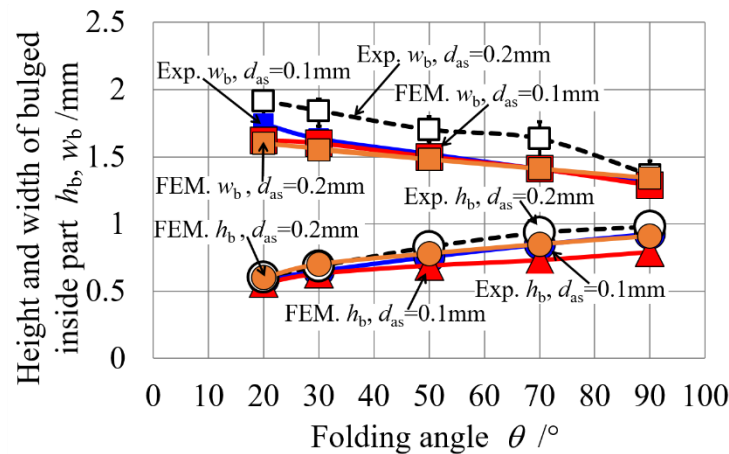


Fig. 3-26 Height and width of bulged inside profile with respect to folding angle. In the FEM simulation, the length of de-laminated area was $L = 2.4$ mm, the lamination was 8 layers, the scored depth was $d_{as} = 0.1$ and 0.2 mm, the detaching criteria was based on the fluffing plus shear glue of $s_t = 11$ MPa.

3.5.6 Effects of length of delaminated zone

In order to verify the effects of the delaminated zone on the folding deformation, the length of delamination zone was varied. **Figure 3-27** shows the FEM bending moment resistance with the folding angle. Here, the length of the delaminated zone was chosen as $L = 1.6$ mm (based on the width of channel die), 2.4 mm and 6.2 mm. The scored depth was chosen as $d_{as} = 0.2$ mm, and the breaking criteria was based on the fluffing model of USPRNG plus the shear glue parameter of $s_t = 11$ MPa. Seeing this figure, the saturated bending moments appeared to be similar to each other. **Figure 3-28** shows the sectional views of folded part at the folding angle $\theta = 20^\circ$ and 70° , while **Fig. 3-29** shows the height and the width of bulged inside profile for the folding angle $\theta = 20^\circ, 30^\circ, 50^\circ$ and 70° .

Through the comparison of these three conditions ($L = 1.6, 2.4$ and 6.2 mm), it was found that the effect of the length of delaminated area was a little different between the case of $L = 1.6$ and $L = 6.2$ mm, as shown in **Fig. 3-28**, while the deformation profile of $L = 6.2$ mm was similar to that of $L = 2.4$ mm. The height of bulged inside part well matched for $L = 1.6, 2.4$ and 6.2 mm. Synthetically, the length of delaminated zone ought to be chosen as $L/B > 1.5$ ($L > 2.4$ mm).

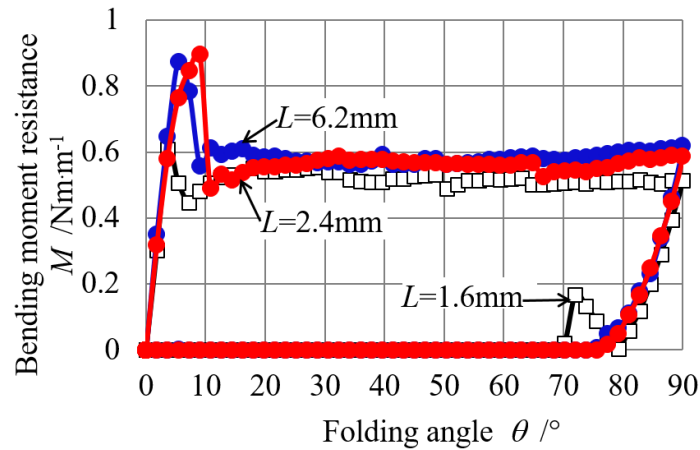


Fig. 3-27 Relation between bending moment resistance and folding angle in the FEM simulation. The lamination was 8 layers, the length of de-laminated area was chosen as $L = 1.6$ (based on the width of channel die), 2.4 and 6.2 mm. The scored depth was $d_{as} = 0.2$ mm, and the detaching criteria was based on the fluffing plus shear glue of $s_t = 11$ MPa.

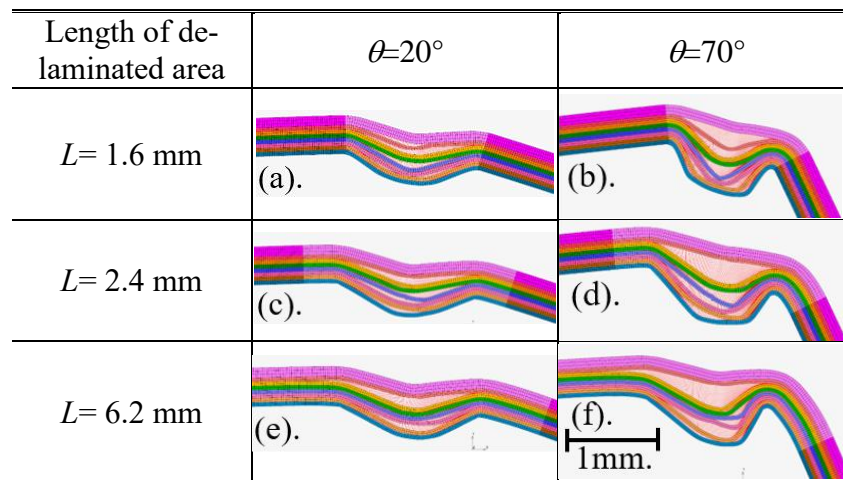


Fig. 3-28 Sectional views of the folded part of FEM model. (a)–(b): $L = 1.6$ mm, (c)–(d): $L = 2.4$ mm, and (e)–(f): $L = 6.2$ mm, the scored depth was $d_{as} = 0.2$ mm, the lamination was 8 layers, and the detaching criteria was based on the fluffing plus the shear glue of $s_t = 11$ MPa.

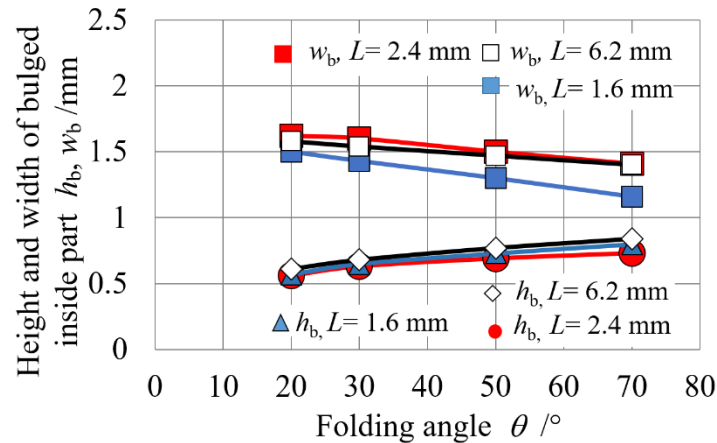


Fig. 3-29 Height and width of the bulged inside profile with respect to the folding angle.

The scored depth was $d_{as} = 0.2$ mm, the length of delaminated area was chosen as $L = 1.6, 2.4,$ and 6.2 mm, the lamination was 8 layers, the detaching criteria was based on the fluffing plus the shear glue of $s_t = 11$ MPa.

3.5.7 Effects of fluffing model on the creasing and folding process

In order to discuss with the effect of fluffing model, the full distributed version of USPRNG plus the shear strength parameter $s_t = 11.0$ MPa was compared with (a) the unused version without USPRNG in the cored zone plus the shear strength parameter $s_t = 1.63$ MPa, and (b) the unused version without USPRNG plus the shear strength parameter $s_t = 11.0$ MPa. The permanent scored depth was representatively chosen as $d_{as} = 0.1$ mm in the experiment and FEM simulation. Also, the experimental result was referred by **Fig. 3-19**. **Figure 3-30** shows the bending moment response that was mentioned above. It was found that the fluffing springs should not be removed when $d_{as} = 0.1$ mm due to insufficient scoring, and the s_t should be 11 MPa because the folding pressure is partially high and then the friction of relatively large. Therefore, the condition of $s_t = 11$ MPa and full springs is necessary.

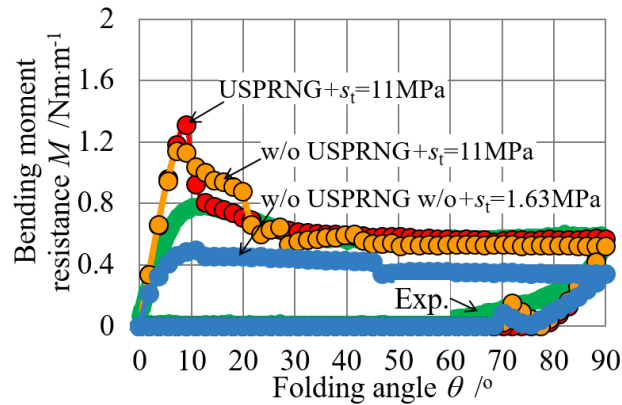


Fig. 3-30 Relationship between bending moment resistance and folding angle.

Simulated conditions were as follow: the scored depth $d_{as} = 0.1$ mm, the number of delamination was numerically performed of 8 layers, the length of delaminated zone $L = 2.4$ mm. The bonding restriction on the specified of the detaching layer (creasing area) was as follow: the detaching layer was modeled as the full length of USPRNG plus the shear strength parameter $s_t = 11.0$ MPa (based on **Fig. 3-11** and **Fig. 3-12**) (the simulated conditions were the same as that of **Fig. 3-19**), without using USPRNG plus the shear strength parameter $s_t = 1.63$ MPa and without using USPRNG plus the shear strength parameter $s_t = 11.0$ MPa.

3.5.8 Softening effect model on the creasing and folding process under the shallow indentation and the indentation depth

According to the softening area, (Li et al., 2018) described the softening area after damage beginning. They have studied the occurrence of damage of fiber-fiber bonds due to shear stress and normal stress. In this section, the authors have investigated the softening area by using the simulation model which compared to the experimental result. **Figure 3-31** and **Fig. 3-32** shows the simulation model of scoring and folding stage. All the conditions were same as that of the section 3.4.2 (FEM simulation model for scoring) and 3.4.3 (FEM simulation model for folding). In order to discuss with the softening effect model on the creasing and folding stage, the spring area of each layer was perfectly deleted at the left and right outside of the bonding area (USPRNG+ s_t) as shown in **Fig. 3-31** and **Fig. 3-32**. Here, at the left and right outside of the bonding area, it was assumed as the softening area. Moreover, the scored depth $d_{as} = 0.06$ mm (it was called as under the shallow indentation) and the scored depth $d_{as} = 0.2$ mm (it was called as under the indentation depth) were discussed.

length of USPRNG area was reasonably similar to the experimental result, whereas the bending moment resistance of the case of FEM of the specialized area (unused spring) was reasonably different for the folding angle at $\theta=10\text{--}35^\circ$. Regarding the mismatching for the folding angle at $\theta=10\text{--}35^\circ$ in the case of the specialized area (unused spring) due to the indentation is shallow, the sheared strain was too small. Then, the softening effect or shearing deformation does not contribute to make delamination in the interlayers. The threshold of delamination breakage is not performed by the small shearing strain. Another mechanism is derived from the geometrical depth of center score. Since the bending moment distribution along the beam body is not even and the right side is subjected to a large bending moment, compared to the left side due to the canti-lever bending, the right side is easily bulged as shown in **Fig 3-33** (experimental case). If the scoring depth is sufficiently deep, the unbalance of moment distribution along the beam body is relatively relaxed by the initial scoring depth.

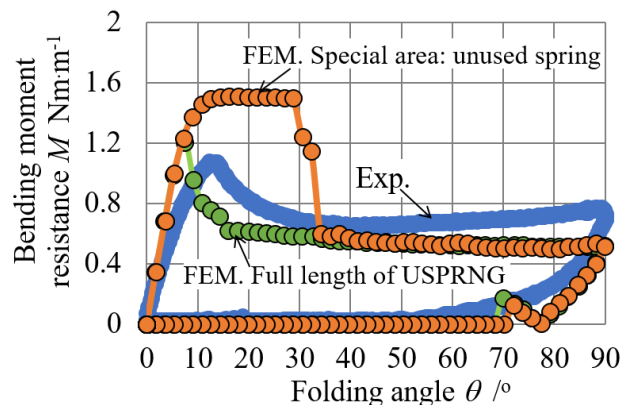


Fig. 3-33 Relationship between bending moment resistance and folding angle.

Simulated conditions were as follow: the scored depth $d_{as} = 0.06$ mm the number of delamination was numerically performed of 8 layers, the length of delaminated zone $L = 2.4$ mm. The bonding restriction on the specified of the detaching layer (creasing area) was modeled as the full length of USPRNG (based on **Fig. 3-11** and **Fig. 3-12**) and special area (unused spring) (based on **Fig. 3-31** and **Fig. 3-32**: under the creasing rule, the bonding area was 0.8mm). The detaching criteria was the fluffing plus the shear strength parameter $s_t = 11.0$ MPa.

Figure 3-34 shows the sectional views of the FEM result and the experimental result of folded parts for the folding angle of $\theta = 20^\circ, 90^\circ$. **Figure 3-34 (a)–(b)**

represented the experimental result of the folding angle at $\theta=20, 90^\circ$. **Figure 3-34 (c)–(d)** illustrated the FEM simulation result of the full length of USPRNG area at the folding angle of $\theta=20, 90^\circ$, whereas the **Fig. 3-34 (e)–(f)** illustrated the FEM simulation result of the specialized area (unused spring) at the folding angle of $\theta=20, 90^\circ$, when choosing the scored depth of $d_{as}=0.06$ mm. The FEM deformation profile seems to be slightly different with the experimental result in the cases of $d_{as}=0.06$ mm.

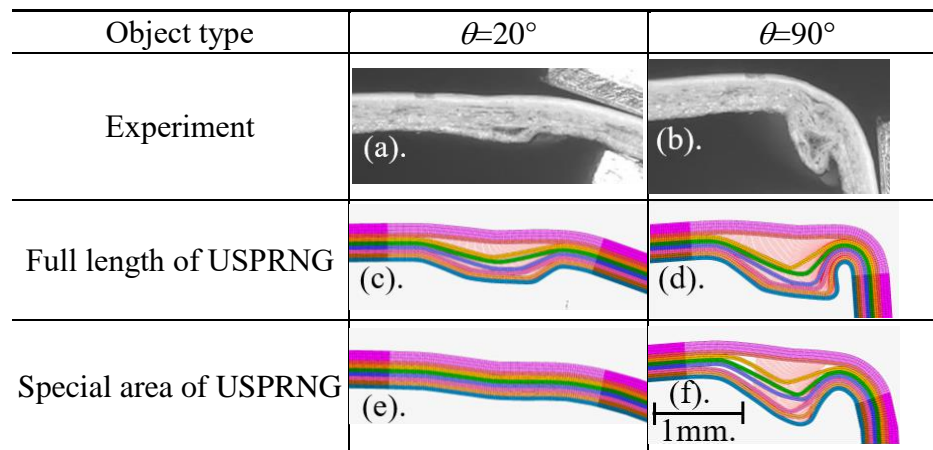


Fig. 3-34 Sectional views of the folded part of FEM model and experimental result. (a)–(b): Experiment, (c)–(d): FEM simulation model for full length of USPRNG, and (e)–(f): FEM simulation model for the specialized area (unused spring), the scored depth was $d_{as} = 0.06$ mm, the lamination was 8 layers, and the detaching criteria was based on the fluffing plus the shear glue of $s_t = 11$ MPa.

Figure 3-35 shows the relationship between the bending moment resistance M and folding angle θ when choosing the scored depth $d_{as}=0.1$ mm. Here, the FEM model conditions were as follow: the length of the delaminated area was $L= 2.4$ mm, the delamination resistance was considered into two sections. Firstly, the full length of USPRNG area as shown in **Fig. 3-11** and **Fig. 3-12** plus the shear glue parameter of $s_t= 11$ MPa. Secondary, the specialized area (unused spring) as shown in **Fig. 3-31** and **Fig. 3-32** plus the shear glue parameter of $s_t= 11$ MPa. From the **Fig. 3-35**, it was indicated in the case of the specialized area (unused spring) tended to decrease the overshoot response at the early stage ($\theta=0\sim 10^\circ$). Relatively, this partial deletion of

fluffing springs made better the bending moment response for closing to the experiment.

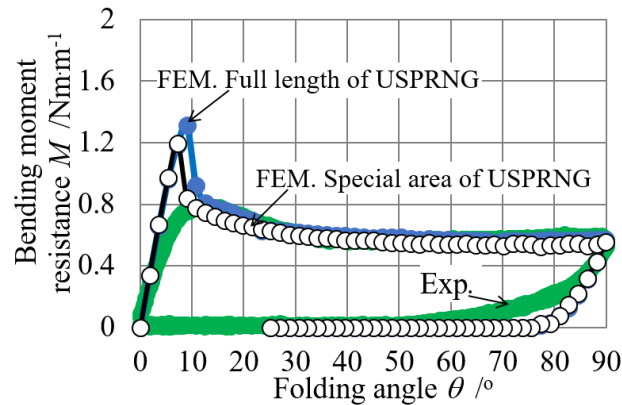


Fig. 3-35 Relationship between bending moment resistance and folding angle. Simulated conditions were as follow: the scored depth $d_{as} = 0.1$ mm, the number of delamination was numerically performed of 8 layers, the length of delaminated zone $L = 2.4$ mm. The bonding restriction on the specified of the detaching layer (creasing area) was modeled as full length of USPRNG (the simulated conditions were the same as that of **Fig. 3-11** and **Fig. 3-12**) and special area (unused spring) (based on **Fig. 3-31** and **Fig. 3-32**: under the creasing rule, the bonding area was 0.8mm). The detaching criteria was the fluffing plus the shear strength parameter $s_t = 11.0$ MPa.

Figure 3-36 shows the experimental relationship between the bending moment resistance M and folding angle θ when choosing the scored depth $d_{as} = 0.2$ mm. Here, the FEM model conditions were as follow: the length of the delaminated area was $L = 2.4$ mm, the de-lamination resistance was considered into two sections. Firstly, the full length of USPRNG area as shown in **Fig. 3-11** and **Fig. 3-12** plus the shear glue parameter of $s_t = 11$ MPa. Secondary, the specialized area (unused spring) as shown in **Fig. 3-31** and **Fig. 3-32** plus the shear glue parameter of $s_t = 11$ MPa. From the **Fig. 3-36**, it was found that the applicability of the specialized area (unused spring) has decreased a large overshoot at the early stage ($\theta = 0 \sim 15^\circ$).

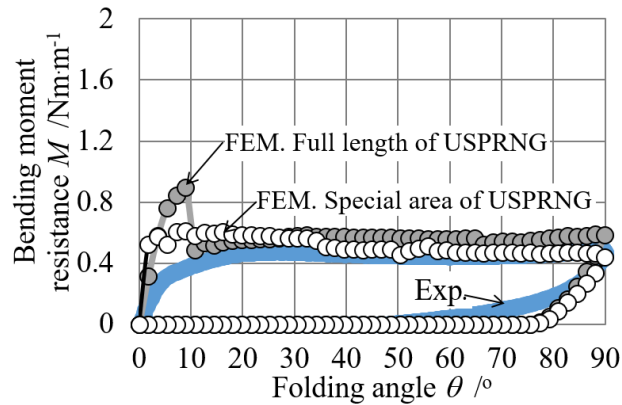


Fig. 3-36 Relationship between bending moment resistance and folding angle. Simulated conditions were as follow: the scored depth $d_{as} = 0.2$ mm, the number of delamination was numerically performed of 8 layers, the length of delaminated zone $L = 2.4$ mm. The bonding restriction on the specified of the detaching layer (creasing area) was modeled as full length of USPRNG (the simulated conditions were the same as that of **Fig. 3-11** and **Fig. 3-12**) and special area (unused spring) (based on **Fig. 3-31** and **Fig. 3-32**: under the creasing rule, the bonding area was 0.8mm). The detaching criteria was the fluffing plus the shear strength parameter $s_t = 11.0$ MPa.

Object type	$\theta=20^\circ$	$\theta=90^\circ$
Experiment	(a).	(b).
Full length of USPRNG	(c).	(d).
Special area of USPRNG	(e).	(f).

Fig. 3-37 Sectional views of the folded part of FEM model. (a)–(b): Experiment, (c)–(d): FEM simulation model for full length of USPRNG, and (e)–(f): FEM simulation model for the specialized area (unused spring), the scored depth was $d_{as} = 0.2$ mm, the lamination was 8 layers, and the detaching criteria was based on the fluffing plus the shear glue of $s_t = 11$ MPa.

Figure 3-37 shows the sectional views of the FEM and experiment folded parts for the folding angle of $\theta = 20^\circ, 90^\circ$ when choosing the scored depth of $d_{as} = 0.2$ mm. Here, the case of the experimental result was shown in the subfigures (a) and (b), the case of the full length of USPRNG area was shown in the subfigures (c) and (d), the case of the specialized area (unused spring) was shown in the subfigures (e) and (f), respectively.

Comparing the full length of USPRNG area and the specialized area (unused spring). It was found that the FEM deformation profile in the case of the specialized area (unused spring) well described the inside bulging and delamination state at the center zone.

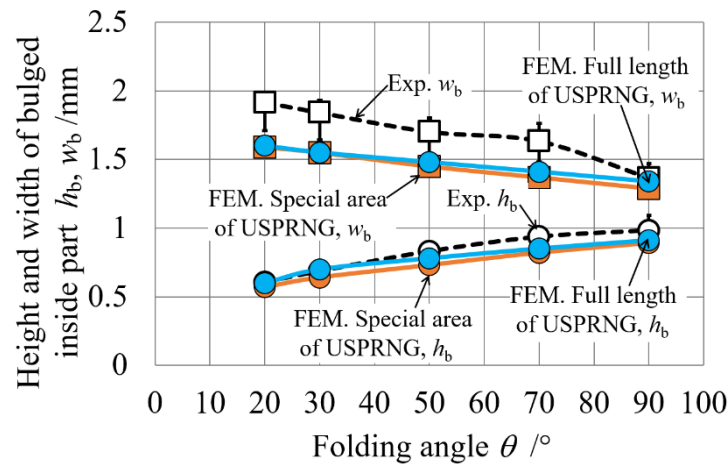


Fig. 3-38 Height and width of bulged inside profile with respect to folding angle. In the FEM simulation, the length of de-laminated area was $L = 2.4$ mm, the lamination was 8 layers, the scored depth was $d_{as} = 0.2$ mm, the detaching criteria was based on the fluffing plus shear glue of $s_t = 11$ MPa. The bonding restriction on the specified of the detaching layer (creasing area) was modeled as full length of USPRNG (based on **Fig. 3-11** and **Fig. 3-12**) and the specialized area (unused spring) (based on **Fig. 3-31** and **Fig. 3-32**: under the creasing rule, the bonding area was 0.8mm).

Figure 3-38 shows the height h_b and the width w_b of the bulged inside part of the experiment and the FEM simulation for the folding angle $\theta = 20^\circ, 30^\circ, 50^\circ, 70^\circ$ and 90° , when choosing $d_{as} = 0.2$ mm. Seeing this figure, the height h_b and the width w_b of the bulged inside part between the full length of USPRNG area and the specialized area (unused spring) were fairly similar with each other. On the other hand, the width w_b of

FEM simulation (full length of USPRNG area and the specialized area) was similar but a little smaller (15%–24%) than that of the experiment for the folding angle of 20° – 90° , while the height h_b of FEM simulation was well matched to the experimental result for the folding angle.

3.6 Conclusions

The cantilever type folding test of a creased paperboard of 0.43-mm thickness was experimentally and numerically performed by varying the indentation depth. The folding behavior of the 8 layers of the paperboard was discussed with respect to the detaching resistance based on the fluffing of ZDTT and the shear glue strength parameter s_t . In the FEM model, the bending stiffness was modeled by the in-plane tensile characteristics, and the scored depth was varied to verify the bulging behavior of creased part. The features of the developed FEM model were revealed as follows:

- (i) A combined model of the out-of-plane fluffing resistance and the in-plane shear glue resistance is necessary for determining the initial bulging mode as well as the scored geometrical profile is the primary factor at the creased part. Its bending moment resistance well matched with the corresponding experimental results for the folding angle $20^\circ < \theta < 90^\circ$.
- (ii) An appropriate shear glue strength parameter s_t was detected as $s_t/\tau_{B(\text{inMD})} = 6.7$ for the scored permanent depth of $d_{as} = 0.1$ – 0.32 mm against the thickness of $t=0.43$ mm when using the groove width of $B = 1.6$ mm. The shear resistance was predicted in a range of the lower bound shear test value and the Mises shear yield stress as the in-plane material property. In case of deep scoring, the value of shear glue parameter s_t seems to be lower bound value, while the value of s_t seems to be the upper bound value in case of shallow scoring, due to existence of a high pressure state in the de-laminated zone.
- (iii) The initial gradient of the bending moment resistance was characterized by the scored depth (geometrical condition) and the Young's modulus. Namely, the initial gradient " G_i " is determined by the combination of elastic modulus and geometrical stiffness.
- (iv) In the FEM model, the span length L of the initial delaminated area was not

sensitive enough to determine the bulging and bending moment resistance under a folding process, if $L/B > 1.5$. Here, B is the groove width. This is caused by the existence of dead point of Z character folding.

- (v) Under satisfying the experiment based bulging mode (Z character folding) at the folded portion, the bending moment resistance was characterized by the Mises yield stress for the saturated stage, $\theta > 40^\circ$. When the bulging mode was a sort of triangle form, it was a little different from the experimental result, the bending moment was also fairly different from that of Z-character mode. Hence, the bulging mode is a primary factor to determine the bending resistance.
- (vi) According to the softening effect in the case of shallow indentation ($d_{as} = 0.06\text{mm}$), the scoring did not contribute to make the delamination in the interlayers. The delamination breakage was not performed by the small shearing strain. Thus, the full assigned model of fluffing non-linear springs was suitable for simulating the bulging and bending moment resistance. In the case of middle scored depth $d_{as} = 0.1\text{-}0.2\text{mm}$, the softening effect model (partially deleted at the high strain zone) was possibly adjustable for fitting the overshoot and/or undershoot response of bending moment.
- (vii) In the case of deep indentation (scored depth $d_{as} > 0.2\text{mm}$), the scoring is sufficiently contribute to make de-lamination in the scored zone. In this state, the high strained zone can be assume to be completely detached state (fluffing non-linear spring was deleted).
- (viii) From the items (vi), (vii), the distribution of fluffing springs must be calibrated from the shearing strain distribution. In the current work, due to the restriction of MARC system (USPRING function), since a simple pattern as the partial deleting of spring assignment was possible, the partial deletion model was verified and its effect was revealed. This means that a sort of scoring history function for calibrating the fluffing non-linear springs is necessary for making remedy of unexpected overshoot at the early stage of bending moment simulation.
- (ix) As for restriction of this modeling, since the parameters in fluffing non-linear springs were considered in a certain feed velocity, when expanding this model to the higher deformation rate, the parameters must be measured furthermore.

References

- American Society for Testing and Materials (ASTM), Standards and Literature References for Composite Materials, 2nd Ed. (1990), D3846–79.
- Baum, G. A., Brennan, D. C. and Habeger, C. C., Orthotropic elastic constants of paper, *Tappi Journal*, Vol.64, No.8 (1981), pp.97–101.
- Beex, L. A. A. and Peerlings, R. H. J., An experimental and computational study of laminated paperboard creasing and folding, *International Journal of Solids and Structures*, Vol.46, No.24 (2009), pp.4192–4207, DOI: 10.1016/j.ijsolstr.2009.08.012.
- CST-J-1, Katayama Steel Rule Die Inc., Tokyo, Japan (online), available from <diemex.com/sale/cst_e.html>, (accessed on May, 2013).
- Giampieri, A., Perego, U. and Borsari, R., A constitutive model for the mechanical response of the folding of creased paperboard, *International Journal of Solids and Structures*, Vol.48, (2011), pp.2275–2287, DOI: 10.1016/j.ijsolstr.2011.04.002.
- Hicks, B. J., Mullineux, G., Berry, C., McPherson, C. J. and Medland, A. J., Energy method for modelling delamination buckling in geometrically constrained systems, *Proceedings of the Institution of Mechanical Engineers, Part C: Journal of Mechanical Engineering Science*, Vol.217, (2003), pp.1015–1026, DOI: 10.1243/095440603322407254.
- Jina, W., Nagasawa, S. and Chaijit, S., Estimation of detaching resistance of a peeled in-plane layer of a white-coated paperboard using fluffing resistance and an isotropic elasticity model, *Journal of Advanced Mechanical Design, Systems, and Manufacturing*, Vol.11, No.2 (2017), pp.1–12, DOI: 10.1299/jamdsm.2017jamdsm0018.
- Kirwan, J. M., *Handbook of Paper and Paperboard Packaging Technology*, 2nd ed. (2013), pp.280–292, Wiley-Blackwell.
- Komiyama, Y., Kon, W., Nagasawa, S. and Fukuzawa, Y., Effect of Structural Shape of Corrugated Medium on Flat Crush Characteristics of Corrugated Fiberboard, *Journal of the Chinese Society of Mechanical Engineers, Transactions of the Chinese Institute of Engineers, Series C*, Vol.34, No.4 (2013), pp.361–369.
- Li, Y., Reese, S., and Simon, J., Evaluation of the out-of-plane response of fiber networks with a representative volume element model, *Tappi Journal*, (2013), pp.1–20.

- MSC Software, Marc document: Theory and User Information), Vol. A, (2010a), pp.567–568, 655.
- MSC Software, Marc document: User Subroutines and Special Routines), Vol.D, (2010b), pp.265–267.
- Murayama, M., Nagasawa, S., Fukuzawa, Y., Yamaguchi, T. and Katayama, I., Orthotropic effect and strain dependency of paperboard on load characteristic of center bevel cutter indented on paperboard, *Journal of Materials Processing Technology*, Vol.159, (2005), pp.199–205, DOI:10.1016/j.jmatprotec.2004.03.033.
- Nagasawa, S., Fukuzawa, Y., Yamaguchi, D., Nagae, S., Katayama, I. and Yoshizawa, A., Deformation characteristics of on creasing of paperboard under shallow indentation, *Proceedings of 10th International Conference on Fracture (Advances in Fracture Research, Elsevier Sci.)* (2001), Article ID: ICF10-0202-1-6, Hawaii, USA.
- Nagasawa, S., Karasawa, M. and Fukuzawa, Y., Cutting characteristics of piled-up cardboards subjected to a wedge indentation, *Journal of Japan Society for Technology of Plasticity*, Vol.50, No.585 (2009), pp.946–950, DOI: 10.9773/sosei.50.946.
- Nagasawa, S., Komiyama, Y. and Mitsomwang, P., Finite Element Analysis of Corrugated Board on Rotary Creasing Process, *Journal of Advanced Mechanical Design, Systems, and Manufacturing*, Vol.7, (2013a), pp.103–114, DOI: 10.1299/jamdsm.7.103.
- Nagasawa, S., Mitsomwang, P., Chaijit, S. and Wongpatsa, W., Finite Element Analysis of Two Dimensional Deformation of Double-wall Corrugated Board on Creasing Process, *Proceedings of the 3rd International Symposium on Engineering, Energy and Environments*, Bangkok, (2013b), pp.338–343.
- Nagasawa, S., Yamagata, D., Fukuzawa, Y. and Murayama, M., Stress analysis of wedged rupture in surface layer of coated paperboard, *Journal of Materials Processing Technology Elsevier Science*, Vol.178, (2006), pp.358–363, DOI: 10.1016/j.jmatprotec.2006.04.116.
- Nagasawa, S., Nasruddin M. and Shiga, Y., Bending Moment Characteristics on Repeated Folding Motion of Coated Paperboard Scored by Round-Edge Knife,

- Journal of Advanced Mechanical Design, Systems, and Manufacturing, Vol.5, No.1 (2011), pp.385–394, DOI: 10.1299/jamdsm.5.385.
- Nagasawa, S., Fukuzawa, Y., Yamaguchi, T., Tsukatani, S. and Katayama, I., Effect of crease depth and crease deviation on folding deformation characteristics of coated paperboard, Journal of Materials Processing Technology, Vol.140, (2003), pp.157–162, DOI: 10.1016/S0924-0136(03)00825-2.
- Nagasawa, S., Endo, R., Fukuzawa, Y., Uchino, S. and Katayama, I., Creasing characteristic of aluminum foil coated paperboard, Journal of Materials Processing Technology, Vol.201, (2008), pp.401–407. DOI:10.1016/j.jmatprotec.2007.11.253.
- Nagasawa, S., Ozawa, S. and Fukuzawa, Y., Effects of folding numbers, scoring depth and bending velocity on bending-moment relaxation of creased paperboard, Mechanical Engineering Journal, Vol.2, No.1 (2015), pp.1–9, DOI: 10.1299/mej.14-00346.
- Nagasawa, S., Tran Xuan, Q. and Jina, W., Estimation of Bending Characteristics of Creased White-Coated Paperboard Subjected to In-Plane Compressive Load Using V-Block Fixtures, Modern Environmental Science and Engineering, Vol.2, No.4 (2016), pp.211–216, DOI: 10.15341/mese(2333-2581)/04.02.2016/001.
- Reinhard, S., Werner, A., Werner, K. and Martin, T., Chapter 17 Surface Sizing and Coating, Handbook of paper and board (ed., Holik, H.), Vol.2, (2013), pp.747–772, WILEY-VCH Verlag and KGaA, Weinheim.
- Sudo, A., Nagasawa, S., Fukuzawa, Y. and Katayama, I., Analysis of exfoliation of laminated layers and creasing deformation of paperboard, Proceedings of The Hokuriku-Shinetsu District Annual Conference of Japan Society of Mechanical Engineers, No.047-1, (2005), pp.35–36 (in Japanese), DOI: 10.1299/jsmehs.2005.42.35.

CHAPTER 4

ANALYSIS OF FOLDING PROCESS OF CREASED PAPERBOARD SUBJECTED TO IN-PLANE COMPRESSIVE LOAD USING THE COMBINATION MODEL

4.1 Introduction

In this chapter, the author intends to apply the in-plane tensile properties to simulate the in-plane compressive mode of a creased white-coated paperboard. Nagasawa et al. (2016) have demonstrated a simple evaluation method for knowing the creasing characteristics on a folded line of paperboard under an in-plane compressive load by using a set of V-Block fixtures as shown in **Fig. 4-1**. Hicks et al. (2003) reported the delamination bucking and this mechanism that was same as the V-Block bending model. Therefore, the coated paperboard is popularly used in the packaging production owing to its advantages such as a high strength-to-weight ratio, high surface smoothness, printability, sustainability including recyclability. In the production of packaging boxes, wedge-pushed cutting, creasing by the flatbed die cutter and the folding of creased lines are necessary and determine the quality of packages (Kirwan, 2013). In the development of blank patterns made of paperboard, an appropriate residual stiffness of the creased parts is necessary for preparing the fold of the paperboard in an automatic folder–gluer machine, and the creased lines must be stably folded without any surface ruptures.

Concerning the estimation of the crease deviation in the folds of eccentrically creased paperboards and the quasistatic folding stiffness concerning the creaser indentation depth were reported by (Nagasawa et al., 2001, 2008). Some bending strength testers were developed to investigate the bending moment and to record the deformation profile of the creased part during a folding process (Nagasawa et al., 2001, 2003, 2011, 2016). The bending strength testers were developed to examine the bending moment and to record the deformation characterization of the creased part during a folding process. One of the bending moment measurement apparatuses (CST-J-1, Katayama Steel Rule Die Inc., Tokyo, Japan) is effective for controlling the bending

rotation velocity and its sleeping time at a specified angle position of the creased part of a worksheet (CST-J-1, 2013; Nagasawa et al., 2015). Therefore, in this chapter, to reveal a deformation characteristic of a creased white-coated paperboard under an in-plane compressive load by using a set of V-Block fixtures. In this work, the FEM simulation was applied the in-plane tensile properties to simulate the in-plane compressive mode of a creased white-coated paperboard, an internal breaking criteria was numerically analyzed using the combination of the fluffing normal and the shear glue strength. The bending moment response and bulging mode of folded portion in the experimental have been discussed with the FEM simulation.



(a) Under compressive test (non-creasing stage) (b) Under compressive test (creasing stage)

Fig. 4-1 Deformation profile based compressive test using V-Block fixtures

4.2 Preliminary investigation and experimental methods

4.2.1 Specimens

The test specimens for this study were designed using the laminated paperboard which is composed of eight layers of bonded fibers structure. The structure of a white-coated paperboard is composed of a pulp fiber structure matrix and a clay coated layer. Some researchers have reported the coated layer is a mixture of ground calcium carbonate, kaolin, and binder, while the fiber layer consists of multiple plies (Reinhard et al., 2013). In this work, to characterize the mechanical properties of a commercially recycled white-coated paperboard which had a thickness of $t = 0.43$ (0.42-

0.44) mm and a nominal basis weight of $350 \text{ g}\cdot\text{m}^{-2}$ was chosen. Its fiber and pulp analysis were summarized in **Table 4-1**, while the in-plane tensile properties of the paperboard in the making machine direction (MD) were shown in **Table 4-2**. These mechanical properties were almost the same as that reported in the previous work (Jina et al., 2017).

Table 4-1 Size of fiber and the pulp combination ratio of white-coated paperboard 350 (measured by Kajaani-FS300) L-BKP: Broad-leaved lumber (hard wood), bleaching kraft pulp; N-BKP: Needle-leaved lumber (soft wood), bleaching kraft pulp; NTMP: Needle-leaved, thermal mechanical pulp; L(n): based on number of fibers in each fibrillation index class; L(l): based on length weighted number of fibers in each fibrillation index class; L(w): based on weight-weighted number of fibers in each fibrillation index class; CWT: Wall thickness of cell; Width: average width of fiber (Jina et al., 2017).

Unit	Pulp combination ratio/%			Projected length of fiber/mm			Size/ μm		Section area/ μm^2
	L-BKP	N-BKP	N-TMP	L(n)	L(l)	L(w)	Width	CWT	CSA
Value	64.7	16.0	19.3	0.56	0.99	1.52	18.2	4.8	256.6

Table 4-2 In-plane tensile properties of a white-coated paperboard in the machine direction (MD). Tensile feed velocity was $0.33 \text{ mm}\cdot\text{s}^{-1}$ (strain rate: 0.00183 s^{-1}). The tensile procedure was based on JIS-P8113. The average (minimum – maximum) of five samples was shown.

	Young's modulus E/MPa	Yield strength σ_Y/MPa	Tensile strength σ_B/MPa	Breaking strain ε_B
MD	5400 (5350–5460)	27.2 (26.6–27.6)	43.2 (42–43.86)	0.021 (0.02–0.022)

4.2.2 Out-of-plane detaching resistance model of specimens based on ZDTT

Out-of-plane tensile test in the thickness direction was conducted to investigate the detaching resistance of the fiber layer. Especially, the ZDTT model was applied for fixing the detaching layers (the interfaces of plies) of paperboard. Jina et al. (2017) proposed the ZDTT model to examine the peeling resistance of a weak-bonded layer of paperboard. Therefore, the relations between the tensile stress and elongation in the thickness direction was investigated by ZDTT as shown in **Fig.4-2**.

Figure 4-2 (a) indicates the schematic of the experimental apparatus of ZDTT. An acrylic-based double-sided adhesive tape NWK-15S was inserted beneath the lower worksheet and upper the worksheet for stacking the lower crosshead. The feed velocity in the experiment of ZDTT was chosen as 0.1 mm s^{-1} . In this report, the specimens were prepared 10 pieces as a square sheet with a length of $L_{\text{ZDTT}} = 10 \text{ mm}$, a width of $B_{\text{ZDTT}} = 10 \text{ mm}$, and a thickness of 0.45 mm . In this work, the average thickness of the paperboard was updated as 0.43 mm , due to a new population. **Figure 4-2 (b)** shows the tensile stress response diagram of the ZDTT and shows the fitting state between the experimental data and approximation curves. Here, the elongation e_z was subdivided into three zones: zone1, zone2, and zone3 as shown in **Fig. 4-2 (b)**. Here, $e_z (= x)$ is equal to a displacement of the lower crosshead. The tensile stress σ was approximated with e_z by using Eqs. (4-1) – (4-3), respectively (Jina et al., 2017).

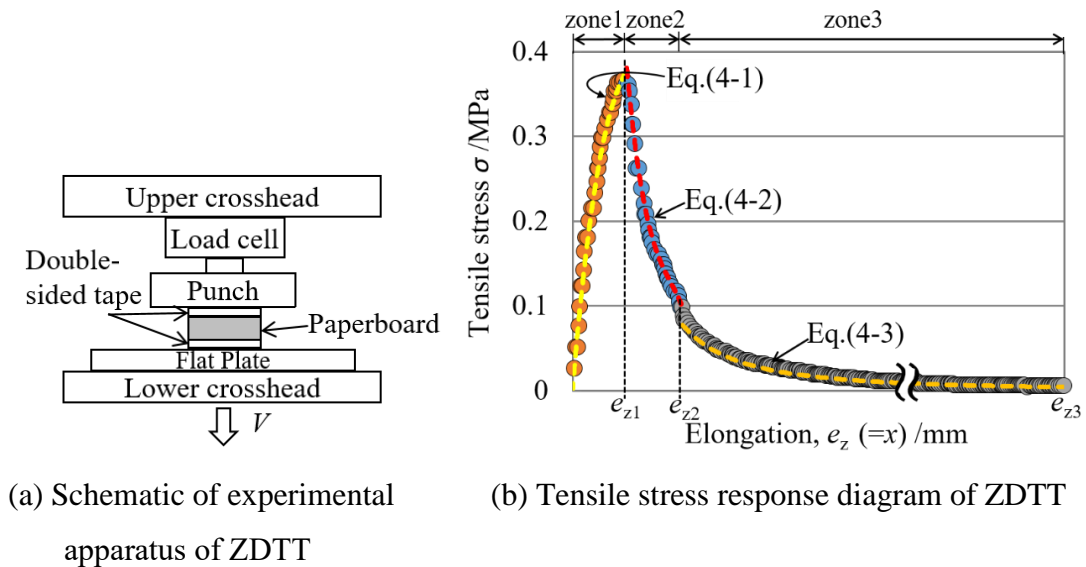


Fig. 4-2 Relationship between tensile stress and elongation in the thickness direction (Jina et al., 2017) ($t = 0.45 \text{ mm}$).

Table 4-3 shows the coefficient values of Eqs. (4-1) – (4-3). The generated thickness of the weak-bonded layer was estimated as $t_{\text{p ZDTT}} = 0.11$ ($0.10 \sim 0.11$) mm. The first zone of $0 < e_z < e_{z1}$ shows the elastic or elasto-plastic behavior before breaking at the weak-bonded layer. The zone of second and third periods of $e_{z1} < e_z < e_{z3}$ is a sort of anaphase yielding behavior which is caused by the fluffing resistance of delamination.

The nominal tensile stress σ is described with the detaching distance of e_z as Eqs.(4-1)–(4-3), and this seems to be caused by fluffing or the drawing phenomena of fibers. Therefore, the anaphase yielding resistance of ZDTT is applied to the resistance of detaching layers during a folding process of the creased part. This fluffing model can be described using a user-defined subroutine of USPRNG (MSC software, 2010a, 2010b). Here, all the side edges of the specimen were simply cut off by using a shaving knife, and any additional notches were not processed on the side edges.

$$\sigma = a_1 e_z^3 + a_2 e_z^2 + a_3 e_z + a_4 \quad (0 < e_z < e_{z1}) \quad (4-1)$$

$$\sigma = b_1 e_z^3 + b_2 e_z^2 + b_3 e_z + b_4 \quad (e_{z1} < e_z < e_{z2}) \quad (4-2)$$

$$\sigma = c_1 e_z^2 \quad (e_{z2} < e_z < e_{z3}) \quad (4-3)$$

Table 4-3 Stiffness coefficient values of Eqs. (4-1)–(4-3) (Jina et al., 2017).

e_{z1}	0.0835	e_{z2}	0.178	e_{z3}	2.192		
a_1	14.1	a_2	-5.35	a_3	0.71	a_4	0.0006
b_1	-0.56	b_2	0.27	b_3	-0.04	b_4	0.003
c_1	0.0015	c_2	-1.04				

In this user-defined subroutine, the bonding line force $f = \sigma L_{ZDTT}$ is specified by the stiffness K and the distance U between the first and second ends of the nonlinear spring, as shown in Eq. (4-4).

$$\sigma = (K \cdot L_{ZDTT}^{-1}) \cdot U \quad (4-4)$$

In the implementation of a user-defined subroutine, Eq. (4-4) was replaced with Eqs. (4-1)–(4-3) using $e_z = U$. When $U > e_{z3}$, the nonlinear spring force is defined as zero. Namely, this is the breaking criteria based on the ZDTT model.

4.2.3 Estimation of the in-plane shear strength properties

The in-plane shear yielding stress test is employed to estimate the bonding ability of the fiber structure of paperboard in the uniaxial tension test. Several reports applied the shear loading for determining the shear strength of single fiber crossings (Mohlin, 1974; Schniewind et al. 1964; McIntosh, 1963; Mayhood et al. 1962). The in-plane shear yielding stress test seems to be related to the creasing deformation. Therefore, the in-plane shear yielding test (based on ASTM-D3846-79, 1990) was conducted for estimating the breaking shear yielding stress under a free compressive state in the thickness direction. It seems to be a sort of a lower bound shear strength. On the other hand, the upper bound of shear strength is expected as the in-plane yielding shear stress of the worksheet. To investigate the lower bound shear strength, the MD direction was considered. **Figure 4-3** shows the schematic of the shearing test apparatus and the specimen size. The specimen was fixed by an acrylic-based double-sided adhesive tape NWK-15S that was inserted between the metal plate and the worksheet. The velocity in the experiment of the shearing test was chosen as $0.1 \text{ mm}\cdot\text{s}^{-1}$. The specimens were prepared as 10 pieces of a rectangle sheet, the notches of which was made by a hand knife. The specimen had an effective length of $l_{\text{dn}} = 3 \text{ mm}$ and a width of $w_s = 10 \text{ mm}$. Namely, the nominal area of the in-plane sheared zone was 30 mm^2 . The thickness of double-sided tape $t_{\text{ds}} = 0.14 \text{ mm}$ and the thickness of metal plate $t_m = 0.22 \text{ mm}$ were used. The lower side of the metal plate was fixed, whereas the upper side of the metal plate was pulled up. **Figure 4-4** shows the relationship between the nominal shear stress $\tau = P/(w_s \cdot l_{\text{dn}})$ and the displacement of the metal plate. In the figure, the shear strength $\tau_{\text{B(inMD)}}$ (lower bound) was a breaking value recorded as the maximum $\tau_{\text{B(inMD)}} = 1.63(1.23\text{--}2.03) \text{ MPa}$, whereas the in-plane MD shearing yield strength (upper bound) was estimated as $\sigma_Y/1.732 = 15.7 \text{ MPa}$ from **Table 4-2**. The strain energy with areal density until the breakage was roughly estimated as $2.2 \text{ J}\cdot\text{mm}^2$ from **Fig. 4-4**.

In this work, due to the use of a general purpose FEM code (MSC.MARC 2015), the shear-stress-yield-based glue model was employed. Since the normal breaking resistance of delaminated layers is considered as the fluffing resistance (ZDTT based nonlinear spring model), only the shear resistance of delaminated layers is considered as the glue breaking model, which is controlled by the GLUED CONTACT option

(MSC software, 2010a). The glued contact is generally released when Eq. (4-5) is satisfied. Here, τ_{if} and σ_{if} are the contact shear and normal stress, respectively. s_t , s_n , and m are the user-defined parameters of breakage. In this model, the normal resistance s_n was assumed to be 0 MPa, and then the index of m was assumed to be 2. Therefore, $s_t=11$ MPa was assumed to be as an appropriate amplified factor of the shear strength parameter s_t as mentioned in chapter 3.

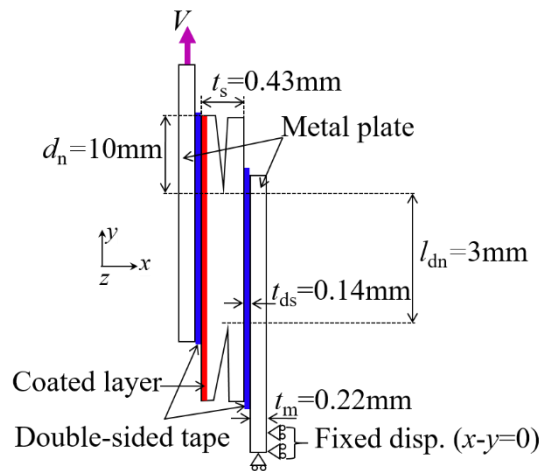


Fig. 4-3 Schematic of the shearing test apparatus

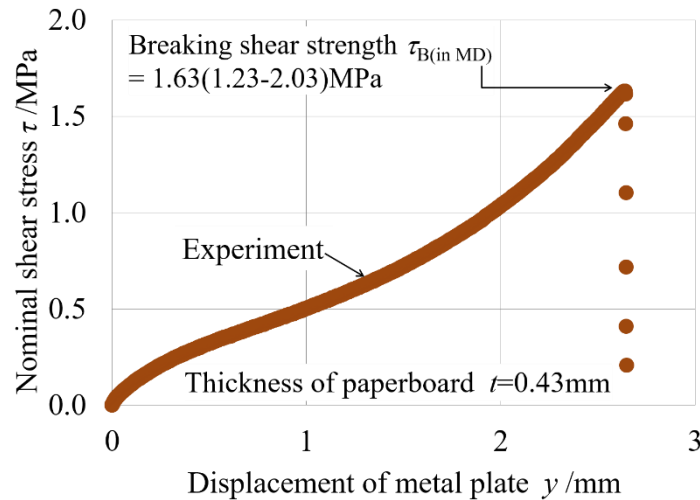


Fig. 4-4 Relation between the nominal shear stress and displacement of the metal plate in the in-plane shearing test.

When any node is released on the delaminated layer due to the breaking criteria of Eq. (4-6), the node on the delaminated layer obeys the rule of frictional CONTACT (MSC software, 2010a) between the two bodies (upper/lower layers). The contact stress

is calculated using the contact force divided by equivalent areas for shell elements. The glue breaking criteria was fundamentally defined by the in-plane shear stress of the shearing test.

$$(\sigma_{if}/s_n)^m + (\tau_{if}/s_t)^m = 1 \quad (4-5)$$

$$(\tau_{if}/s_t) = 1 \quad (4-6)$$

4.2.4 Experimental initial creasing and working conditions

The specimens were prepared as 5 pieces of a rectangle formed white-coated paperboard, which had a width of $W_{vb} = 20$ mm and length $L_{vb} = 20$ mm. All the paperboard specimens were kept at a temperature of 296 ± 1 K and a relative humidity of $50\% \pm 1\%$ in a controlled room for 24 h. The creasing stage was performed in the same room. Measurements were performed five times for each case. **Figure 4-5** shows the scoring state of a paperboard specimen using a round-edged knife (a creasing rule with a radius of $r = 0.355$ mm and thickness of $b = 0.71$ mm) with the rubber fixtures, of which the shore hardness was 40 A. The height difference (step) of rubber from the creasing rule was 1.4 mm, and the height of rubber was 7 mm. Using the paperboard thickness t and the thickness of the creasing rule b , the groove width B was empirically chosen as $2t + b = 1.6$ mm. The paperboard was scored by the creasing rule with a changing indentation depth d . The quantity $\gamma = 2d/B$ is defined here as the normalized indentation depth (Kirwan, 2013; Nagasawa et al., 2015). The creaser direction angle ϕ was chosen as 90° with respect to the MD, as shown in **Fig. 4-6**. The value of γ was chosen as 0 (none scored) and 0.7. The feed velocity was chosen as $V = 0.0167$ mm·s⁻¹. **Figure 4-7** shows the depth and width profile of the scoring process. **Figure 4-7 (a)** shows the indentation depth of creasing rule d , whereas **Figure 4-7 (b)** shows the profile after scoring, namely, the depth after scoring d_{as} and the width after scoring w_p . **Table 4-4** shows the indentation depth of creasing rule d and the profile parameters d_{as} and w_p after scoring.

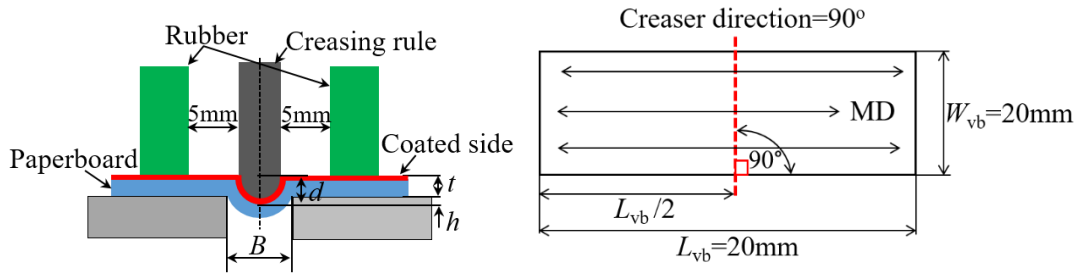


Fig. 4-5 Schematic of the scoring apparatus **Fig. 4-6** Creaser direction of paperboard

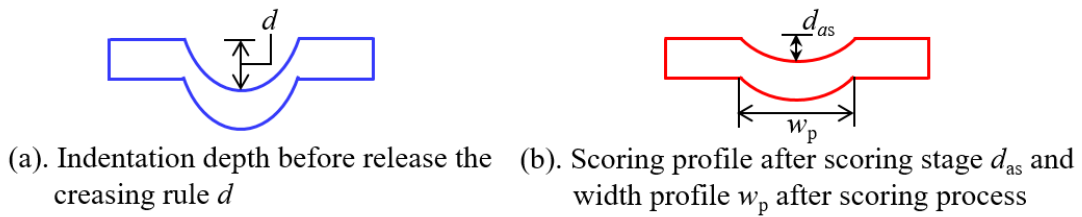


Fig. 4-7 Depth and width profile of the scoring stage.

Table 4-4 Scoring profile of experiment.

Normalized indentation depth γ	Indentation depth before release d /mm	Profile after scoring	
		Depth d_{as} /mm	Width w_p /mm
0.7	0.56	0.2 (0.18–0.2)	1.97 (1.79–2.08)

4.2.5 Experimental compressive load using V-Block fixtures

To estimate the folding characteristic which was analyzed by using the V-Block fixtures. An in-plane compressive load by using a set of V-Block fixtures were conducted. **Figure 4-8** shows an example of the deflected state of a specimen mounted on the V-Block stand apparatus and a general view of the compressive loading test (Nagasawa et al., 2016). The vertical distance of upper and lower V-Blocks was initially set up as $L_{V0} = L_{vb}$. The specimen mounted between the upper and lower of V-Block fixtures as shown in **Fig. 4-8 (a)**. **Figure 4-8 (b)** shows the loaded and deflected state of a specimen. The lower V-Block fixture was moved upward with the feed velocity $1 \text{ mm}\cdot\text{s}^{-1}$ until the deflected specimen contacted to the inside surface of V-Blocks. In this duration of compressing test, the relationship between the compressive load per unit width $F_V / W_{vb} = f_V \text{ N/mm}$ and the displacement $\delta_V = L_{V0} - L_V$ was measured. Its maximum displacement was 4.2 mm, while the equivalent of $L_{V0} = 20 \text{ mm}$. The average

rotation velocity of folding was estimated as $\omega_V = 90/360/4.2s = 0.06$ rps. **Figure 4-9** shows an example of the loading response when choosing $\gamma = 0.7$. The maximum line load $f_{V_{peak}} = F_{V_{peak}}/W_{vb}$ was detected as the buckling strength for the nominal shear strain γ , and also the saturated state load $f_{st} = f_{st}/W_{vb}$ was evaluated. Here, the maximum compressive load $f_{V_{peak}}$ was calculated as $\delta \approx 0 - 1$ mm, while the saturated state f_{st} was computed as $1 < \delta < 4.2$ mm. All the specimens were folded on the right side as shown in **Fig. 4-8 (b)**, due to the protector mounted on the left side of the lower V-Block fixture. In this investigation, a digital video camera recorded the deformation profile, and each deflected specimen was recorded when discretely choosing the folded angle α_V such as 10, 20, 30, 40 ..., 70°. The compressive line force f_V and the lateral deflection δ_V were recorded as seen in **Fig. 4-8 (b)** and **Fig. 4-9**. The equivalent bending moment of V-Block M_V was calculated using Eq. (4-7).

$$M_V = f_V \cdot \delta_V / W_{vb} \quad (4-7)$$

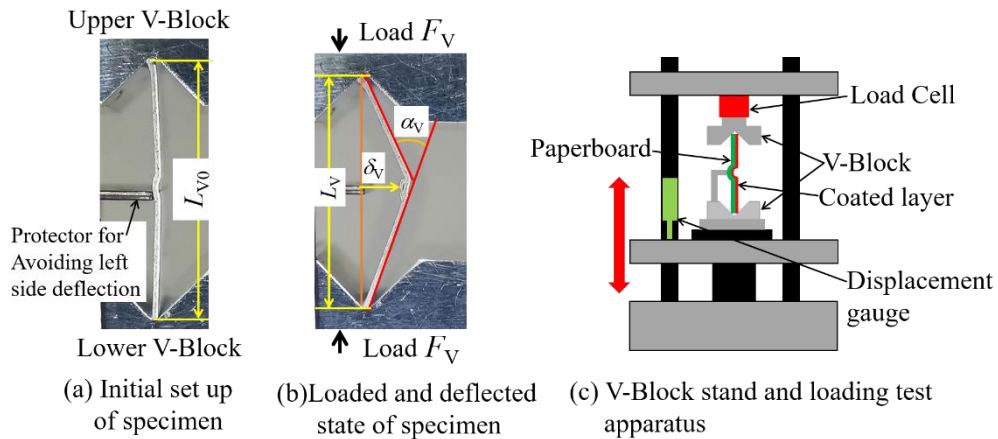


Fig. 4-8 Detail of set up of specimen and layout of V-Block stand apparatus
(Nagasawa et al., 2016)

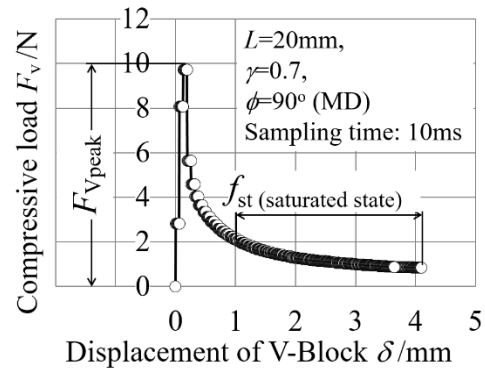


Fig. 4-9 Relationship between folding load response and displacement of V-Block

4.3 FEM simulation model

4.3.1 FEM simulation model for non-scoring

A general purpose finite element code, MSC.MARC 2015, was employed for simulating the non-scoring process. The updated Lagrange procedure and a large strain analysis were used for a two dimensional model (plane strain). The thickness of the worksheet was $t = 0.43$ mm. **Figure 4-10** shows the FEM non-scoring model based on the compressive stage. The compressive model was two dimensional (plane strain), an isotropic elasto-plastic model was assumed by using the in-plane tensile testing properties in the MD. The mesh model was made of a full model because the folding deformation was not symmetric with the center position. Here, the deformable body assumed to be the thick layer which was the thickness that of $t=0.43\text{mm}$, and the folding resistance of worksheet is characterized by the in-plane yielding stress.

The size of the specimen and boundary condition were shown in **Fig. 4-10**. The longitudinal length was assumed to be $L_{vb} = 20$ mm. The number of divided elements of the worksheet was 13600, whereas that of the total nodes was 53644. The eight-node plane strain quadrilateral element type 27 was adopted. The Young's modulus of the deformable body was assumed to be 5400 MPa from **Table 4-2**, and the Poisson's ratio was $\nu = 0.2$ (Baum et al., 1981). The yield stress was assumed to be 27.2 MPa (**Table 4-2**) and perfect-plastic. According to the friction coefficient between the deformable body and the upper-lower rigid body μ_{td} were assumed to be 0.1 as shown in **Table 4-**

5. The upper rigid body was fixed, as shown in the vertical and horizontal axes (x , y -axis) in **Fig. 4-10**, whereas the lower rigid body was moved upward in the vertical axes.

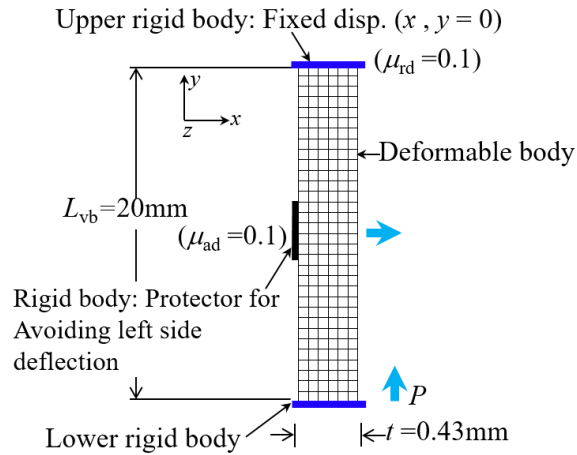


Fig. 4-10 Schematic of the non-scoring apparatus for FEM model. The interlayers were not delaminated.

4.3.2 FEM simulation model for scoring

The FEM model was employed for simulating the scoring process. The updated Lagrange procedure and a large strain analysis were used for a two dimensional model (plane strain). The thickness of the worksheet was $t = 0.43$ mm. **Figure 4-11** shows the FEM scoring model based on the experimental scoring process. Since the bending was two dimensional (plane strain), an isotropic elasto-plastic model was assumed by using the in-plane tensile testing properties in the MD. The mesh model was made of a full model because the folding deformation was not symmetric with the scored-center position. Although the mechanical properties of thickness direction are different from this isotropic model, since the scored zone is initially de-laminated and the geometrical profile is fitted to the real experimental scored depth, the bending resistance seems to be characterized by the in-plane stiffness and resistance. Here, the layer detaching resistance is considered as the bonding resistance, and the bending resistance of each layer is characterized by the in-plane yielding stress. Therefore, an appropriate of the number of plies were 8 as reported in chapter 3. The upper layer defined as the 1st layer had the thickness of $c_b = 0.11$ mm (Jina et al., 2017), whereas the other layers were defined as 0.046 mm for the 2nd–8th layers.

The breaking criteria of the bonded interfaces in the creasing zone were based on the fluffing model and the shear breaking glue model. Namely, a new combination model was introduced. The subroutine USPRNG that described the detaching resistance of ZDTT with Eqs. (4-1)–(4-3) was adopted. The shear breaking glue model was assumed to have the glue tangential strength parameter s_t chosen as 11 MPa (6.8 times of 1.63 MPa), also estimated as the Mises shear yield of $\sigma_Y/1.732 = 15.7$ MPa).

The size of the specimen and boundary condition were shown in **Fig. 4-11**. The longitudinal length was assumed to be $L_{vb} = 20$ mm. The number of divided elements of the worksheet was 13600, whereas that of the total nodes was 53644. The eight-node plane strain quadrilateral element type 27 was adopted. The Young's modulus of the deformable body was assumed to be 5400 MPa from **Table 4-2**, and the Poisson's ratio was $\nu = 0.2$ (Baum et al., 1981). The yield stress was assumed to be 27.2 MPa (**Table 4-2**) and perfect-plastic. According to the scored depth d_{as} was chosen as 0.2mm (it was called as under the indentation depth) as reported in chapter 3. Hence, the spring area of each layer was perfectly deleted from the left and right outside of the bonding area (USPRNG+ s_t) as shown in **Fig. 4-11**. It was called the softening area under the high-pressure state of the creasing rule and die. Therefore, the softening area, (Li et al., 2018) described the softening area after damage beginning. They have studied the occurrence of damage of fiber-fiber bonds due to shear stress and normal stress. Here, at the left and right outside of the bonding area, it was assumed as the softening area. Since in the case of the indentation depth under a high pressured state, the interlayers were delaminated. The deformable body comprised three parts: (1) Each layer was permanently fixed at the left and right outside, (2) The spring area of each layer was perfectly deleted at the left and right outside of the bonding area (USPRNG+ s_t) as shown in **Fig. 4-11** and (3) Each layer was bonded by the USPRING joints of Eq. (4-4) and the shear glue of Eq. (4-6) at the central creased zone. The tools were assumed to be rigid bodies as following: creasing rule (round-edge knife), die (grooved counter plate) and rubber fixtures.

Regarding the friction coefficient of tools and worksheet, the kinetic friction coefficient between the noncoated paperboard and the counter plate was 0.4 (Murayama et al., 2005). The friction coefficient of the postal cardboard against the postal cardboard was also measured as 0.5–0.7 (Nagasawa et al., 2009). In this simulation work, to avoid any unstable state of FEM execution, all the friction coefficients were assumed to be

appropriate values for each area as shown in **Table 4-5**. The friction coefficient μ_{el} with the interlayers of the paperboard was 0.7. The sliding condition of contact area against the tools was assumed to be slippery. Namely, the friction coefficients μ_b , μ_d of the creasing rule and the grooved plate (channel die) against the paperboard were 0.1. The friction coefficient μ_r of the rubber fixture against the paperboard was assumed to be zero (no friction). The edge radius of the groove was 0.1 mm, whereas the width of the groove (channel die) was 1.6 mm. The lower grooved counter plate (die) was fixed, as shown in the vertical and horizontal axes (x , y -axis) in **Fig. 4-11**.

The indentation depth of the creasing rule was chosen as shown in **Table 4-6**. Seeing **Table 4-4**, the indentation depth of creasing rule d , and the permanent depth after scoring d_{as} were fairly different with each other due to the spring back effect. It seems to be caused by the in-plane isotropic assumption of elasto-plastic behavior against the real orthotropic behavior. In order to compare the experimental result and the simulation, the permanent scoring depth based on the experimental result was approximately prepared in the simulation. Here, the $d_{as}=0.2$ mm was chosen for simulating the folding process. This parameter d_{as} was used in the simulation for discussing the folding of the worksheet as shown in **Table 4-6**. Therefore, the length of the detached zone was chosen as 2.4 mm (1.5 times of channel die width).

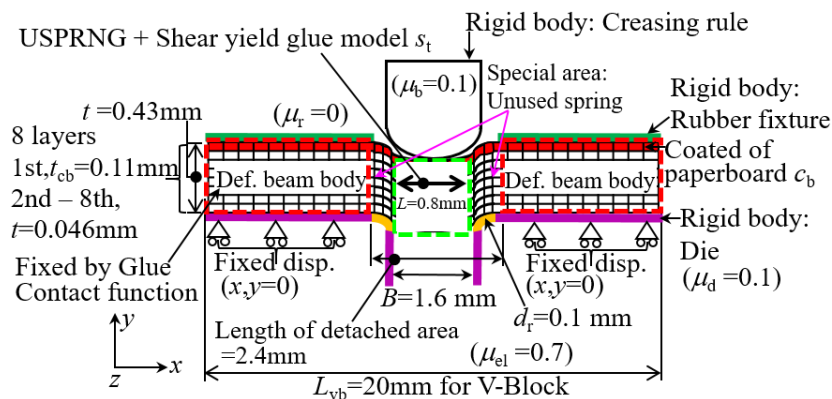
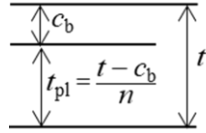


Fig. 4-11 Schematic of the scoring apparatus for FEM model. The bonding restriction on the specified of the detaching layer (bonding area under the creasing rule was 0.8mm) was modeled by the user's subroutine USPRNG using the criteria of Eqs. (4-1)–(4-3) and the shear yield glue model.

Table 4-5 Model conditions for FEM simulation.

Object type	Worksheet	Friction coefficients:
Young's modulus E /MPa	5400	$\mu_{el} = 0.7$,
Poisson's ratio	0.2	$\mu_{rd}, \mu_b, \mu_d, \mu_{vb}, \mu_{ad} = 0.1$
Yield strength σ_Y /MPa	27.2	$\mu_t = 0$ (no friction)
Thickness of worksheet t /mm	0.43	Shear strength parameter of glue joint: $s_t = 11.0$ /MPa
Thickness of 1st layer c_b /mm	0.11	
t_{pl} /mm for 2nd–8th layers, in case of $n = 7$	0.046	



Definition of the thickness of interlayers when assuming $(n+1)$ plies

t_{pl} : the thickness of each interlayer, n : the number of interlayers

Table 4-6 Scoring profile of FEM.

Indentation depth before release d /mm	Profile after scoring	
	Depth d_{as} /mm	Width w_p /mm
0.23	0.2	1.65

4.3.3 FEM simulation model for compressive load using V-Block fixtures

In order to compare with the experimental observations described in section 4.2.5 and to predict the behavior of folding and bulging of the creased part, an in-plane compressive load by using a set of V-Block fixtures was carried out as shown in **Fig. 4-12**. This simulation was taken over from the scoring stage described in section 4.3.2. Additional conditions were as follows: the friction coefficient of the upper-lower V-Block fixtures against the paperboard μ_{vb} was 0.1, the protector for avoiding left side deflection against the paperboard μ_{ad} was 0.1. Here, the upper-lower V-Block fixtures and the protector for avoiding left side deflection were assumed to be rigid bodies. The upper V-Block fixture was fixed, as shown in the vertical and horizontal axes (x, y-axis) in **Fig. 4-12**, whereas the lower V-Block fixture was moved upward in the vertical axes. The maximum displacement was 4.2 mm. The loadcase properties were as follows: the total loadcase time was 4.2 seconds, the constant time step was chosen as 0.021 seconds for each step in the simulation and the total increment was 200 steps for simulating the folding stage.

The simulation was discussed as follows: (i) in order to verify the applicability of the in-plane tensile properties that was applied to the bending mode as discussed in

chapter 3. In this chapter, the in-plane tensile properties and the combination of the fluffing normal and the shear glue strength $s_t=11$ MPa were applied to the compressive mode by using a set of V-Block fixtures as shown in **Fig. 4-12**. (ii) The bending moment response and the bulged profile were discussed with the experimental results.

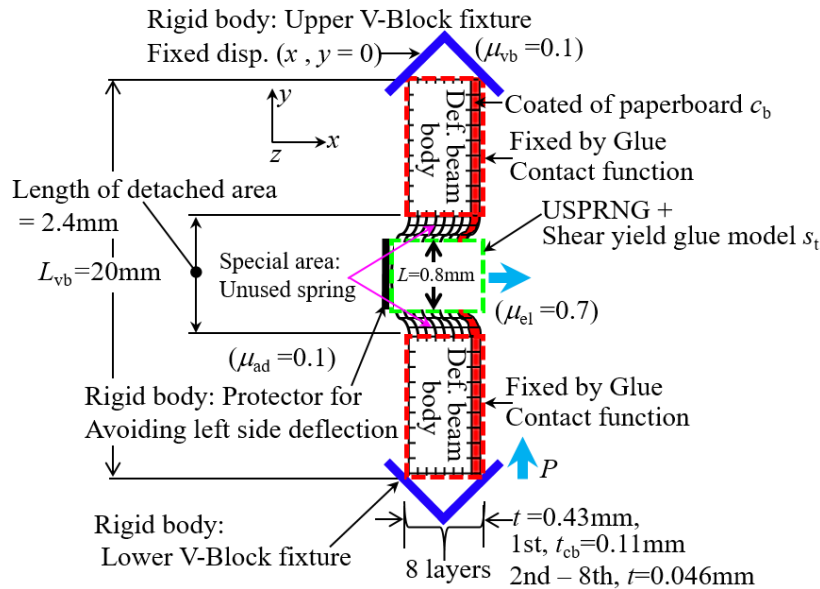


Fig. 4-12 Size definition and boundary condition of FEM V-Block model. The bonding restriction on the specified of the detaching layer (the bonding area under the creasing rule was 0.8mm) was modeled by the user's subroutine USPRNG using the criteria of Eqs. (4-1)–(4-3) and the shear yield glue model.

4.4 Estimation method of bending moment response under compressive load using V-Block fixtures

The bending moment response under compressive load using V-Block fixtures was derived by **Fig. 4-13**. The component of force was composed of the force in the vertical (F_v) and horizontal (F_h) directions. In the **Fig. 4-13** shows the estimation method of the force in the vertical (F_v) and horizontal (F_h) directions. The bending moment response was estimated by using the Eq. (4-8). Therefore, the present calculation (FEM) is an ideal condition. Due to in the experiment is difficult to estimate the force in the horizontal direction (F_h). Hence, the relationship between the force in the vertical and deflection of the worksheet ($F_v \times \delta_v$) is a part of the component force,

not full component. The occurrence of the bending moment response must be based on F_v , and F_h component is a new discussion. The mismatching of $F_v \times \delta_v$ between the experiment and FEM result is another problem.

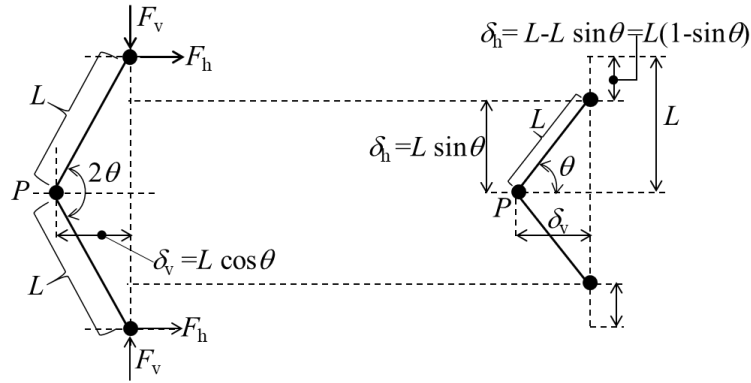


Fig. 4-13 Estimation method of force in the vertical (F_v) and horizontal (F_h) directions

$$\begin{aligned}
 M &= F_v \times \delta_v + F_h \times \delta_h \\
 &= F_v \times L \cos \theta + F_h \times L \sin \theta \\
 &= L \times (F_v \cos \theta + F_h \sin \theta) / W_{vb}
 \end{aligned} \tag{4-8}$$

4.5 Results and discussion

4.5.1 Experimental compressive load using V-Block fixtures

Figure 4-14 shows the relationship between compressive load and displacement of the lower V-Block fixture when choosing the scored depth $d_{as} = 0$ mm (non-scored) and $d_{as} = 0.2$ mm. The compressive load tended to decrease with the scored depth d_{as} . It was found that in the case of the F_{vpeak} of $d_{as} = 0$ mm was higher than that of the $d_{as} = 0.2$ mm. The ratio of $d_{as} = 0$ mm by $d_{as} = 0.2$ mm was about 2.4 times, and the f_{st} of $d_{as} = 0$ mm was higher than that of the $d_{as} = 0.2$ mm. The ratio of $d_{as} = 0$ mm by $d_{as} = 0.2$ mm was about 3.6 times.

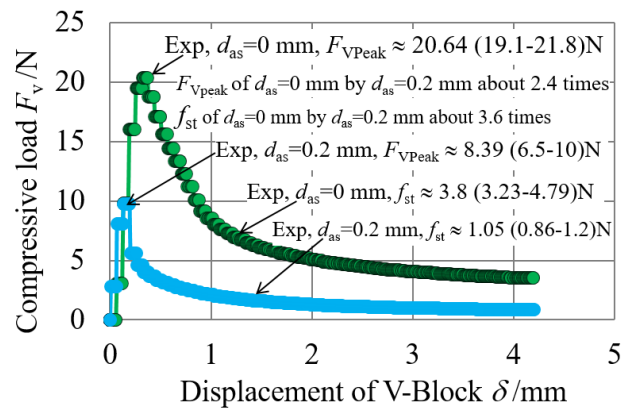


Fig. 4-14 Relationship between compressive load and displacement of lower V-Block fixture in the experiment when choosing $d_{as}=0$ and 0.2 mm.

4.5.2 Compressive load response of the worksheet on the simulation model using V-Block fixtures

Figure 4-15 shows the relationship between compressive load and displacement of the lower V-Block fixture. In the case of FEM simulation was shown the force in the vertical direction (F_v). Here, the permanent scored depth was representatively chosen as $d_{as}=0$ mm (non-scored). When choosing the $d_{as}=0$ mm, in the case of the F_{vpeak} of FEM simulation was higher than that of the experimental result. The ratio of FEM by experiment was about 12.9 times, and the f_{st} of FEM was higher than that of the experimental result. The ratio of FEM by experiment was about 2.2 times. **Figure 4-16** shows the relationship between compressive load and displacement of the lower V-Block fixture of FEM simulation. Therefore, the force in the horizontal direction (F_h) of $d_{as}=0$ mm was about 0.64N. Its value quite small compared to the force in the vertical direction (F_v). Since the shape of lower rigid body assumed to be the flat shape. The authors avoided the unstable state in the FEM simulation. Hence, the flat shape of the lower rigid body was applied.

Figure 4-17 shows the relationship between compressive load and displacement of the lower V-Block fixture. In the case of FEM simulation was shown the force in the vertical direction (F_v). When choosing the $d_{as}=0.2$ mm, in the case of the F_{vpeak} of FEM simulation was higher than that of the experimental result. The ratio of FEM by experiment was about 4.8 times, and the f_{st} of FEM was higher than that of the experimental result. The ratio of FEM by experiment was about 3.7 times. **Figure**

4-18 shows the relationship between compressive load and displacement of the lower V-Block fixture. In the case of FEM simulation was shown the force in the horizontal direction (F_h). When choosing the $d_{as}=0.2$ mm, in the case of the $F_{h\text{peak}}$ of FEM simulation was higher than that of the $F_{v\text{peak}}$ of the experimental result. The ratio of FEM by experiment was about 3.8 times, and the f_{st} of FEM was higher than that of the experimental result. The ratio of FEM by experiment was about 3.7 times.

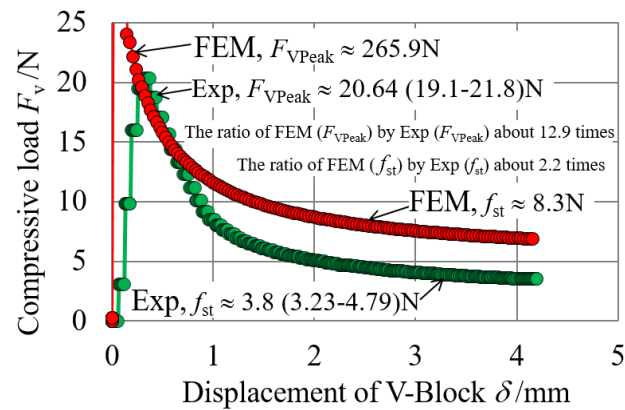


Fig. 4-15 Relationship between compressive load and displacement of lower V-Block fixture. In the case of FEM simulation was shown the force in the vertical direction (F_v). Simulated conditions were as follow: the scored depth $d_{as} = 0$ mm (non-scored), the number of layers 8, and the detaching criteria of interlayer was not delaminated.

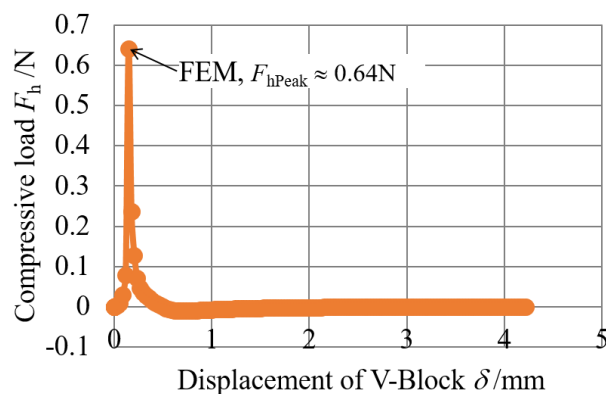


Fig. 4-16 Relationship between compressive load and displacement of lower V-Block fixture. In the case of FEM simulation was shown the force in the horizontal direction (F_h). Simulated conditions were as follow: the scored depth $d_{as} = 0$ mm (non-scored), the number of layers 8, and the detaching criteria of interlayer was not delaminated.

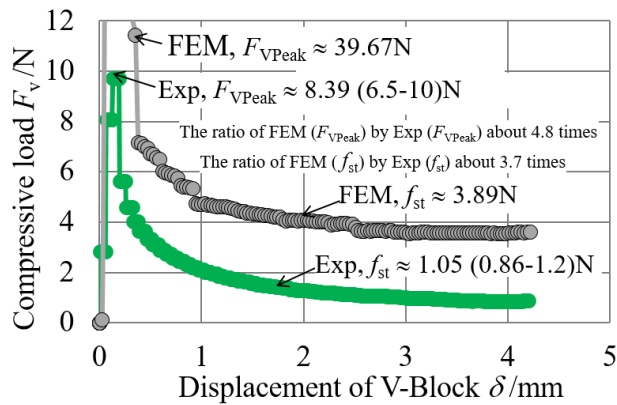


Fig. 4-17 Relationship between compressive load and displacement of the lower V-Block fixture. In the case of FEM simulation was shown the force in the vertical direction (F_v). Simulated conditions were as follow: the scored depth $d_{as} = 0.2$ mm, the number of layers 8, the length of delaminated zone $L = 2.4$ mm, and the detaching criteria (bonding area under the creasing rule was 0.8mm) was the fluffing plus the shear strength parameter $s_t = 11.0$ MPa.

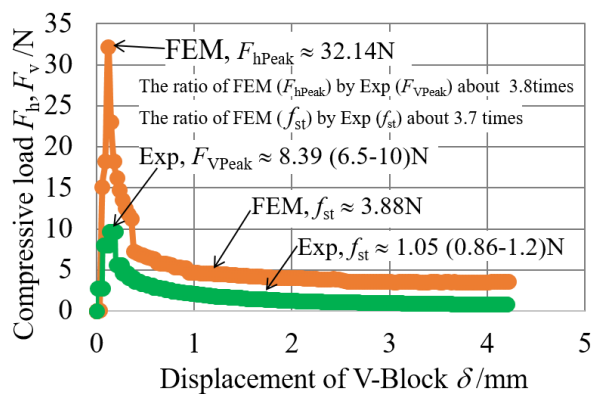


Fig. 4-18 Relationship between compressive load and displacement of the lower V-Block fixture. In the case of FEM simulation was shown the force in the horizontal direction (F_h). Simulated conditions were as follow: the scored depth $d_{as} = 0.2$ mm, the number of layers 8, the length of delaminated zone $L = 2.4$ mm, and the detaching criteria (bonding area under the creasing rule was 0.8mm) was the fluffing plus the shear strength parameter $s_t = 11.0$ MPa.

4.5.3 Equivalent bending moment response under compressive load using V-Block fixtures for non-scoring

Figure 4-19 shows the relationship between bending moment resistance M_v under the compressive load and folding angle α_v of the paperboard. Here, the non-scored depth was representatively chosen as $d_{as}=0$ mm in the experiment and FEM simulation. In order to verify the plastically collapse moment M_{PC} . The M_{PC} was estimated using Eq. (4-9). Therefore, the M_{PC} of the in-plane tensile properties in MD was calculated as $1.26 \text{ Nmm}\cdot\text{mm}^{-1}$. Comparing the M_{PC} in the in-plane tensile properties and the simulation result as shown in **Fig. 4-19** they are also reasonably similar between each other. Regarding the experimental result as shown in **Fig. 4-19** the bending moment response at the folding angle $\alpha_v > 30^\circ$ tended to be remarkably smaller than that of the simulation result.

$$M_{PC} = \sigma_Y \cdot t^2/4 \quad (4-9)$$

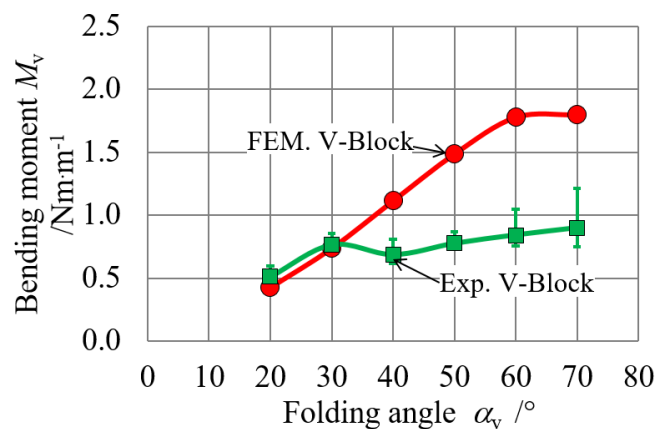


Fig. 4-19 Relationship between bending moment resistance under the compressive load and folding angle. Simulated conditions were as follow: the scored depth $d_{as} = 0$ mm (non-scored), the number of layers 8, the length of delaminated zone $L = 2.4$ mm, and the detaching criteria (bonding area under the creasing rule was 0.8mm) was the fluffing plus the shear strength parameter $s_t = 11.0$ MPa.

Figure 4-20 shows the vector diagrams of maximum σ_{p1} (tensile state) and minimum σ_{p2} (compressive state) principal stresses at the folding angle of 70° for $d_{as} = 0$ mm (non-scored). Seeing the **Fig. 4-20 (a)** the upper side was shown the tensile state σ_{p1} , whereas the **Fig. 4-20 (b)** the lower side was shown the compressive state σ_{p2} .

Figure 4-21 show contour band diagrams with the magnitude of the maximum σ_{p1} and minimum σ_{p2} principal stresses when choosing the folding angle of 70° for $d_{as} = 0$ mm (non-scored). Here, the case of tensile state σ_{p1} was shown in the subfigure (a), the case of compressive state σ_{p2} was shown in the subfigure (b), respectively. From this figure, the subsequent features were shown: (i) A high tensile state, shown by the yellow band ($\sigma_{p1} > 38.54$ MPa), was detected in the upper zone. (ii) A high compressive stress was distinguished in the center of the lower zone.

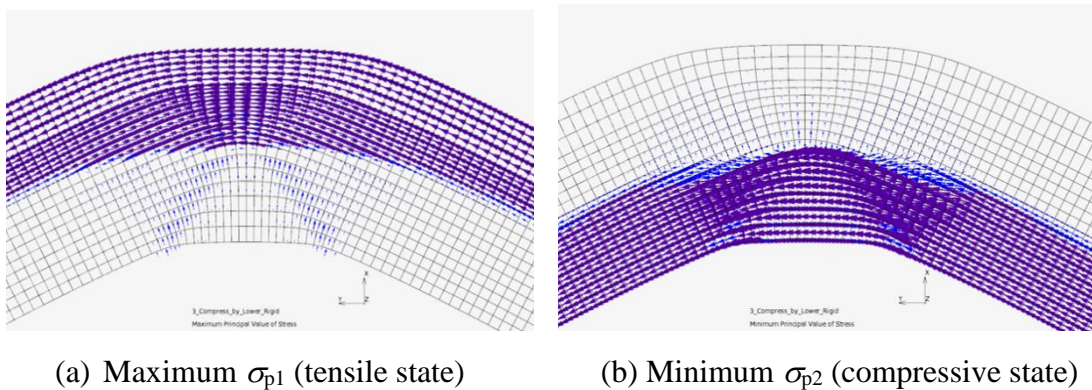


Fig. 4-20 Vector diagrams of σ_{p1} and σ_{p2} principal stresses at the folding angle of 70° for $d_{as} = 0$ mm (non-scored).

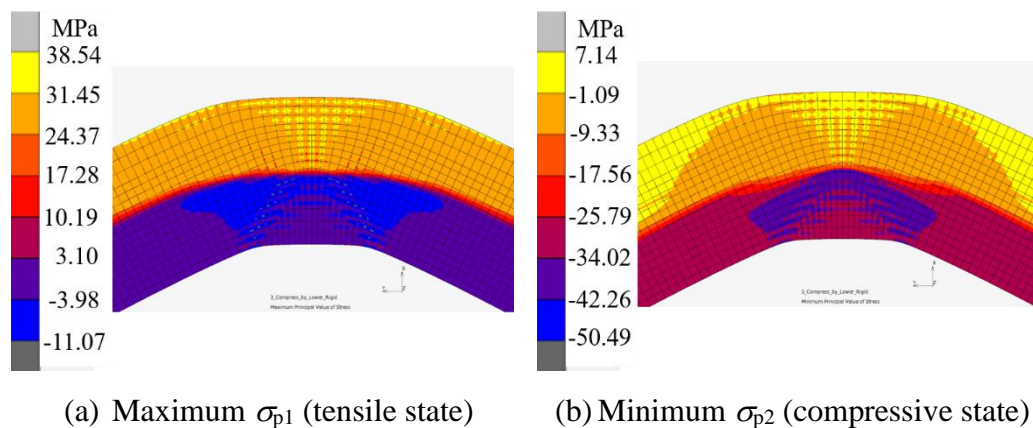


Fig. 4-21 Contour band diagrams of σ_{p1} and σ_{p2} principal stresses at the folding angle of 70° for $d_{as} = 0$ mm (non-scored).

Figure 4-22 shows the norm of σ_{p1} and σ_{p2} were detected along the center of the thickness direction. The σ_{p1} was estimated in length between of 0–0.27mm, whereas the

σ_{p2} was estimated in length between of 0.29–0.43mm. The average value of σ_{p1} was 33.13 MPa, whereas the σ_{p2} was -35.87 MPa

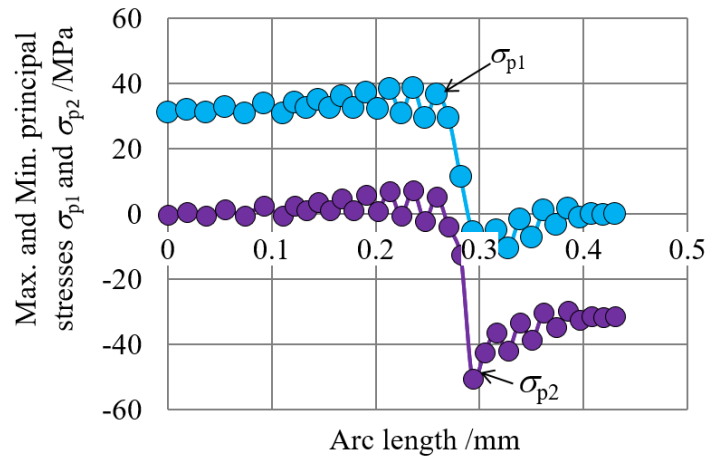


Fig. 4-22 Magnitude of σ_{p1} and σ_{p2} principal stress of worksheet at the folding angle of 70° for $d_{as} = 0$ mm (non-scored).

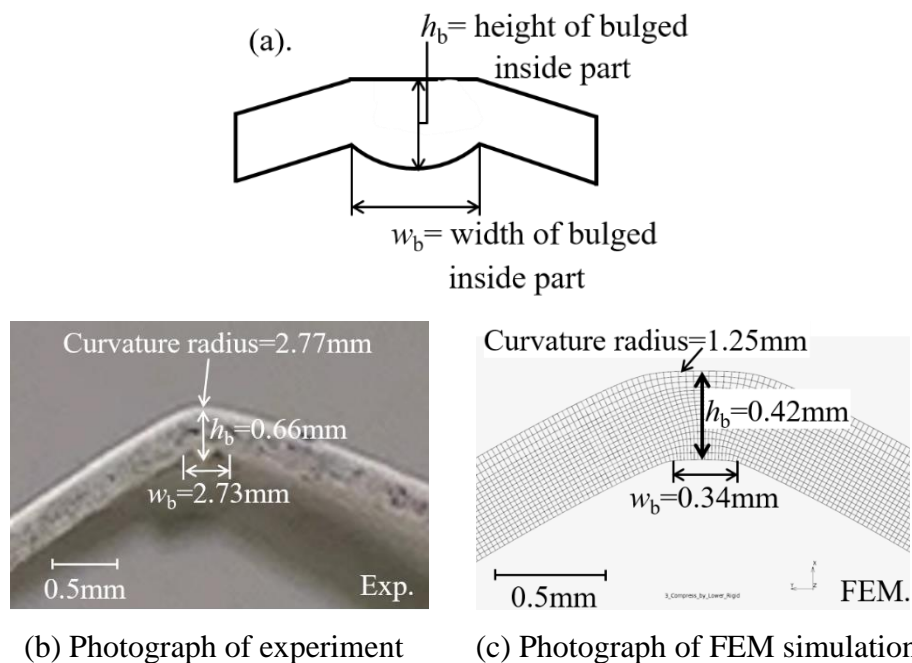


Fig. 4-23 Sectional views of folded part of paperboard in the FEM simulation and experimental result with respect to 70° . (a) Definition of the height and the width for the bulged profile. (b): experiment. (c): FEM simulation. In the FEM simulation, the interlayers were not delaminated.

According to the mismatching between the FEM simulation and the experimental result for the folding angle larger than 30° , this mismatch seems to be caused by the mismatching of the curvature radius, the height of bulged inside part h_b and the width of bulged inside part w_b as shown in **Fig. 4-23**. **Figure 4-23** shows the sectional views of the FEM and experiment folded parts for the folding angle of $\theta = 70^\circ$.

4.5.4 Equivalent bending moment response under compressive load using V-Block fixtures for scoring

Figure 4-24 shows the relationship between bending moment resistance M_v under the compressive load and folding angle α_v of the paperboard. Here, the scored depth was representatively chosen as $d_{as}=0.2$ mm in the experiment and FEM simulation.

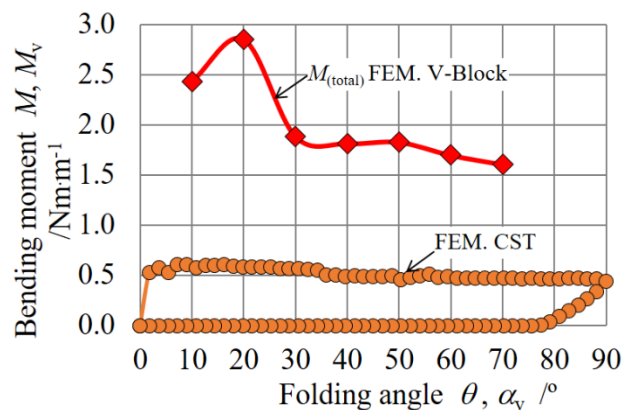


Fig. 4-24 Relationship between bending moment resistance under the compressive load of FEM-V-Block and FEM CST concerning the folding angle. Simulated conditions were as follow: the scored depth $d_{as} = 0.2$ mm, the number of layers 8, the length of delaminated zone $L = 2.4$ mm, and the detaching criteria (bonding area under the creasing rule was 0.8mm) was the fluffing plus the shear strength parameter $s_t = 11.0$ MPa.

To convert the force of each direction to the bending moment response of FEM V-Block. The FEM V-Block was discussed with the force in the vertical (F_v) and horizontal (F_h) directions. Then the summation of the force in the vertical (F_v) and horizontal (F_h) were discussed with the FEM-CST that was mentioned in chapter 3.

Hence the Eq. (4-8) was applied to convert the bending moment response. It was found that the FEM simulation based bending moment of FEM V-Block under compressive load tended to be remarkably larger than that of the FEM-CST as shown in **Fig. 4-24**.

Figures 4-25 show contour band diagrams with the magnitude of the maximum (principal) shear stress τ_{pmax} of FEM-V-Block at the folding angle of 70° . Seeing the contour band diagrams, the Mises shear stress (yielding level) of $15.7 \text{ MPa} = \sigma_y/\sqrt{3}$ occurred at the contact zone of interlayers. This seems to be caused by the frictional shear sliding under a high pressured contact with the interlayers. Namely, it is found that the shear strength parameter s_t does not determine the maximum shear stress, but affects the early stage slipped pattern of interlayers.

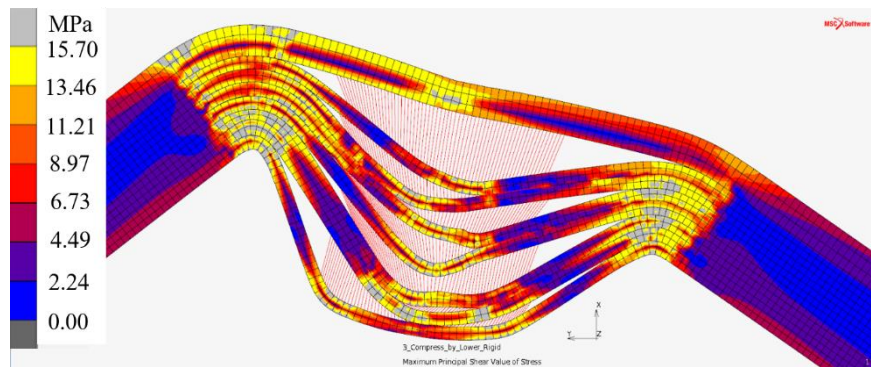


Fig. 4-25 Contour bands diagram of the maximum shear stress τ_{pmax} when choosing $s_t = 11.0 \text{ MPa}$ for the folding angle of 70° . Other simulated conditions were as follows: the scored depth $d_{as} = 0.2 \text{ mm}$, the length of delamination zone $L = 2.4 \text{ mm}$, and detaching criteria (bonding area under the creasing rule was 0.8mm) was the fluffing plus the shear strength.

Figure 4-26 shows the sectional views of the FEM and experiment folded parts of V-Block for the folding angle of $\theta = 20^\circ, 50^\circ, 70^\circ$. **Fig. 4-26 (a)** defines the height h_b and the width w_b of bulged inside part. **Figure 4-26 (b)–(d)** illustrated the experimental result at the folding angle of $\theta = 20, 50^\circ, 70^\circ$. **Figure 4-26 (e)–(g)** illustrated the FEM simulation result at the folding angle of $\theta = 20, 50^\circ, 70^\circ$. Here, the FEM model conditions were as follow: the length of the delaminated area was $L = 2.4 \text{ mm}$, the de-lamination resistance was considered as the fluffing model of USPRNG plus the shear glue parameter of $s_t = 11 \text{ MPa}$. The bonding area under the creasing rule

was 0.8mm. Seeing these figures, it was shown that the FEM deformation profile was well described the inside bulging and delamination state of the experimental result.

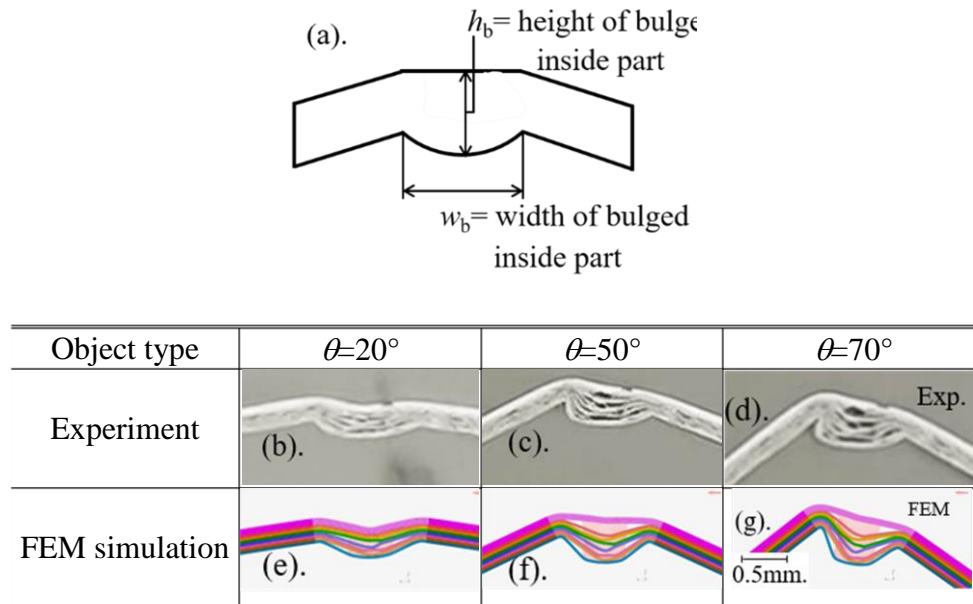


Fig. 4-26 Sectional views of folded part of paperboard in the FEM simulation and experimental result with respect to 20° , 50° and 70° . (a) Definition of the height and the width for the bulged profile. (b) - (d): experiment. (e) - (g): FEM simulation. In the FEM simulation, $L = 2.4$ mm, the lamination was 8 layers, and the detaching criteria (bonding area under the creasing rule was 0.8mm) was based on the fluffing resistance plus shear glue of $s_t = 11$ MPa.

Figure 4-27 shows the height h_b and the width w_b of the bulged inside part of the experiment and the FEM simulation for the folding angle $\theta = 20^\circ, 30^\circ, 50^\circ$ and 70° . Seeing this figure, the width w_b of FEM simulation was similar but a little smaller (11%–12%) than that of the experiment for the folding angle of 20° – 70° , while the height h_b of FEM simulation was almost matched to the experimental result for the folding angle.

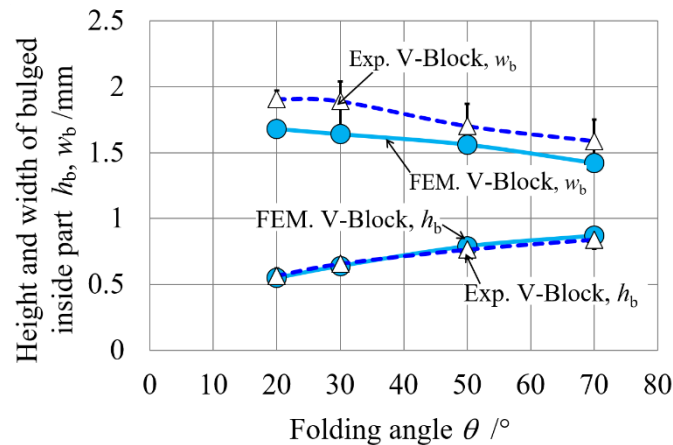


Fig. 4-27 Height and width of bulged inside profile with respect to folding angle. In the FEM simulation, the length of the de-laminated area was $L = 2.4$ mm, the lamination was 8 layers, the scored depth was $d_{as} = 0.2$ mm, the detaching criteria (bonding area under the creasing rule was 0.8mm) was based on the fluffing plus shear glue of $s_t = 11$ MPa.

4.6 Conclusions

The applicability of the in-plane tensile properties was applied to an in-plane compressive load test of a creased white-coated paperboard through the FEM simulation. The compressive load test of a 0.43-mm-thick coated paperboard was investigated by varying the scored depth $d_{as} = 0$ and 0.2 mm using a set of upper/lower V-Block fixtures. Through these investigations, the followings were revealed.

(i) According to the experimental results, the compressive load tended to decrease with the scored depth d_{as} .

(ii) In the case of the scored depth $d_{as} = 0$ mm (non-scored), the bending moment at the folding angle 60° and 70° is controlled by the value of the yield strength.

(iii) The combination of the fluffing normal and the shear glue strength $s_t = 11$ MPa was well described the bulging mode of folded portion in the experimental result for the scored depth of $d_{as} = 0.2$ mm.

References

- American Society for Testing and Materials (ASTM), Standards and Literature References for Composite Materials, 2nd Ed, Philadelphia, PA, D3846-79, (1990).
- Baum, G. A., Brennan, D. C. and Habeger, C. C., Orthotropic elastic constants of paper, *Tappi Journal*, Vol.64 No.8 (1981), pp.97–101.
- CST-J-1, Katayama Steel Rule Die Inc., Tokyo, Japan (online), available from <diemex.com/sale/cst_e.html>, (accessed on May, 2013).
- Hicks, B.J.,Mullineux, G.,Berry, C.,McPherson, C.J.,and Medland, A.J., Energy method for modelling delamination buckling in geometrically constrained systems. *Proceedings of the Institution of Mechanical Engineers, Part C: Journal of Mechanical Engineering Science* 217, (2003), pp.1015–1026.
- Jina, W., Nagasawa, S. and Chaijit, S., Estimation of detaching resistance of a peeled in-plane layer of a white-coated paperboard using fluffing resistance and an isotropic elasticity model, *Journal of Advanced Mechanical Design, Systems, and Manufacturing*, Vol. 11, No.2 (2017), pp.1–12.
- Kirwan, J. M., *Handbook of Paper and Paperboard Packaging Technology* 2nd ed., (2013), pp.280-292, Wiley-Blackwell.
- Li, Y., Reese, S., and Simon, J., Evaluation of the out-of-plane response of fiber networks with a representative volume element model, *Tappi Journal*, (2013), pp.1–20.
- Mayhood C. H, Kallmes O. J, Cauley M. M. Measured Shear Strength of Individual Fiber to Fiber Contacts. *Tappi* 1962; 45 (1): 69.
- McIntosh D. C. Tensile and Bonding Strengths of Loblolly Pine Kraft Fibers Cooked to Different Yields. *Tappi* 1963; 46 (5): 273.
- Mohlin U.-B. Determination of interfibre bond strength. *Svensk Papperstidning* 1974; 77 (4): 131.
- MSC Software, *Marc document: Theory and User Information*), Vol. A, (2010a), pp.567–568, 655.
- MSC Software, *Marc document: User Subroutines and Special Routines*), Vol.D, (2010b), pp.265–267.
- Murayama, M., Nagasawa, S., Fukuzawa, Y., Yamaguchi, T. and Katayama, I., Orthotropic effect and strain dependency of paperboard on load characteristic of

- center bevel cutter indented on paperboard, *Journal of Materials Processing Technology*, Vol. 159, (2005), pp. 199–205, DOI:10.1016/j.jmatprotec.2004.03.033.
- Nagasawa, S., Endo, R., Fukuzawa, Y., Uchino, S. and Katayama, I., Creasing characteristic of aluminum foil coated paperboard, *Journal of Materials Processing Technology*, Vol. 201, (2008), pp.401-407. Doi:10.1016/j.jmatprotec.2007.11.253.
- Nagasawa, S., Fukuzawa, Y., Yamaguchi, D., Nagae, S., Katayama, I. and Yoshizawa, A., Deformation characteristics of on creasing of paperboard under shallow indentation, *Proceedings of 10th International Conference on Fracture, (Advances in Fracture Research, Elsevier Sci.)*, (2001), Article ID: ICF10-0202-1-6, Hawaii, USA.
- Nagasawa, S., Fukuzawa, Y., Yamaguchi, T., Tsukatani, S. and Katayama, I., Effect of crease depth and crease deviation on folding deformation characteristics of coated paperboard, *Journal of Materials Processing Technology*, Vol. 140, (2003), pp. 157-162, DOI: 10.1016/S0924-0136(03)00825-2.
- Nagasawa, S., Karasawa, M. and Fukuzawa, Y., Cutting characteristics of piled-up cardboards subjected to a wedge indentation, *Journal of Japan Society for Technology of Plasticity*, Vol.50, No.585 (2009), pp.946–950, DOI: 10.9773/sosei.50.946.
- Nagasawa, S., Nasruddin M. and Shiga, Y., Bending Moment Characteristics on Repeated Folding Motion of Coated Paperboard Scored by Round-Edge Knife, *Journal of Advanced Mechanical Design, Systems, and Manufacturing*, Vol. 5, No.1 (2011), pp.385–394, DOI: 10.1299/jamdsm.5.385.
- Nagasawa, S., Ozawa, S. and Fukuzawa, Y., Effects of folding numbers, scoring depth and bending velocity on bending-moment relaxation of creased paperboard, *Mechanical Engineering Journal*, Vol. 2, No.1 (2015), pp.1-9.
- Nagasawa, S., Tran Xuan, Q. and Jina, W., Estimation of Bending Characteristics of Creased White-Coated Paperboard Subjected to In-Plane Compressive Load Using V-Block Fixtures, *Modern Environmental Science and Engineering*, Vol. 2, No.4 (2016), pp.211–216, Doi: 10.15341/mese(2333-2581)/04.02.2016/001.

Reinhard, S., Werner, A., Werner, K., and Martin, T., Chapter 17 Surface Sizing and Coating, Handbook of paper and board (ed., Holik, H.), Vol.2, (2013), pp.747-772, WILEY-VCH Verlag and KGaA, Weinheim.

Schniewind A. P, Nemeth L. J, Brink D. L. Shear Strength of Single-Fiber Crossings. Tappi 1964; 47 (4): 244.

CHAPTER 5

CONCLUSIONS AND PROSPECTS

5.1 Conclusions

In this research work, the author aims to develop a numerical simulation model of the folding process of a creased paperboard and to reveal the deformation characteristics of the creased paperboard. Therefore, in this work, in order to characterize the delamination and bulging deformation, an internal breaking criteria was numerically analyzed using a new combination model. A general purpose finite element method (FEM) code was applied to develop a combination model comprising the out-of-plane fluffing subroutine and the in-plane shear glue strength. To verify the folding mechanics of the creased part, the following methods were considered: (i) an internal breaking criteria and transient de-lamination of a weak-bonded layer of paperboard was experimentally investigated through a peel cohesion test (PCT). (ii) A cantilever type bending moment measurement apparatus was experimentally examined the creased part of paperboard. (iii) A simple evaluation method has been developed for knowing the creasing characteristics on a folded line of paperboard under an in-plane compressive load by using a set of V-Block fixtures. Through experimental and numerical results, the following features were disclosed:

In chapter 2, When, the stiffness coefficient value was derived by the z-directional (out-of-plane) tensile test (ZDTT), which applied to the peeling model. It was found that FEM simulation results showed good similarity with experimental results and revealed that the peeling deformation of the coated paperboard. Equivalent fibers based fluffing model that were derived from a ZDTT experiment (approximated as discretely distributed nonlinear springs) well explains the existence of the peak point of peeling force and saturated peel resistance.

In chapter 3, as for the deformation characteristics of the creased paperboard, the experimental and FEM simulation results disclosed the following characteristics: first, the initial gradient of the bending moment resistance is characterized by the scored depth. Second, a combined model of the out-of-plane fluffing resistance and the in-plane shear glue well matched with the corresponding experimental results. Third, the

applicability of the specialized area (unused spring area) was applied to reduce the overshoot response at the folding stage, because a high sheared strain state was intensively / partially generated by the indentation of creaser knife against the worksheet supported by the rectangular groove. Such a high sheared state was extremely delaminated as observed in the experimental result. Fourth, the in-plane shear glue strength characterizes the deformation pattern of delaminated zone in the folding process of the scored zone. The shear strength parameter s_t does not determine the maximum shear stress, but affects the early stage slipped pattern of interlayers. As the result, the formation of bulged layers was affected by the shear strength parameter s_t . Finally, FEM simulation results showed that an appropriate shear glue strength parameter s_t was chosen as $s_t/\tau_{B(\text{inMD})} \approx 6.7$ for the scored depth of $d_{\text{as}} = 0.1\text{--}0.32$ mm when using the groove width of $B = 1.6$ mm.

In chapter 4, when the in-plane tensile properties were applied to the compressive mode of a creased white-coated paperboard, the breaking criterion based on a combined model of the out-of-plane fluffing resistance and the in-plane shear glue. The FEM simulation and the experimental result were found that the compressive load tended to decrease with the scored depth d_{as} . In the case of the FEM simulation, the bending moment response is controlled by the value of the yield strength. The combination of the fluffing normal and the shear glue strength was well described the bulging mode of folded portion in the experimental.

5.2 Prospects

The FEM simulations of folding mechanics of the creased part were conducted and discussed based on the detaching resistance of a white-coated paperboard. In this study, the stiffness coefficient value of the interlayer was derived by the z-directional (out-of-plane) tensile test (ZDTT), which applied to the peeling and folding model. The detaching resistance was estimated with a fluffing model using a finite element method (FEM) code. Since this fluffing model is not limited to apply to any dissimilar laminated solid materials, therefore, it can be applied to another material such as carbon fiber, milk carton and composite materials, and also possibly be applied to analyze the non-linear folding mechanics of a new laminated material.

Appendix A

User-defined subroutine of USPRNG

How to write the User Subroutine code

- 1.) To write and edit the source code by using the editor's software such as Notepad++, Force 2.0, Eclipse, Simple Fortran, etc.
- 2.) After choosing the above software, then write the source code as shown in **Fig A.**
- 3.) Save file as .f file.

```

1:      SUBROUTINE USPRNG(RATK,F,DATAK,U,TIME,N,NN,NSPRNG)
2:      IMPLICIT REAL*8 (A-H, O-Z)
3:      DIMENSION RATK(2), DATAK(2), U(2), TIME(2), N(2), F(2)
4: c RATK(1) : is the ratio of the present value of spring stiffness to the
5: c data value given in the option input; to be defined by the user
6: c U(1) : For mechanical springs
7: c F(1) : is the force to be defined by the user: spring force
8:      D=U(1)
9:      IF(D. LE. 0.0835) GO TO 1
10:     IF(D. GT. 0.0835. AND. D. LE. 0.1781) GO TO 2
11:     IF(D. GT. 0.1781. AND. D. LE. 2.1918) GO TO 3
12:     IF(D. GT. 2.1918) GO TO 4
13: c ez1
14:     1 RATK(1)=0.
15:     F(1)=14.1*D*D*D-5.35*D*D+0.71*D+0.0006
16:     GO TO 98
17: c ez2
18:     2 RATK(1)=0.
19:     F(1)=-0.56*D*D*D+0.27*D*D-0.04*D+0.003
20:     GO TO 98
21: c ez3
22:     3 RATK(1)=0.
23:     F(1)=0.0015*D**(-1.04)
24:     GO TO 98
25:     4 RATK(1)=0.
26:     F(1)=0.
27:     GO TO 98
28: c
29:     98 write(6,*) "user subroutine I love you"
30:     RETURN
31:     END
32:
33:

```

Fig. A.1 User-defined subroutine of USPRNG

How to call the User Subroutine file on MARC Mentat 2015

- 1.) After preparing the FEM model and User Subroutine code.
- 2.) Select No.1 (Job1) as shown in **Fig. A2.**
- 3.) Select No.2 (Run) as shown in **Fig. A3.**
- 4.) Select No.3 (User Subroutine File) as shown in **Fig. A4.**
- 5.) Select No.4 (User Subroutine File) as shown in **Fig. A4.**
- 6.) Select No.5 (Save Model) as shown in **Fig. A4.**
- 7.) Select No.6 (Submit (1)) as shown in **Fig. A4.**

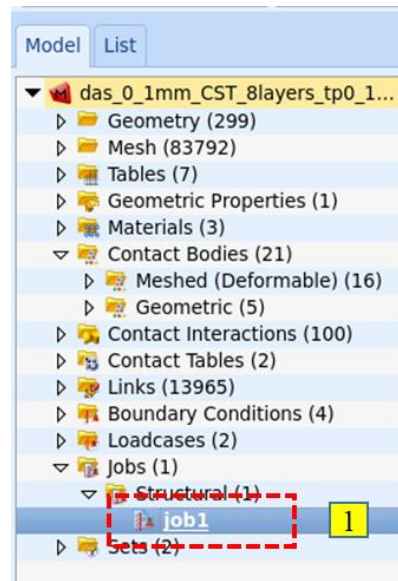


Fig. A.2

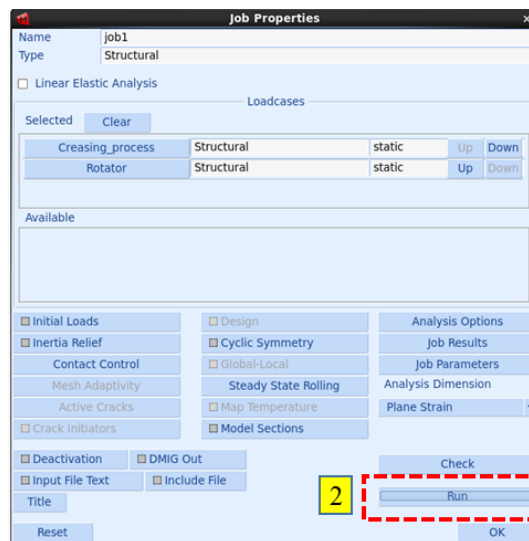


Fig. A.3

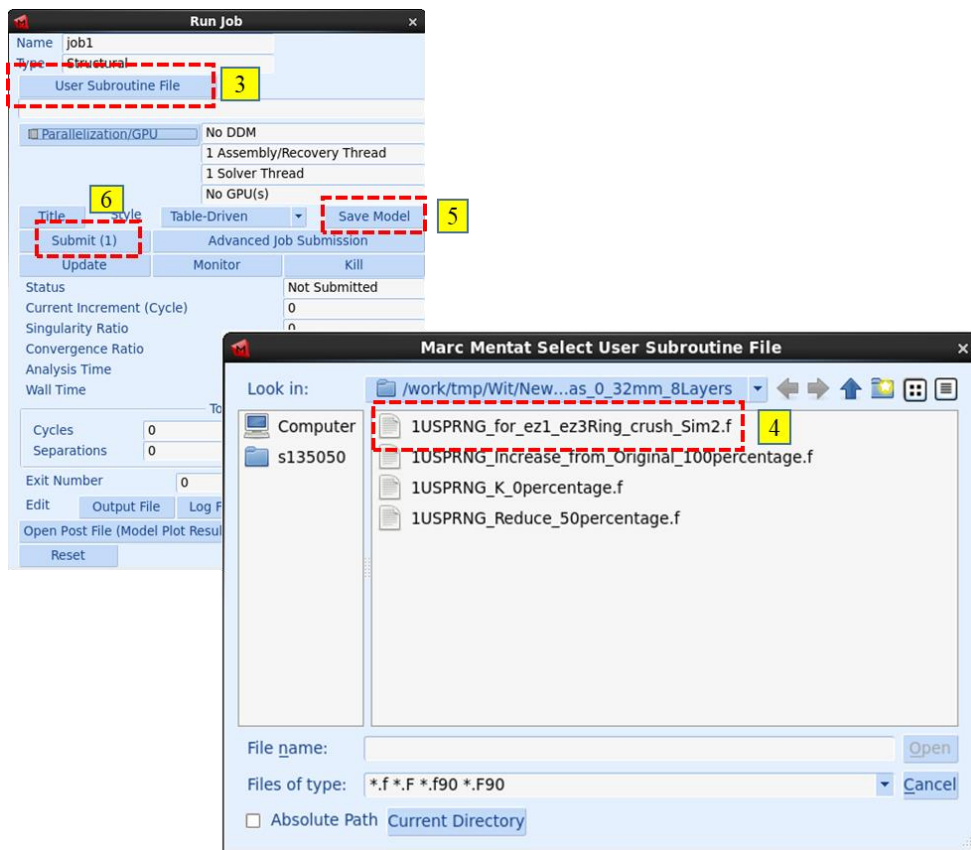


Fig. A.4

How to check the output file of the User Subroutine on MARC Mentat 2015

- 1). Open result file (file name .out) in Excel or WordPad.
- 2). To check the correctness of the source code that was combined with the FEM model, search the sentence (user subroutine I love you) as shown in **Fig. A5**.
- 3). The sentence as shown in **Fig. A5** that means the FEM simulation was completed.

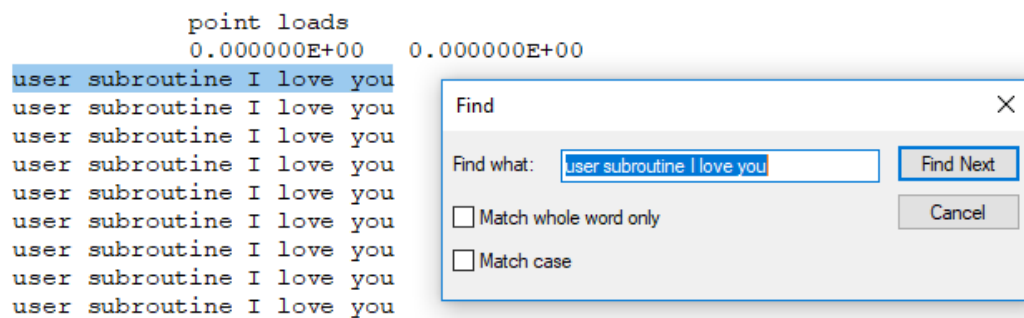


Fig. A.5

Appendix B

Apparatuses and tools

Table B.1 Lists of apparatuses and tools


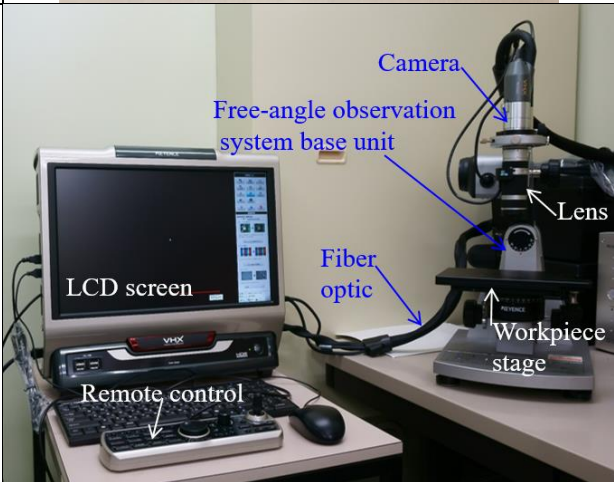
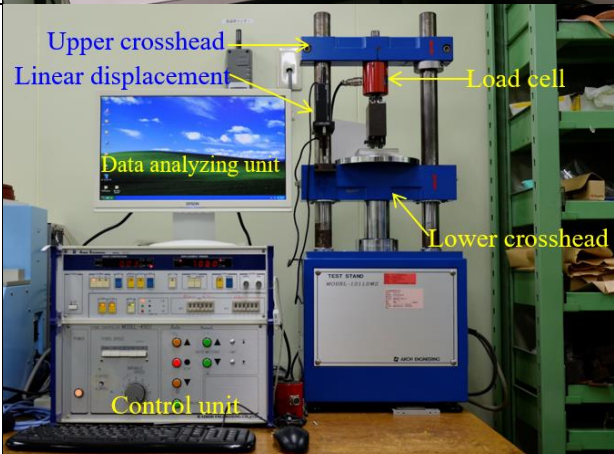
Apparatus/ tool	Photograph of apparatus/tool	Specification/ capacity
Double-sided adhesive tape (NWK - 15 S)		Adhesive: acrylic type. Thickness: 0.14 mm.
Optical microscope (VHX-2000)		<ul style="list-style-type: none"> - Power supply: 100 ~ 240VAC 50/60HZ, 340VA max. - Shutter speed = 1/15 ~ 1/19000 s. - Image sensor: 2.11 million-pixels.
Compression machine (Aiko engineering machine, model 1311DWS)		<ul style="list-style-type: none"> - Power supply: 100 VAC 50/60HZ - Load cell: 50N, 50kgf, 500kgf.

Table B.1 Lists of apparatuses and tools (Continued)

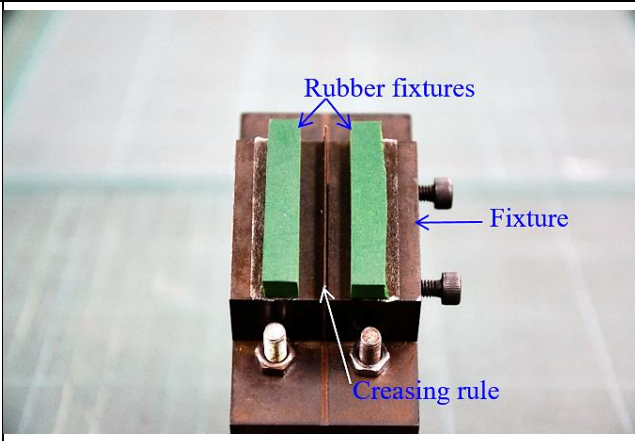
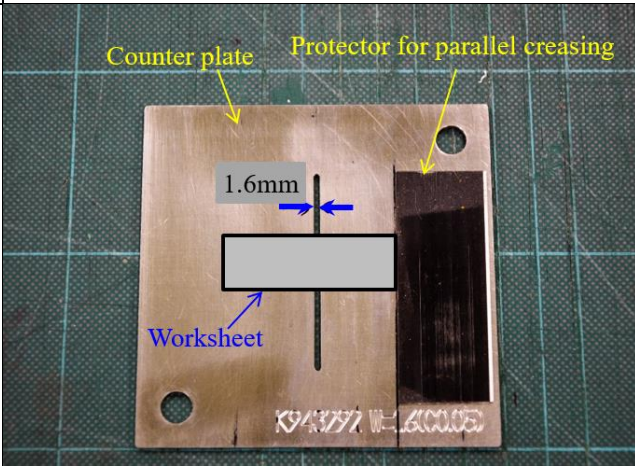
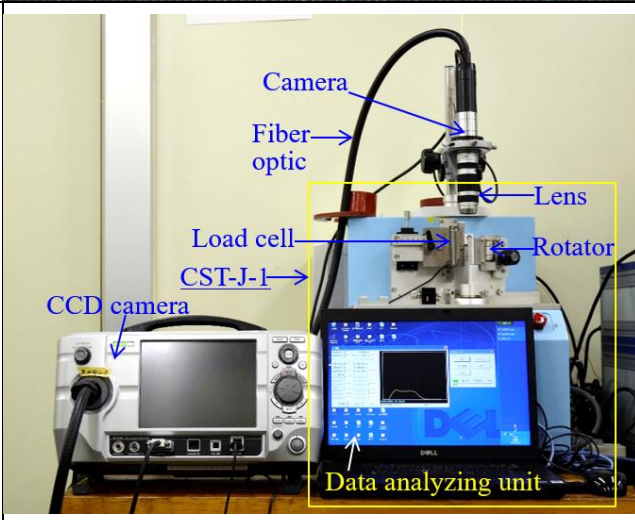
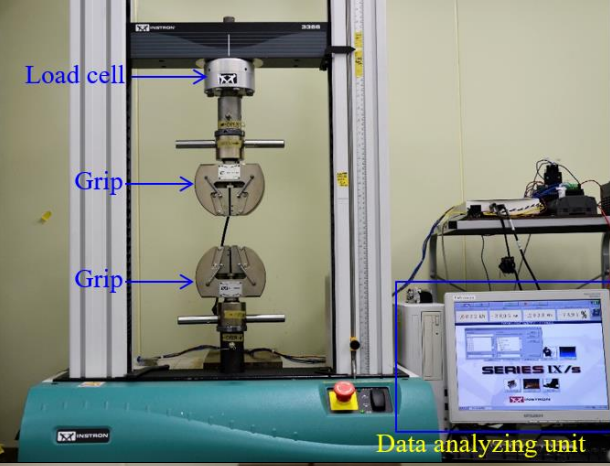
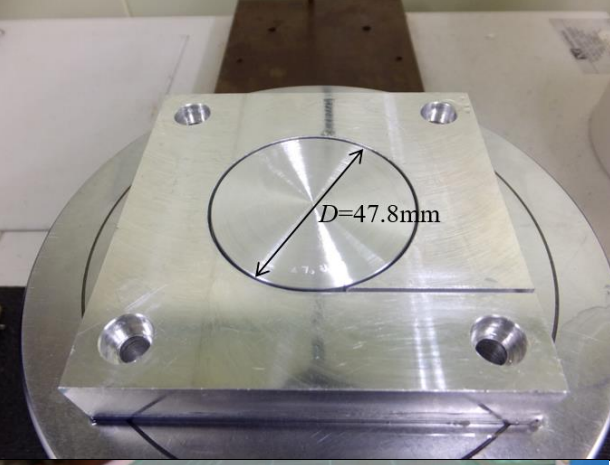
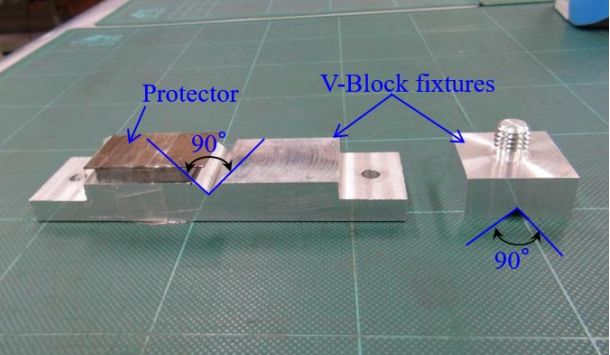
Apparatus/ tool	Photograph of apparatus/tool	Specification/ capacity
Rubber fixtures and creasing rule		<ul style="list-style-type: none"> - Thickness of creasing rule: 0.71mm, radius of creasing rule: 0.355mm. - Hardness of creasing rule: 600HV. -Shore hardness of rubber fixtures: 40A.
Die (grooved counter plate)		<ul style="list-style-type: none"> -Counter plate: SUS630. -Width of groove: 1.6mm. -Chamfer: 0.16mm. -Hardness of counter plate: 510HV.
Bending stress tester system (CST-J-1)		<ul style="list-style-type: none"> - Power supply: 100VAC 50/60HZ -Maximum load 10N. - Measurement Speed: 0-1 rotation/second (1 rotation 36000PULS) -Measurement angle: 1-130°

Table B.1 Lists of apparatuses and tools (Continued)

Apparatus/ tool	Photograph of apparatus/tool	Specification/ capacity
Universal testing machine (Instron 3366)		<ul style="list-style-type: none"> - Capacity of load cell = 10 kN. - Max. testing speed = 500 mm·min⁻¹. - Vertical test space = 1193 mm.
Schematic diagram of ring crush test		<ul style="list-style-type: none"> -Standard: JIS-P8126, 2005. - Diameter of annular groove: 47.8mm. - Depth of groove:6.34mm
V-Block fixtures		<p>Compressive test material: Aluminum AA5051</p>

Appendix C

List of publications

List of journal publications

- [1] Nagasawa, S., Tran Xuan, Q. and Jina, W., Estimation of Bending Characteristics of Creased White-Coated Paperboard Subjected to In-plane Compressive Load Using V-block Fixtures, *Modern Environmental Science and Engineering*, Vol. 2, No. 4, 2016, pp. 211-216.
- [2] Jina, W., Nagasawa, S. and Chaijit, S., Estimation of detaching resistance of a peeled in-plane layer of a white-coated paperboard using fluffing resistance and an isotropic elasticity model, *Journal of Advanced Mechanical Design, Systems and Manufacturing*, Vol. 11, No. 2, 2017, pp. 1-12.
- [3] Jina, W. and Nagasawa, S., Finite Element Analysis of Folding Process of Creased White-coated Paperboard using Combination Model of Fluffing Resistance and Shear Yield Glue, *Journal of Advanced Mechanical Design, Systems and Manufacturing*, Vol. 12, No. 2 , 2018, pp. 1-15.

List of international conferences

- [1] Jina, W., Mitsomwang, P., Nagasawa, S. and Chaijit, S., Estimation of detaching yield resistance in the contact area on peeling model of white-coated paperboard, *The 4th International GIGAKU Conference in Nagaoka*, Nagaoka University of Technology, Niigata, Japan, (2015), MO-17, pp.116.
- [2] Jina, W. and Nagasawa, S., Introduction to processing analysis of ductile resin sheet based on elasto-plastic dynamics subjected to punch/die shearing., *Daihatsu automobile company*, Osaka, Japan, (2016).
- [3] Nagasawa, S., Uehara, M., Matsumoto, C., Kambe, H. and Jina, W., Estimation of stress and displacement around nick zone of zipper pull tab formed on paperboard., *Proceedings of the 2017 International Conference on Materials and Processing ICMP2017*, Los Angeles, CA, USA, (2017), No. 4303, pp. 1-6.
- [4] Jina, W. and Nagasawa, S., Analysis of folding characteristics of creased paperboard, and development of fluffing resistance model for characterizing delamination, *MSC Software 2017 Users Conference*, Tokyo, Japan, (2017).
- [5] Takano, Y., Jina, W., Nagasawa, S., Phookerd, P., Yoshizawa, K., Furumi, T and Mohri, Y., Development of refuse paper and plastic fuel molding machine and feasibility study of crush cutting characteristics of disposable paper diaper, *The 6th International GIGAKU Conference in Nagaoka*, Nagaoka University of Technology, (2017), RD-022, pp.31.

List of national conferences

- [1] Jina, W. and Nagasawa, S., Estimation of Bending Characteristics of Creased White-Coated Paperboard subjected to In-Plane Compressive Load using V-Block Fixtures, *Proceeding of Japanese Spring Conference for the Technology of Plasticity*, Nippon Institute of Technology, Saitama, Japan, (2016), No.142, pp. 63-64.
- [2] Uehara, M., Jina, W. and Nagasawa, S., Tearing characteristic of zipper pull tap of paperboard, 3rd report., *Proceeding of Japanese Spring Conference for the Technology of Plasticity*, Nippon Institute of Technology, Saitama, Japan, (2016), No.115, pp. 23-24.
- [3] Jina, W. and Nagasawa, S., Estimation of Bending Characteristics of Creased White-Coated Paperboard subjected to In-Plane Compressive Load using V-Block Fixtures, report 2nd, *Proceeding of Japanese Spring Conference for the Technology of Plasticity*, Gyuroku Plaza, Gifu, Japan, (2017), No.408, pp. 181-182.

Biography

Personal details

Full name	:	JINA WEERAYUT
Address	:	80, Maetam, Phayamengrai, Chiang rai, 57290, Thailand.
Place of Birth	:	Chiang rai, Thailand.
Date of Birth	:	January 12, 1987.

Educational background

May 2003 – March 2006.	Kanchanapisek Chiangrai Technical College, Chiang rai, Thailand.
May 2006 – August 2010.	Pathumwan Institute of Technology, Bangkok, Thailand. Bachelor of Engineering in Mechatronics Engineering.
Sep. 2013 – August 2015.	Nagaoka University of Technology, Niigata, Japan. Master of Engineering in Mechanical Engineering.
Sep. 2015 – Aug. 2018.	Nagaoka University of Technology, Niigata, Japan. Doctor of Engineering in Information Science and Control Engineering.

Working experience

Nov. 2011 – Jan. 2013	Joined Bangkok Komatsu Company Limited, Amatanakorn Industrial Estate, Chonburi, Thailand. Maintenance Engineer.
-----------------------	--

Research field

Application of finite element analysis in sheet material, Material processing technologies, Mechanics of materials processing.